ISSN 1454-8518

ANNALS OF THE UNIVERSITY OF PETROŞANI

ELECTRICAL ENGINEERING

VOL. 18 (XLV)

UNIVERSITAS PUBLISHING HOUSE
PETROŞANI - ROMANIA 2016

Annals of the University of Petrosani, Electrical Engineering, 18 (2016)

ISSN 1454-8518

Editorial office address: Ec. Radu Ioan, University of Petroşani, 20 University Street, 332006 Petroşani, Romania, Phone: (40) 254/54.29.94; 54.25.80; 54.25.81; 54.33.82; Fax: (40) 254/54.34.91; 54.62.38,

Contact person: **Susana ARAD**, e-mail: susanaarad@yahoo.com

This publication is spread in 28 countries.

CONTENTS

Annals of the University of Petrosani, Electrical Engineering, 18 (2016)

THE UTILIZATION OF THE S-FUNCTION BLOCK IN SIMULATION OF THE MATHEMATICAL MODEL OF INDUCTION MOTOR WITH IRON LOSS

OLIMPIU STOICUTA[1]

Abstract: In this paper is presented the procedure of using Matlab-Simulink's S-Function blocks for simulating the mathematical mode of the induction motors with the squirrel-cage rotor, in which the iron losses are not negligible.

Keywords: induction motors, mathematical models, simulation, iron losses.

1. INTRODUCTION

Mathematical modeling of the induction motor is an important problem for the accuracy of this operation, depending on the dynamic performance of the control systems. The most commonly used mathematical models of the induction motor, in control systems, are those that take in account the following assumptions [1]:

- the motor is not saturated, the permeability of the iron parts is infinite;
- the iron losses are negligible;
- the motor presents perfect symmetry electrical, magnetic and constructive;
- the power supply system must be three-phase, sinusoidal and symmetric;
- the air-gap is considered to be uniform;
- the magnetic field from the air-gap is considered to have a sinusoidal space variation;
- the rotor and stator windings are replaced with equivalent concentrated windings;
- the rotor windings variables and parameters are reported to the stator;

the squirrel-cage winding type is replaced with an equivalent three-phase winding, with the same number of whirls and the same repartition factor as the stator winding;

[1] *Associate Professor, Eng., PhD, University of Petrosani, Romania*

- the pelicular effect and variation with temperature of the motor's parameters are not taken in consideration.

In present, the most commonly used mathematical models for the induction motors, obtained considering the assumptions from above, are [1], [2]:

- *the stator currents-rotor fluxes model*. This model is defined by the following mathematical relations:

$$\frac{d}{dt}\begin{bmatrix}\underline{i}_s\\ \underline{\psi}_r\end{bmatrix}=\begin{bmatrix}a_{11} & a_{13}-j\cdot a_{14}\cdot z_p\cdot\omega_r\\ a_{31} & a_{33}+j\cdot z_p\cdot\omega_r\end{bmatrix}\cdot\begin{bmatrix}\underline{i}_s\\ \underline{\psi}_r\end{bmatrix}+\begin{bmatrix}b_{11}\\ 0\end{bmatrix}\cdot\underline{u}_s \tag{1}$$

$$\frac{d}{dt}\omega_r=H_{m1}\cdot\mathrm{Im}\left(\underline{\psi}_r^*\cdot\underline{i}_s\right)-H_{m2}\cdot\omega_r-H_{m3}\cdot M_r \tag{2}$$

where $\underline{i}_s=i_{ds}+j\cdot i_{qs}$; $\underline{\psi}_r=\psi_{dr}+j\cdot\psi_{qr}$; $\underline{\psi}_r^*=\psi_{dr}-j\cdot\psi_{qr}$; $\underline{u}_s=u_{ds}+j\cdot u_{qs}$; $j=\sqrt{-1}$;

$$a_{11}=-\left(\frac{1}{T_s\cdot\sigma}+\frac{1-\sigma}{T_r\cdot\sigma}\right);\ a_{13}=\frac{L_m}{L_s\cdot L_r\cdot T_r\cdot\sigma};\ a_{14}=\frac{L_m}{L_s\cdot L_r\cdot\sigma};\ a_{31}=\frac{L_m}{T_r};\ a_{33}=-\frac{1}{T_r};$$

$$b_{11}=\frac{1}{L_s\cdot\sigma};T_s=\frac{L_s}{R_s};T_r=\frac{L_r}{R_r};\sigma=1-\frac{L_m^2}{L_s\cdot L_r};H_{m1}=\frac{3}{2}\cdot\frac{z_p}{J}\cdot\frac{L_m}{L_r};H_{m2}=\frac{F}{J};H_{m3}=\frac{1}{J}$$

.

- *the stator currents-rotor currents model.* The equations that define this model, are:

$$\frac{d}{dt}\begin{bmatrix}\underline{i}_s\\ \underline{i}_r\end{bmatrix}=\begin{bmatrix}a_{11}-j\cdot a_{12}\cdot z_p\cdot\omega_r & a_{13}-j\cdot a_{14}\cdot z_p\cdot\omega_r\\ a_{31}+j\cdot a_{32}\cdot z_p\cdot\omega_r & a_{33}+j\cdot a_{34}\cdot z_p\cdot\omega_r\end{bmatrix}\cdot\begin{bmatrix}\underline{i}_s\\ \underline{i}_r\end{bmatrix}+\begin{bmatrix}b_{11}\\ b_{31}\end{bmatrix}\cdot\underline{u}_s \tag{3}$$

$$\frac{d}{dt}\omega_r=H_{m1}\cdot\mathrm{Im}\left(\underline{i}_s\cdot\underline{i}_r^*\right)-H_{m2}\cdot\omega_r-H_{m3}\cdot M_r \tag{4}$$

where

$$\underline{i}_s=i_{ds}+j\cdot i_{qs};\ \underline{i}_r=i_{dr}+j\cdot i_{qr};\ \underline{i}_r^*=i_{dr}-j\cdot i_{qr};\ \underline{u}_s=u_{ds}+j\cdot u_{qs};\ j=\sqrt{-1};$$

$$a_{11}=-\frac{1}{T_s\cdot\sigma};\ a_{12}=\frac{1-\sigma}{\sigma};\ a_{13}=\frac{L_m}{L_s\cdot T_r\cdot\sigma};a_{14}=\frac{L_m}{L_s\cdot\sigma};a_{31}=\frac{L_m}{L_r\cdot T_s\cdot\sigma};\ a_{32}=\frac{L_m}{L_r\cdot\sigma};$$

$$a_{33}=-\frac{1}{T_r\cdot\sigma};\ a_{34}=\frac{1}{\sigma};\ b_{11}=\frac{1}{\sigma\cdot L_s};\ b_{31}=-\frac{L_m}{L_s\cdot L_r\cdot\sigma};\ T_s=\frac{L_s}{R_s};\ T_r=\frac{L_r}{R_r};$$

$$H_{m1}=\frac{3}{2}\cdot\frac{z_p}{J}\cdot L_m;\ H_{m2}=\frac{F}{J};\ H_{m3}=\frac{1}{J};\ \sigma=1-\frac{L_m^2}{L_s\cdot L_r}.$$

- *the stator fluxes-rotor fluxes model*. The mathematical model is defined by the following equations:

$$\frac{d}{dt}\begin{bmatrix}\underline{\psi}_s\\ \underline{\psi}_r\end{bmatrix}=\begin{bmatrix}a_{11} & a_{13}\\ a_{31} & a_{33}+j\cdot z_p\cdot\omega_r\end{bmatrix}\cdot\begin{bmatrix}\underline{\psi}_s\\ \underline{\psi}_r\end{bmatrix}+\begin{bmatrix}1\\0\end{bmatrix}\cdot\underline{u}_s \tag{5}$$

$$\frac{d}{dt}\omega_r=H_{m1}\cdot\mathrm{Im}\left(\underline{\psi}_s\cdot\underline{\psi}_r^*\right)-H_{m2}\cdot\omega_r-H_{m3}\cdot M_r \tag{6}$$

where $\underline{\psi}_s=\psi_{ds}+j\cdot\psi_{qs}$; $\underline{\psi}_r=\psi_{dr}+j\cdot\psi_{qr}$; $\underline{\psi}_r^*=\psi_{dr}-j\cdot\psi_{qr}$; $\underline{u}_s=u_{ds}+j\cdot u_{qs}$; $j=\sqrt{-1}$

$$a_{11}=-\frac{1}{\sigma\cdot T_s};\ a_{13}=\frac{L_m}{\sigma\cdot L_r\cdot T_s};\ a_{31}=\frac{L_m}{\sigma\cdot L_s\cdot T_r};\ a_{33}=-\frac{1}{\sigma\cdot T_r};\ T_s=\frac{L_s}{R_s};\ T_r=\frac{L_r}{R_r};$$

$$H_{m1}=\frac{3}{2}\cdot\frac{z_p}{J}\cdot\frac{L_m}{L_s\cdot L_r\cdot\sigma};\ H_{m2}=\frac{F}{J};\ H_{m3}=\frac{1}{J};\ \sigma=1-\frac{L_m^2}{L_s\cdot L_r}.$$

- *the stator fluxes-stator currents model*. The mathematical relations that define this model, are:

$$\frac{d}{dt}\begin{bmatrix}\underline{\psi}_s\\ \underline{i}_s\end{bmatrix}=\begin{bmatrix}0 & a_{13}\\ a_{31}-j\cdot a_{32}\cdot z_p\cdot\omega_r & a_{33}+j\cdot z_p\cdot\omega_r\end{bmatrix}\cdot\begin{bmatrix}\underline{\psi}_s\\ \underline{i}_s\end{bmatrix}+\begin{bmatrix}1\\b_{31}\end{bmatrix}\cdot\underline{u}_s \tag{7}$$

$$\frac{d}{dt}\omega_r=H_{m1}\cdot\mathrm{Im}\left(\underline{\psi}_s^*\cdot\underline{i}_s\right)-H_{m2}\cdot\omega_r-H_{m3}\cdot M_r \tag{8}$$

where $\underline{i}_s=i_{ds}+j\cdot i_{qs}$; $\underline{\psi}_s=\psi_{ds}+j\cdot\psi_{qs}$; $\underline{\psi}_s^*=\psi_{ds}-j\cdot\psi_{qs}$; $\underline{u}_s=u_{ds}+j\cdot u_{qs}$; $j=\sqrt{-1}$;

$$a_{13}=-R_s;\ a_{31}=\frac{1}{\sigma\cdot L_s\cdot T_r};\ a_{32}=\frac{1}{\sigma\cdot L_s};\ a_{33}=-\frac{1}{\sigma}\cdot\left(\frac{1}{T_s}+\frac{1}{T_r}\right);\ b_{31}=\frac{1}{\sigma\cdot L_s};$$

$$H_{m1}=\frac{3}{2}\cdot\frac{z_p}{J};\ H_{m2}=\frac{F}{J};H_{m3}=\frac{1}{J};\ T_s=\frac{L_s}{R_s};\ T_r=\frac{L_r}{R_r};\ \sigma=1-\frac{L_m^2}{L_s\cdot L_r}.$$

The current trends in the simulation of the induction motors within Matlab-Simulink program is based on the use of the S-Function blocks. This facilitates the implementing of the mathematical models previously presented , in one graphic block usable in Simulink, written either in the Matlab or C language [1], [3].

Current research in the field of the vector control systems for the induction motors, are based on the mathematical model that takes in account the iron losses. In this sense, this paper presents a mathematical model of the induction motor, in which the iron losses are not neglected. Simulation of the induction motor taking in account

the iron losses is being achieved in Matlab-Simulink using an S-Function block. On the other hand, to highlight the influence of iron losses, in this article is done a comparative analysis by simulation, between the stator currents – rotor fluxes model, and the mathematical model that take in account the iron losses of the induction motor.

2. THE MODEL OF INDUCTION MOTOR WITH IRON LOSS

The equivalent circuit of the induction motor that considers the iron losses is presented in Fig.1. The iron losses, as well as the losses that are happening because of the eddy and hysteresis currents, are modelled using a resistance equivalent to the iron losses, placed parallel with the mutual inductivity [4]. This model is known under de name of the parallel model of the induction motor with iron losses [5].

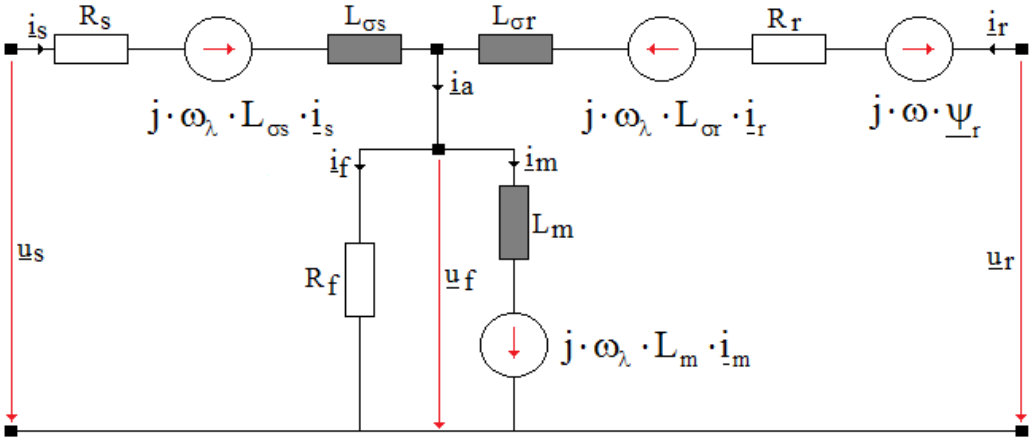

Fig.1. The equivalent circuit of the induction motor with iron losses

Using the circuit from Fig.1, the following equations can be written [6]:

- the equations of the stator voltages:

$$\underline{u}_s = R_s \cdot \underline{i}_s + \frac{d}{dt}\underline{\psi}_s + j \cdot \omega_\lambda \cdot \underline{\psi}_s \tag{9}$$

- equations of the rotor voltages:

$$0 = R_r \cdot \underline{i}_r + \frac{d}{dt}\underline{\psi}_r + j \cdot (\omega_\lambda - \omega) \cdot \underline{\psi}_r \tag{10}$$

- equation of the stator fluxes:

$$\underline{\psi}_s = \underline{\psi}_m + L_{\sigma s} \cdot \underline{i}_s \tag{11}$$

- equation of the rotor fluxes:

$$\underline{\psi}_r = \underline{\psi}_m + L_{\sigma r} \cdot \underline{i}_r \tag{12}$$

- equation of the air-gap fluxes:

$$\underline{\psi}_m = L_m \cdot \underline{i}_m \tag{13}$$

- currents equation:

$$\underline{i}_s + \underline{i}_r = \underline{i}_m + \underline{i}_f \tag{14}$$

- magnetic branch voltage equations:

$$\underline{u}_f = R_f \cdot \underline{i}_f = \frac{d}{dt}\underline{\psi}_m + j \cdot \omega_\lambda \cdot \underline{\psi}_m \tag{15}$$

- motion equation of the induction motor:

$$J \cdot \frac{d}{dt}\omega_r = M_e - F \cdot \omega_r - M_r \tag{16}$$

where M_e is the electromagnetic torque of the induction motor:

$$M_e = \frac{3}{2} \cdot \frac{z_p}{L_{\sigma r}} \cdot \mathrm{Im}\left(\underline{\psi}_r^* \cdot \underline{\psi}_m\right) \tag{17}$$

The equations of the induction motor presented above, are generalized, being written in a orthogonal axis system $d\lambda - q\lambda$, that rotates with an angular speed ω_λ.

By customizing of the axis system, we obtain the following equations:

- for $\omega_\lambda = 0$, the general equations of induction machine in the stator reference system;
- for $\omega_\lambda = \omega_r$, the general equations of induction machine in the rotor reference system.

The equations presented above, can be written in the following matrices forms:

- *stator currents-rotor fluxes-air-gap fluxes model.* The mathematical equations that define this model are:

$$\frac{d}{dt}\begin{bmatrix} \underline{i}_s \\ \underline{\psi}_r \\ \underline{\psi}_m \end{bmatrix} = \begin{bmatrix} a_{11} - j \cdot \omega_\lambda & a_{13} & a_{15} \\ 0 & a_{33} - j \cdot \left(\omega_\lambda - z_p \cdot \omega_r\right) & -a_{33} \\ a_{51} & a_{53} & a_{55} - j \cdot \omega_\lambda \end{bmatrix} \cdot \begin{bmatrix} \underline{i}_s \\ \underline{\psi}_r \\ \underline{\psi}_m \end{bmatrix} + \begin{bmatrix} b_{11} \\ 0 \\ 0 \end{bmatrix} \cdot \underline{u}_s \tag{18}$$

$$\frac{d}{dt}\omega_r = H_{m1}\cdot \mathrm{Im}\left(\underline{\psi}_r^{*}\cdot \underline{\psi}_m\right) - H_{m2}\cdot\omega_r - H_{m3}\cdot M_r \tag{19}$$

where $\underline{i}_s = i_{ds} + j\cdot i_{qs}$; $\underline{\psi}_r = \psi_{dr} + j\cdot\psi_{qr}$; $\underline{\psi}_r^{*} = \psi_{dr} - j\cdot\psi_{qr}$; $\underline{\psi}_m = \psi_{dm} + j\cdot\psi_{qm}$;

$\underline{u}_s = u_{ds} + j\cdot u_{qs}$; $j = \sqrt{-1}$; $a_{11} = -\dfrac{R_s + R_f}{L_{\sigma s}}$; $a_{13} = -\dfrac{R_f}{L_{\sigma s}\cdot L_{\sigma r}}$; $a_{15} = R_f\cdot\dfrac{L_r}{L_{\sigma s}\cdot L_{\sigma r}\cdot L_m}$;

$a_{33} = -\dfrac{R_r}{L_{\sigma r}}$; $a_{51} = R_f$; $a_{53} = \dfrac{R_f}{L_{\sigma r}}$; $a_{55} = -R_f\cdot\dfrac{L_r}{L_{\sigma r}\cdot L_m}$; $b_{11} = \dfrac{1}{L_{\sigma s}}$; $H_{m1} = \dfrac{3}{2}\cdot\dfrac{z_p}{J}\cdot\dfrac{1}{L_{\sigma r}}$;

$$H_{m2} = \frac{F}{J}; H_{m3} = \frac{1}{J};\ L_r = L_{\sigma r} + L_m;\ L_s = L_{\sigma s} + L_m.$$

- *stator currents-rotor currents-magnetizing currents model.* This model is defined by the following relations:

$$\frac{d}{dt}\begin{bmatrix}\underline{i}_s\\ \underline{i}_r\\ \underline{i}_m\end{bmatrix} = \begin{bmatrix} a_{11} - j\cdot\omega_\lambda & a_{13} & -a_{13}\\ a_{31} & a_{33} - j\cdot\left(\omega_\lambda - z_p\cdot\omega_r\right) & -a_{31} - z_p\cdot\omega_r\cdot a_{36}\\ a_{51} & a_{51} & -\left(a_{51} + j\cdot\omega_\lambda\right)\end{bmatrix}\cdot\begin{bmatrix}\underline{i}_s\\ \underline{i}_r\\ \underline{i}_m\end{bmatrix} + \begin{bmatrix} b_{11}\\ 0\\ 0\end{bmatrix}\cdot\underline{u}_s \tag{20}$$

$$\frac{d}{dt}\omega_r = H_{m1}\cdot\mathrm{Im}\left(\underline{i}_m\cdot\underline{i}_r^{*}\right) - H_{m2}\cdot\omega_r - H_{m3}\cdot M_r \tag{21}$$

where $\underline{i}_s = i_{ds} + j\cdot i_{qs}$; $\underline{i}_r = i_{dr} + j\cdot i_{qr}$; $\underline{i}_r^{*} = i_{dr} - j\cdot i_{qr}$; $\underline{i}_m = i_{dm} + j\cdot i_{qm}$; $\underline{u}_s = u_{ds} + j\cdot u_{qs}$;

$j = \sqrt{-1}$; $a_{11} = -\dfrac{R_s + R_f}{L_{\sigma s}}$; $a_{13} = -\dfrac{R_f}{L_{\sigma s}}$; $a_{31} = -\dfrac{R_f}{L_{\sigma r}}$; $a_{33} = -\dfrac{R_r + R_f}{L_{\sigma r}}$; $a_{36} = -\dfrac{L_m}{L_{\sigma r}}$;

$$a_{51} = \frac{R_f}{L_m};\ b_{11} = \frac{1}{L_{\sigma s}};\ H_{m1} = \frac{3}{2}\cdot\frac{z_p}{J}\cdot L_m;\ H_{m2} = \frac{F}{J}; H_{m3} = \frac{1}{J}.$$

Equations (18) and (19), respectively (20) and (21), define the most commonly used mathematical models for the induction motor, obtained under the hypothesis that the iron losses are not negligible.

3. THE INDUCTION MOTOR SIMULATION

The mathematical models for the induction motor, which are to be simulated at the same time, are: stator currents – rotor fluxes model (defined by relations (1) and (2)), respectively, stator currents – rotor fluxes – air-gap fluxes (defined by relations (18) and (19)). The simulations programs are realized using the general equations for the induction motors, using a stator reference system ($\omega_\lambda = 0$).

The program used to simulate the two induction motors, is presented in Fig.2. The program presented in the Fig.2, is created in Matlab – Simulink using S-Function blocks.

The differential equation systems that define the mathematical models for the induction motors, are being solved using the numeric method Dormand – Prince (ode45), using a relative and absolute error $\varepsilon = 10^{-7}$.

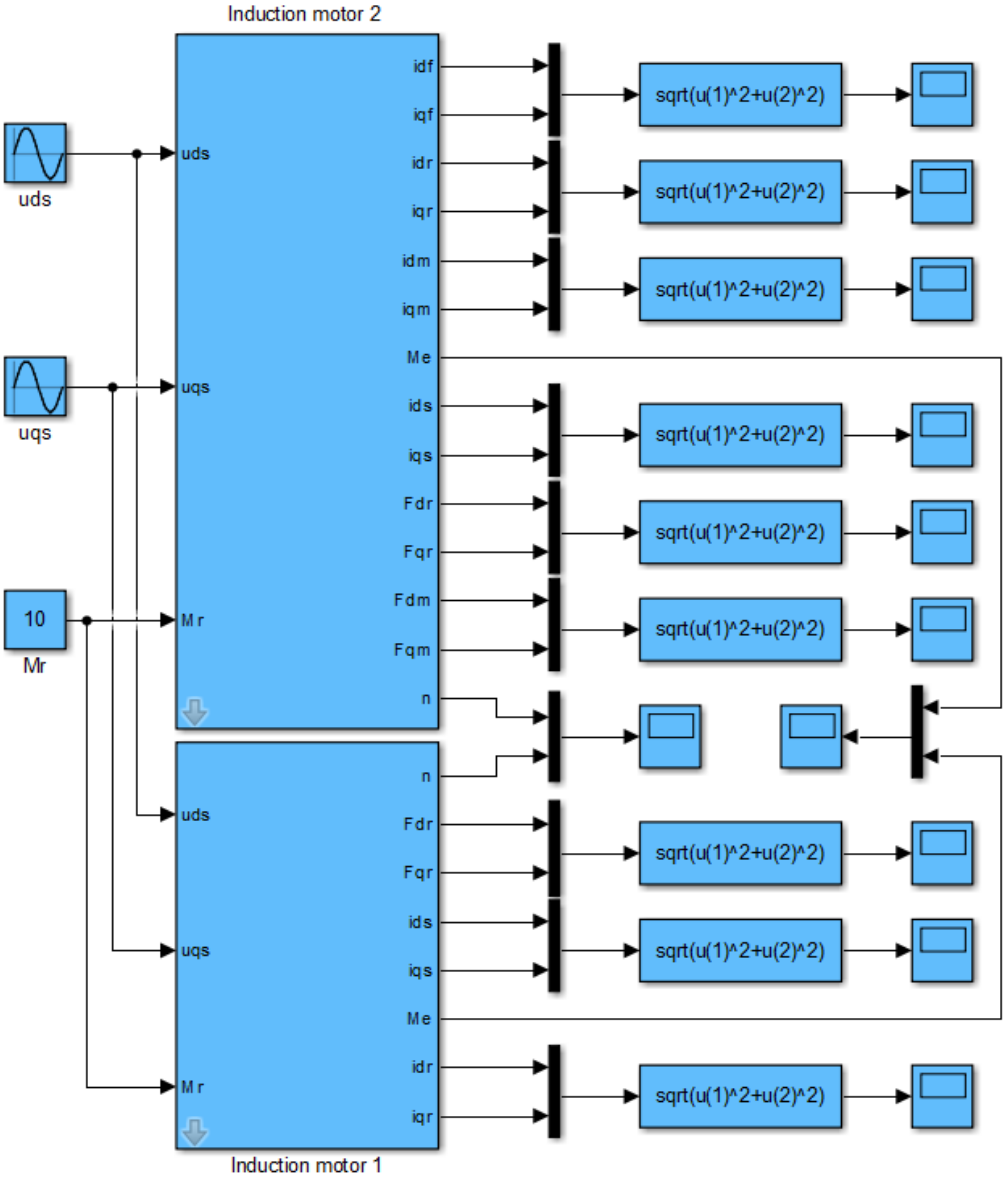

Fig.2. The simulation program in Matlab-Simulink for the two induction motors

The internal structure of the two subsystems from Fig.2, are represented in the following figures.

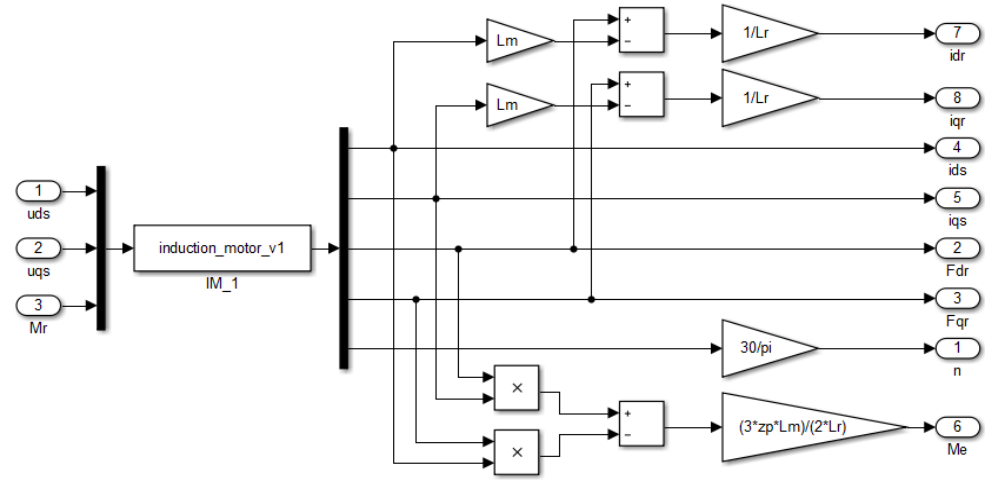

Fig.3. Internal structure of the subsystem "Induction motor 1", which implements the stator currents-rotor fluxes mathematical model.

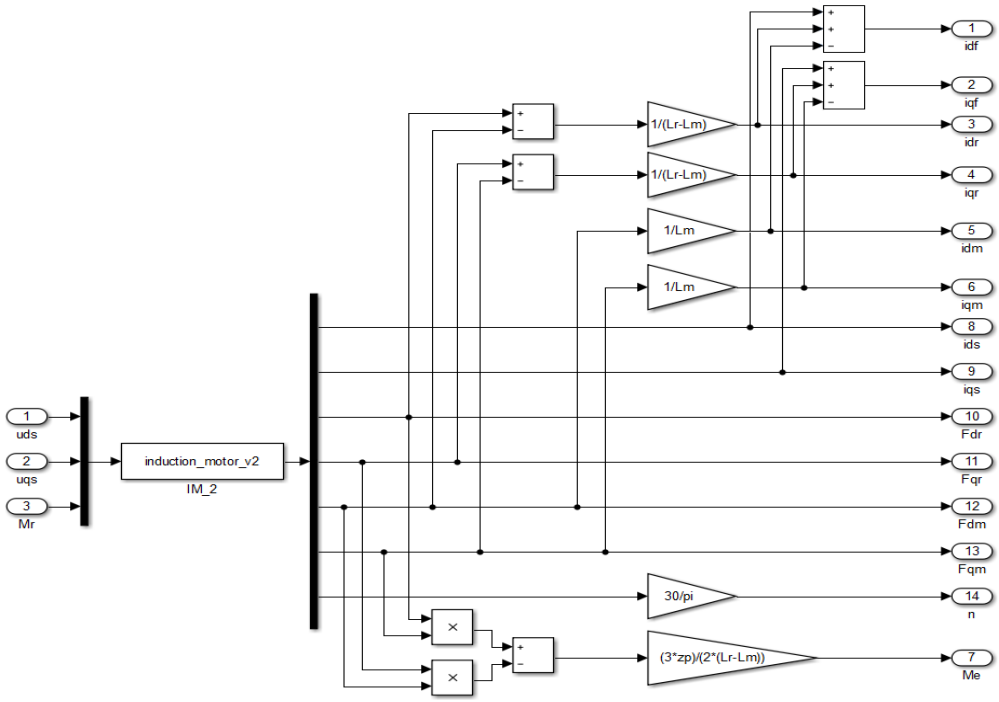

Fig.4. Internal structure of the subsystem "Induction motor 2", which implements the stator currents-rotor fluxes-air-gap fluxes mathematical model.

In Fig.3 and Fig.4, the S-Function blocks are noted by "IM_1", respectively "IM_2". The Matlab programs which are attached to the S-Function blocks, are presented in the following figures.

```
function[sys,x0]=induction_motor_v1(t,x,u,flag,Rs,Rr,Ls,Lr,Lm,J,F,zp)
s=1-(Lm^2/(Ls*Lr));
Ts=Ls/Rs;
Tr=Lr/Rr;
a11=-((1/(Ts*s))+((1-s)/(Tr*s)));
a13=Lm/(Ls*Lr*Tr*s);
a14=Lm/(Ls*Lr*s);
a31=Lm/Tr;
a33=-(1/Tr);
b11=1/(s*Ls);
Hm1=(3*zp*Lm)/(2*J*Lr);
Hm2=F/J;
Hm3=1/J;
if abs(flag)==1
     sys=[a11*x(1)+a13*x(3)+a14*zp*x(5)*x(4)+b11*u(1);
          a11*x(2)-a14*zp*x(5)*x(3)+a13*x(4)+b11*u(2);
          a31*x(1)+a33*x(3)-zp*x(5)*x(4);
          a31*x(2)+zp*x(5)*x(3)+a33*x(4);
          Hm1*x(3)*x(2)-Hm1*x(4)*x(1)-Hm2*x(5)-Hm3*u(3)];
elseif flag==3
   sys=x;
elseif flag==0
   sys=[5 0 5 3 0 0];
    x0=[0;0;0;0;0];
else
   sys=[];
end
```

Fig.5. "IM_1" block code.

The Matlab programs, presented in Fig.5 and Fig.6, are based on the explained differential equations of the analyzed induction motors (for each differential equations whose coefficients and/or variables are of complex type, there are extract both the equation for the real part, and the equation that correspond to the imaginary part). This way, the stator currents – rotor fluxes mathematical model, is defined by 5 differential equations, and the stator currents – rotor fluxes – air-gap fluxes mathematical model, is defined by 7 differential equations.

The components u_{ds} and u_{qs} of the stator voltages (see Fig.2), are defined by the following relation:

$$\begin{cases} u_{ds} = U_N \cdot \sqrt{\dfrac{2}{3}} \cdot \sin\left(\omega \cdot t\right) \\ u_{qs} = U_N \cdot \sqrt{\dfrac{2}{3}} \cdot \sin\left(\omega \cdot t - \dfrac{\pi}{2}\right) \end{cases} \tag{22}$$

where $\omega = 2 \cdot \pi \cdot f$; f is the stator voltages frequency, and U_N is the nominal voltage of the induction motor.

The relations (22) are implemented within the simulation program, using two sinusoidal generators, specific to the Simulink toolbox.

```
function[sys,x0]=induction_motor_v2(t,x,u,flag,Rs,Rr,Rf,Ls,Lr,Lm,J,F,zp)
Lgs=Ls-Lm;
Lgr=Lr-Lm;
a11=-(Rs+Rf)/Lgs;
a13=-Rf/(Lgs*Lgr);
a15=Rf*Lr/(Lgs*Lgr*Lm);
a33=-Rr/Lgr;
a51=Rf;
a53=Rf/Lgr;
a55=-Rf*Lr/(Lgr*Lm);
b11=1/Lgs;
Hm1=(3*zp)/(2*J*Lgr);
Hm2=F/J;
Hm3=1/J;
if abs(flag)==1
     sys=[a11*x(1)+a13*x(3)+a15*x(5)+b11*u(1);
          a11*x(2)+a13*x(4)+a15*x(6)+b11*u(2);
          a33*x(3)-zp*x(7)*x(4)-a33*x(5);
          zp*x(7)*x(3)+a33*x(4)-a33*x(6);
          a51*x(1)+a53*x(3)+a55*x(5);
          a51*x(2)+a53*x(4)+a55*x(6);
          Hm1*x(3)*x(6)-Hm1*x(4)*x(5)-Hm2*x(7)-Hm3*u(3)];
elseif flag==3
   sys=x;
elseif flag==0
   sys=[7 0 7 3 0 0];
    x0=[0;0;0;0;0;0;0];
else
   sys=[];
end
```

Fig.6. "IM_2" block code.

The electrical and mechanical parameters of the induction motor (IM) used to simulation, are given in the Table 1.

Table 1. **Induction Motor Parameters** [7]

	Name	Value		Name	Value
R_s	*Stator resistance*	4.85 [Ω]	F	*Friction coefficient*	0.008[N·m·s/rad]
R_r	*Rotor resistance*	3.805 [Ω]	P_N	*Rated power*	1.5 [kW]
R_f	*Iron loss resistance*	500 [Ω]	n_N	*Rated speed*	1420 [rpm]
L_s	*Stator inductance*	0.274 [H]	z_p	*Number of pole pairs*	2
L_r	*Rotor inductance*	0.274 [H]	f_N	*Rated frequency*	50 [Hz]
L_m	*Mutual inductance*	0.258 [H]	U_N	*Rated voltage*	220 Δ/380 Y [V]
J	*Motor inertia*	0.031[kg·m^2]	M_N	*Rated torque*	10 [N·m]

The tandem simulation of the two mathematical models, relating to analyzed induction motor, is being made for the direct on-line starting case (DOL), in load,

having at the shaft a resistive torque equal with the nominal torque of the induction machine.

Within the simulation, the nominal voltage has the value $U_N = 380[V]$, and the frequency of the supply voltages for the induction motor, has the value $f = 50[Hz]$.

The simulated program from Fig.2, was compiled and ran on a numeric system operating Windows 10- 64b. The hardware structure of the system is built around an I7-4720HQ processor (2.6GHz), with 8 GB of available RAM.

The results from the simulation are presented in the following figures.

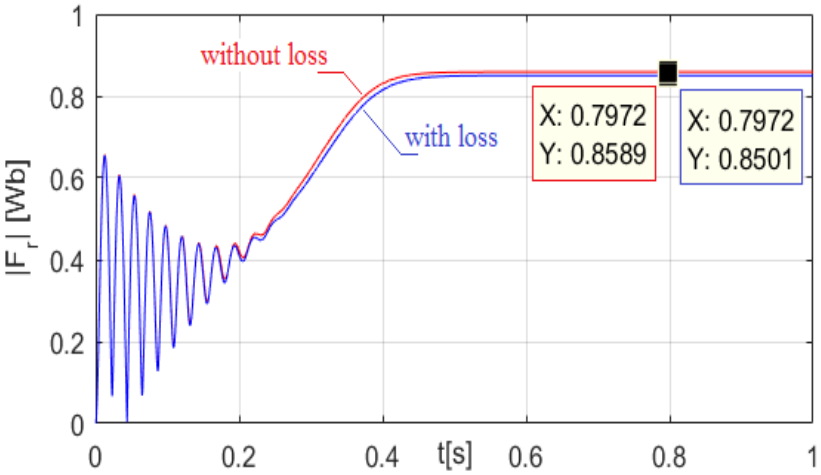

Fig. 7. The module of the rotor flux phasor

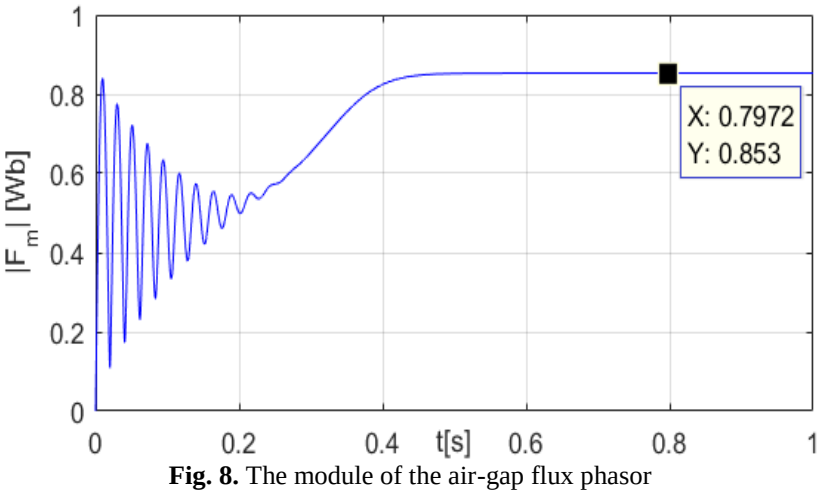

Fig. 8. The module of the air-gap flux phasor

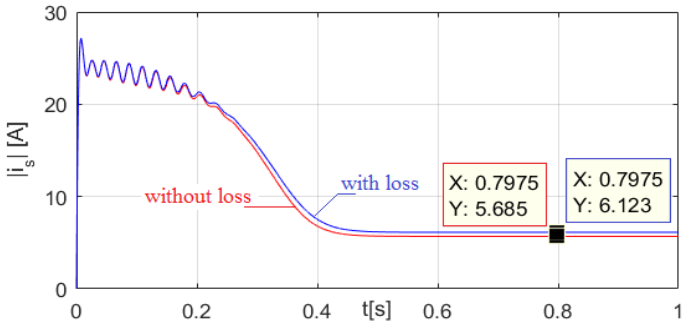

Fig. 9. The module of the stator current phasor

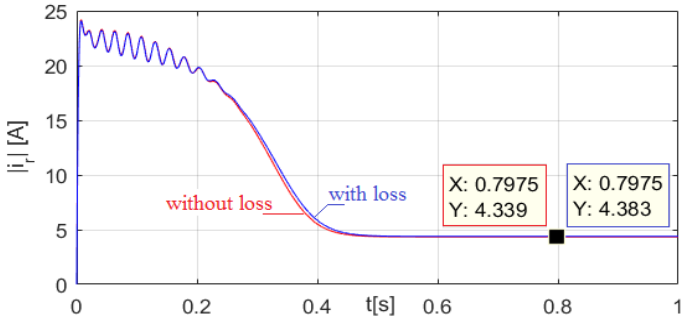

Fig. 10. The module of the rotor current phasor

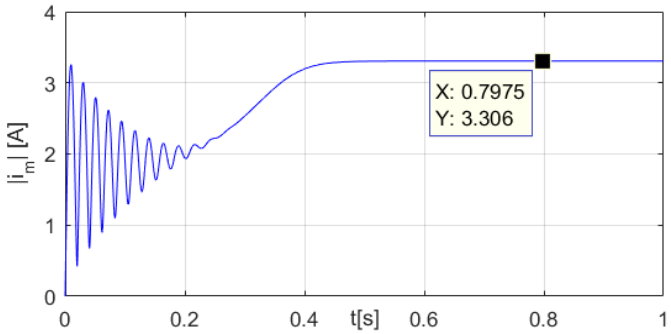

Fig. 11. The module of the magnetizing current phasor

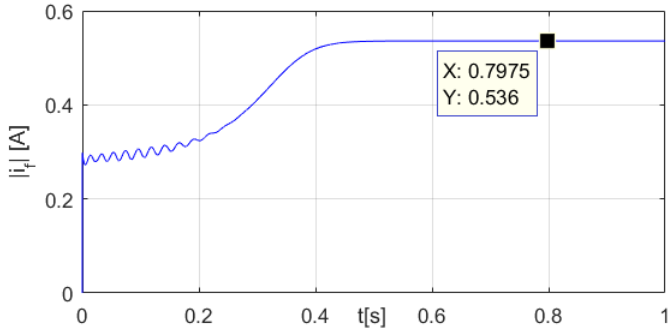

Fig. 12. The module of the "iron loss current" phasor

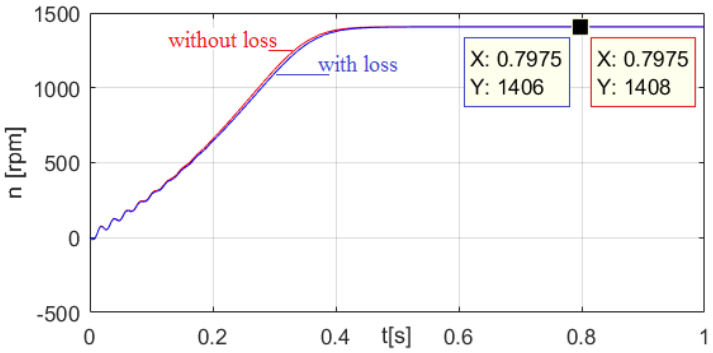

Fig. 13. Speed of the induction motor

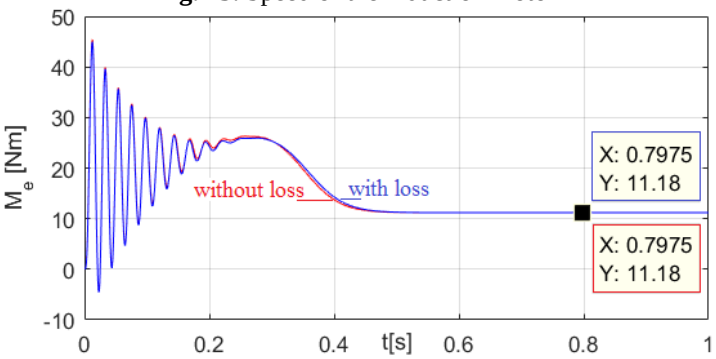

Fig. 14. Electromagnetic torque of the induction motor

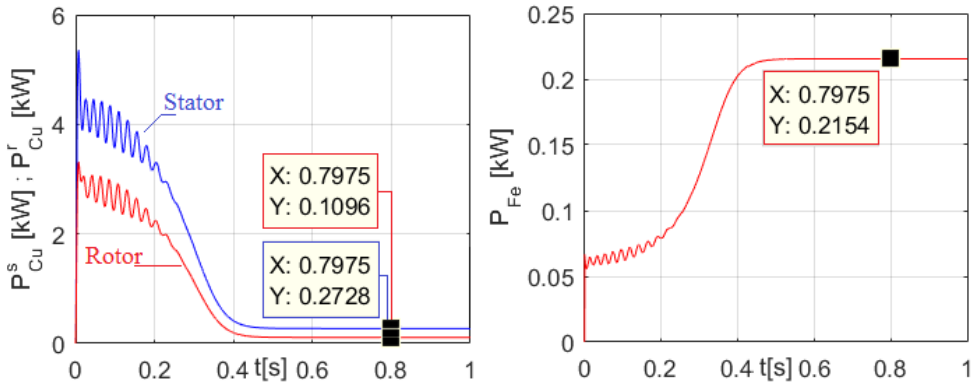

Fig. 15. Losses in copper and iron for the induction motor

From the previously presented graphics, it can be observed that the results obtained after the simulation of the conventional model of the induction motor, are similar to the results obtained based on the mathematical model of the induction motor which takes in account the iron losses. The most significant differences appear in stationary regime (the module of the stator current phasor case – see Fig.9, and also in

the case of the speed – see Fig. 13). The absolute differences between the other variables, obtained by simulation, in stationary regime, have a value lower than 0.05.

From Fig.7 and Fig.8, it can be observed that in stationary regime, the module of the rotor flux phasor is approximately equal to the module of the air-gap flux phasor. From Fig.9 - Fig.12, it is observed that, both in transitory regime, and in the stationary regime, between the modules of the currents phasor of the induction motor, the can be written the following inequalities:

$$|\underline{i}_s| > |\underline{i}_r| > |\underline{i}_m| \gg |\underline{i}_f| \tag{23}$$

Fig.15 presents the cooper and iron losses of the induction motor. The calculus relations of these losses are presented in the following:

- cooper losses (the Joule-Lenz effect), in the stator of the induction motor

$$P_{Cu}^{s} \cong k_n \cdot R_s \cdot \left(i_{ds}^2 + i_{qs}^2\right) = k_n \cdot R_s \cdot |\underline{i}_s|^2 \tag{24}$$

- cooper losses (the Joule-Lenz effect), in the rotor of the induction motor

$$P_{Cu}^{r} \cong k_n \cdot R_r \cdot \left(i_{dr}^2 + i_{qr}^2\right) = k_n \cdot R_r \cdot |\underline{i}_r|^2 \tag{25}$$

- iron losses in the induction motor

$$P_{Fe} \cong k_n \cdot R_f \cdot \left(i_{df}^2 + i_{qf}^2\right) = k_n \cdot R_f \cdot |\underline{i}_f|^2 \tag{26}$$

where $k_n = 3/2$.

From Fig.15, it can be observed that the iron and cooper losses, in stationary regime, satisfy the following inequalities:

$$P_{Cu}^{s} > P_{Fe} > P_{Cu}^{r} \tag{27}$$

From Fig.15, it can be observed that the total cooper and iron losses, in stationary regime, within the induction motor, have an approximate value of 0.6 [kW], which means an approximate value of 40% from the nominal value of the induction motor. Taking account of the relations (14) and (23), we can make the following approximation:

$$\underline{i}_m \cong \underline{i}_s + \underline{i}_r \tag{28}$$

Justification for the approximative relation (28), is presented under graphical form in the following figures.

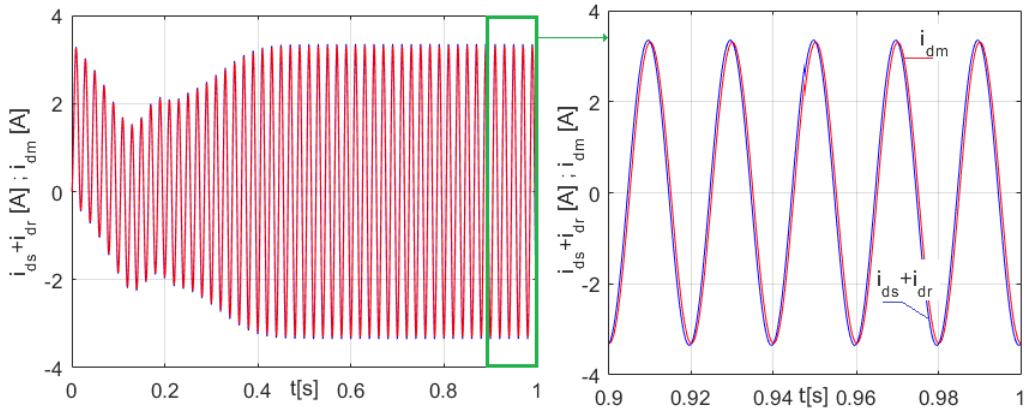

Fig. 16. Magnetizing current approximation on the d axis

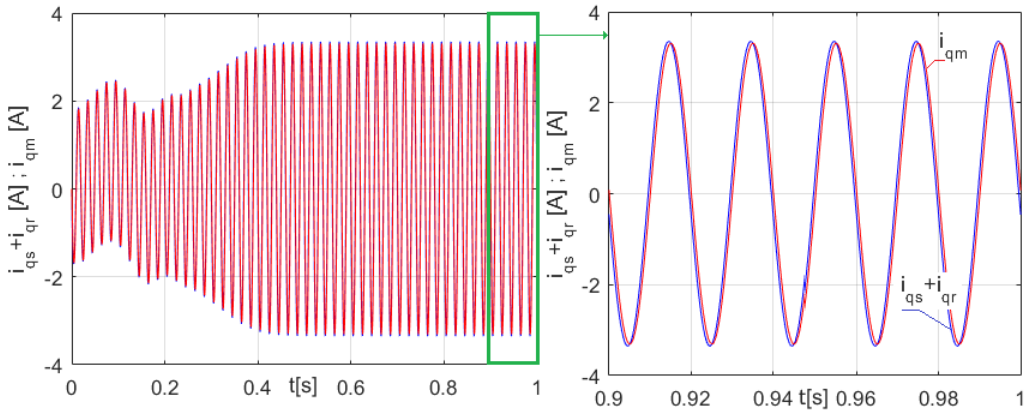

Fig. 17. Magnetizing current approximation on the q axis

The mathematical model of the induction motor, obtained with relation (28), is known in the special literature under the name of the series model of the induction motor with iron losses [9].

On the other hand, from the presented graphics, it is observed that the time for the transitory process is approximate 0.45 [s]. Within the transitory process, the module of the stator current phasor reaches a maximum of approximate 27[A], whilst the module of the rotor current phasor reaches a maximum value of approximate 24[A] (see Fig.9 and Fig.10).

This is being reflected in the cooper losses variation in time, from the stator and the rotor of the induction motor.

This way, the cooper losses from the stator, have a maximum value of approximate 5.3 [kW], while the cooper losses from the rotor, have a maximum value of approximate 3.3 [kW].

4. CONCLUSIONS

Using the S-Function block in simulating of the induction motor, offers the advantage of implementing within a single file written in Matlab or C, all of the non-linear differential equations that define the mathematical model of the induction motor. This file is imported in Simulink, with help of the S-Function block.

The simulation programs contained in this paper are presented in detail, offering a very helpful support for the specialists from automatization field and electric engineering field.

REFERENCES

[1]. **Pana T., Stoicuta O.,** *Stability of the Vector Drive Systems with Induction Motors*, Mediamira Publishers, 2016.

[2]. **Boldea I., Nasar S.A.,** *Vector Control of AC Drives*, CRC Press, 1992.

[3]. **Ong C.H.,** *Dynamic Simulations of Electric Machinery: using Matlab-Simulink*, Prentice Hall, 1998.

[4]. **Boldea I., Nasar S.A.,** *Unified Treatment of Core Losses and Saturation in the Orthogonal-Axis Model of Electric Machines*, IEE Proceedings B, Electric Power Applications, Vol.134, No. 6, pp.355-363, 1987.

[5]. **Levi E.,** *Impact of Iron Loss on Behavior of Vector Controlled Induction Machines*, IEEE Transactions on Industry Applications, vol.31, pp.1287-1296, 1995.

[6]. **Marcu M., Samoila L. B., Popescu F.G.,** *Power Active Filter Based on Synchronous Reference System Theory*, Proceedings of the 1st International Conference on Industrial and Manufacturing Technologies (INMAT '13), Vouliagmeni, Athens, Greece, May 14-16, 2013, pag. 82-87, ISSN: 2227-4596, ISBN: 978-1-61804-186-9.

[7]. **Sung-Dong Wee, Myoung-Ho Shin, Dong-Seok Hyun**, *Stator-Flux-Oriented Control of Induction Motor*, IEEE Transactions on Industrial Electronics, Vol.48, No.3, pp. 602-608, 2001.

[8]. **Aissa K., Eddine K.D.,** *Vector control using Series Iron Loss Model of Induction Motors and Power Loss Minimization*, World Academy of Science, Engineering and Technology, Vol.52, pp. 142-148, 2009.

[9]. **Jung J., Nam K.,** *A Vector Control Scheme for EV Induction Motors with a Series Iron Loss Model*, IEEE Transactions on Industrial Electronics, Vol.45, No.4, pp.617-624, 1998.

ABOUT THE POWER GENERATING PLANTS DEMANDS AS ENERGY MANAGEMENT FEATURE

MARIA DANIELA STOCHITOIU[1]

Abstract: Typically, areas of different power densities also require different network configurations. In this context, the reliability of supply and the supply quality of the electric power distribution system should be paid special attention. The modern society shouldn't exist without a safety, clean and certain electrical energy supply as well as an affordable price.

Keywords: power generating plants, electric power distribution system, climate change, energy quality.

1. INTRODUCTION

Climate change is an issue that has been raising concern from different nations and has triggered actions within them to become more sustainable. It has been proven that besides saving money, energy efficiency reduces environmental impact and creates jobs. For these reasons, it is in every country's best interest to head towards efficiency and reduces energy waste.

The improvement of energy efficiency is one of the most cost-effective ways to concurrently improve the security of supply, reduce energy-related emissions, assure affordable energy prices, and improve economic competitiveness. More specifically, it requires promoting and ensuring the use of high quality, cost-effective energy audits and energy management systems to all final customers.[6]

The electrical energy is one of the base conditions for economical and social development for education, health and all aspects of human life.

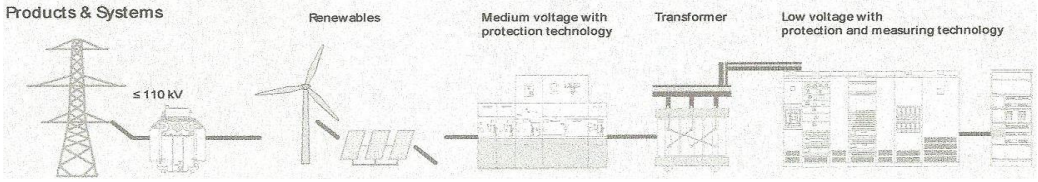

Fig.1 Integrated production and system solution of electrical distribution

[1] *Associate Professor, Eng., PhD, University of Petrosani, Romania*

In the last twenty years, there were major changes in the electrical energy develop system meantime the electrical societies have relied their strategies on the predictable and stable conditions, the industry- which is still powerful regulated – is frequently putting face to face with frameworks of rules and climate reglementations in nowadays.

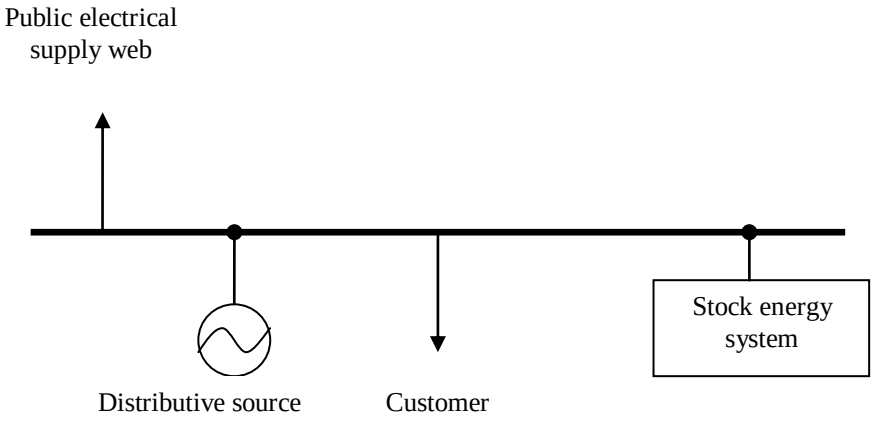

Fig. 2 The distributed supply installation using the stock energy system

As specific particularities of energy sector, it can mention: a high inertia due to interval of time between decision and implementation; along with transport structure is main contributor to environmental pollution and climate changes; it needs important financial investments.[5]

In Romania, the Energy Regulatory Authority (ANRE) is responsible for developing energy efficiency policy. Regarding energy efficiency and promoting the use of renewable energy sources to end-users, the following criteria were mandatory:

• Operators with more than 1,000 toe (41,868 GJ) consumption of energy must have a certified energy manager, declare consumption, perform energy audits and answer an energy analysis questionnaire.

• Energy distributors, distribution system operators and retail power companies must improve their energy efficiency while still providing competitive prices. They must also complete energy audits and measures to improve efficiency to end users, and contribute to mechanisms or energy efficiency funds.

• Towns with 20,000 inhabitants must implement energy efficiency programmer. Romania requires management to be involved with the yearly energy efficiency programmer to ensure buy-in and implementation. Subsequent energy audits must evaluate the implementation of the recommendations of the previous audit.

2. POWER GENERATING PLANTS DEMANDS

Regarding the planning concept for power supply, it is not only imperative to observe standards and regulations, it is also important to discuss and clarify economic and technical interrelations. To this end electric equipment, such as distribution boards and transformers, is selected and rated in such a way that an optimum result for the power system as whole is achieved rather than focusing individual components. All components must be sufficiently rated to withstand normal operating conditions as well as fault conditions.[1]

As a part of energy management, the voltage quality is very important

1. The power generating plants that are incorporated, such as combined heat and power stations (CHP), diesel generator units, gas turbines, wind power stations, and solar systems, should be assigned functions, such as standby power supply, emergency power supply, base load coverage, capping of peak loads. The respective function and the installation sites of power generating plants (centrally or distributed in relation to the main feed-in) have a significant effect on the MV network configuration and the required power system protection.

2. Depending on the design, power generating plants can increase the network short-circuit rating; this can be taken into account when dimensioning the switchgear and equipment.

3. Power generating plants can have a negative effect on the power system and power quality. Examples of this are voltage changes, harmonics, and flicker.

The criterion of selectivity, i.e. the clear identification of the power supply unit affected by the fault and its disconnection, is clearly linked to these requirements. In order to reduce the effects of a system fault as much as possible, the protection must take effect as quickly as possible.

The basic idea behind power system protection is the detection of a fault through the presence of abnormal electrical states, and then to determine which points in the network should be disconnected. The following are characteristic for these faults: • Overcurrent; • Collapse and displacement of the voltages

The protection function is based on the determination and evaluation of these variables. Overcurrent and voltage changes occur not only in the immediate vicinity of the fault location, but in wide areas of the network or throughout the entire network. It is therefore not enough to only measure these variables in order to decide whether a relay that responds to these variables should trip or not.

Usually, additional selection criteria must be introduced in order to be able to decide about the regulation- compliant tripping operation. Particularly important for these additional variables are: • Time; • Energy or current direction

The work involved in the requirement for selectivity mainly depends on the structure of the network to be protected, and is usually greater the more complicated it

is structured. Harmonics are generated by equipment with non-linear current-voltage characteristics such as transformers, gas-discharge lamps, and power electronic devices. It is impaired by faults in the power supply on the one hand and system perturbations caused by the connected appliances, plants, and equipment on the other hand. EN 50160 describes the following main characteristics of the supply voltage.

Important harmonic generators are: • Power electronic devices such as converter drives, static UPS systems, rectifier systems, dimmers; • Fluorescent lamps; • Power supply units for the DC voltage supply of information and communication technology components; • Motors with non-linear current-voltage characteristics; • Converters in DC chargers; • Converters in photovoltaic systems and wind power stations. Harmonics cause, for instance: • Heating of three-phase and alternating current motors; • Fault tripping of circuit-breakers and miniature circuit- breakers and malfunctions of ripple control receivers; • Overloading and destruction of capacitors as a result of thermal overloading; • Overheating of transformers; • Skin effects of cabling resulting in higher temperature loads and a greater voltage drop; • Malfunction of electronic devices and control units as a result of zero-crossing faults; • Problems with the compensation of earth faults.

3. CONCLUSIONS

Power generating plants can have a negative effect on the power system and power quality. The basic challenge in planning is to find the optimum of investment and operating costs on the one hand and a risk estimation (frequency and effects of failures) on the other hand Supply quality = voltage quality + availability + service quality.

REFERENCES

[1]. **Leca A., s.a.** *Managementul energiei,* Editura Agir, Bucuresti 2007.

[2]. **Marcu M.D., Pana, L., Popescu F.G., Slusariuc R.**, *Evaluation the losses power and electrical energy on the basis of the relative load curves, by reference to the basic sizes*. SGEM2014/Conference Proceedings, Vol. Energy and clean technologies, ISBN 978-619-7105-15-5, ISSN 1314-2704, 229 - 236 pp, 17-26 June, Albena, Bulgaria, 2014.

[3]. **Marcu M. D., Popescu F., Samoila L. B.,** *Modeling and Simuling Power Active Filter Using Method of Generalized Reactive Power Theory*, Proceedings of IEEE International Conference on Computer Science and Automation Engineering, vol. 2, 10-12 June, 2011, Shanghai, China, pg. 213-218, ISBN 978-1-4244-8725-7.

[4]. **Stochitoiu M.D.** *The ret development due to energetic mix in the electrical energy production,* Annals of electrical engineering, University.of Petrosani 2015.

[5]. **Stochitoiu M.D., Gruber Cristian** *The distributed supply and the impact above the electrical webs,* Annals of electrical engineering, University.of Petrosani 2013.

[6]. *** www.ec.europa.eu

[7]. *** www.fenercom.com

[8]. *** www.nrcan.gc.ca

BIAXIAL ORIENTATION OF THE PV PANEL FOR HIGHER ENERGY CONVERSION

MARIUS DANIEL MARCU[1], TITU NICULESCU[2], FLORIN-GABRIEL POPESCU[3], RAZVAN SLUSARIUC[4]

Abstract: Due to increasingly human needs of energy, new technologies and energy sources must be used to supply the demand of clean energy in the context of environmental issues. Renewable energy sources like solar energy has one of the most potential and it is studied here. Periods of morning and evening when the sun's rays make an small angle with the solar panel generates a smaller amount of energy. Using 2 actuators for both axes of motion for photovoltaic panel can follow the position of the sun from sunrise to sunset.

Keywords: solar, photovoltaic, energy, conversion, orientation.

1. SOLAR RADIATION DURING CLEAR SKY

Photovoltaic performance meaning electricity generation depends to a large extent of the incident solar radiation on photovoltaic module positioned with different orientations, but most data received from weather stations are based on the horizontal surface. Thus, forecasting solar radiation on inclined surfaces is crucial because as usual photovoltaic panels are inclined to receive maximum sunlight yield as possible.

Direct radiation, diffuse irradiance and reflected irradiance are the components of global radiation on inclined surfaces.

$$R_{Tt} = R_{bt} + R_{dt} + R_{rt} \tag{1}$$

[1] *PhD., Associate Professor, Eng., University of Petrosani*
[2] *PhD., Associate Professor, Eng,. University of Petrosani*
[3] *PhD., Lecturer, Eng., University of Petrosani*
[4] *PhD., Assistant Eng., University of Petrosani*

where R_{Tt} is equivalent radiation, R_{bt} is the direct beam, R_{dt} is the diffuse irradiance R_{rt} is the reflected irradiance.

Direct Solar Irradiance (R_{bt})

Direct solar radiation on inclined plane is mathematically represented as follows:

$$R_{bt} = R_b \cdot \cos\theta_{AOI} \tag{2}$$

Where R_b is the direct radiation on the horizontal surface and θ is the angle of incidence between the normal to the surface and the incoming solar direct beam [1],[3].

Diffuse solar irradiance (R_{dt})

The model of the diffuse irradiance that arrives at a site on inclined solar systems with equal intensity from all direction as sky is considered as isotropic is expressed as:

$$R_{dt} = CR_b \cdot \left[\frac{1+\cos\beta}{2}\right] \tag{3}$$

Where the C is the sky diffuse factor:

$$C = 0.095 + 0.04 \cdot \sin\left[360 \cdot \frac{(N-100)}{365}\right] \tag{4}$$

Reflected Solar Irradiance (R_{rt})

The reflected solar radiation is given by:

$$R_{rt} = \rho \cdot R_b \cdot (\sin\gamma_s + C) \cdot \left[\frac{1-\cos\beta}{2}\right] \tag{5}$$

Where ρ is the reflectance.

The intensity of this radiation depends largely on the reflectivity of the surface at that location.

The equivalent equation of solar radiation incident on a tilted photovoltaic solar panel was rewritten using previous equations:

$$R_{Tt} = E_{\exp}\left(-\frac{k}{\sin\gamma_s}\right) \cdot$$
$$\cdot\left[\cos\gamma_s \cdot \cos(\alpha_s - \phi_{Az}) \cdot \sin\beta + C\left(\frac{1+\cos\beta}{2}\right) + \rho(\sin\gamma_s + C) \cdot \left(\frac{1-\cos\beta}{2}\right)\right] \tag{6}$$

2. ORIENTATION OF THE SOLAR PANEL TOWARDS THE SUN

Biaxial orientation of the photovoltaic panel is required to meet the goal of a performance increase of solar energy conversion into electricity. The orientation of the PV generator so that the incidence of solar radiation beam is perpendicular to the photovoltaic panel obviously will lead to a power generation at full capacity for a longer period of time than if it would have a fixed position [3].

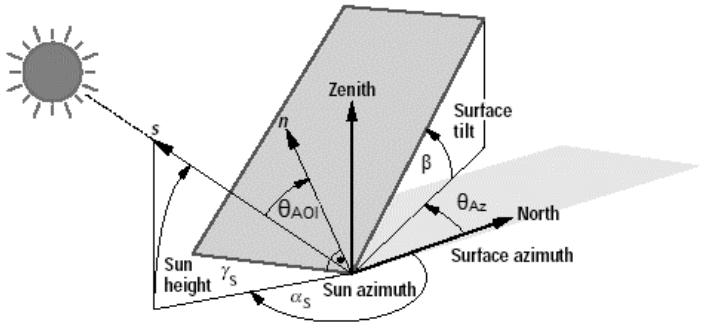

Fig. 1. Sun angles relative to the photovoltaic system

ω - hour angle is the angular displacement of local meridian from east to west due to Earth's rotation on its axis by 15 degrees per hour;

δ – declination angle is the angle between Earth-Sun line and plane along the equatorial circle;

γ_s – solar height is the angle formed by the Earth-Sun line and the horizontal plane of that location;

θ_{AOI} – the angle of incidence is the angle of sunlight beam that comes from the sun and the normal to the surface;

β – inclination of the photovoltaic panel;

ρ - is the reflection coefficient;

n – normal to the photovoltaic panel plan.

Periods of morning and evening when the sun's rays make an small angle with the solar panel generates a smaller amount of energy.

Using 2 actuators for both axes of motion photovoltaic panel can follow the position of the sun from sunrise to sunset. Declination photovoltaic panel is associated with solar altitude, which will change its position every 5 days.

Tracking the sun during a day it is performed by the second actuator that changes the angle of once every 5 minutes.

Simplifying and knowing that the sun moves at an hourly speed of 15 ° / h, the pitch diurnal angle, conducted by the equatorial orientation system, achieves on average a 1° angle of incidence that lasts approx. 1 h / 15° = 60 min / 15° = 4 min /° C.

This period has however momentary different values, depending on the slope of variation of declination during the year, β declination is approximately constant throughout the day, leading to a seasonal variation of the β angle.

The orientation of the photovoltaic panel during the measurements was made to south where the photovoltaic panel had fixed orientation with β with values of 30, 35 and 45 degrees [4].

In the case of biaxial orientation of the solar panel two actuators - one for changing the β angle and one for the surface modification of the panel with respect to the azimuth of the sun - they were operated every 5 minutes corresponding to the position of the sun in order to achieve an perpendicular incidence to the beam coming from the solar disc [5].

3. MEASUREMENTS UPON THE SELECTED OPTIONS

Measurements were carried out for four cases respectively 30, 35, 45 degrees and optimal orientation.

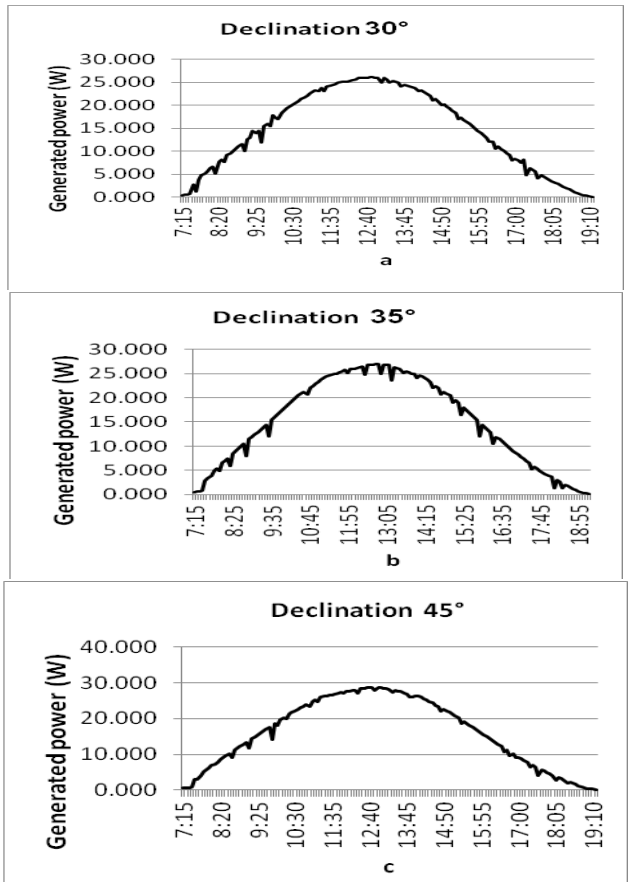

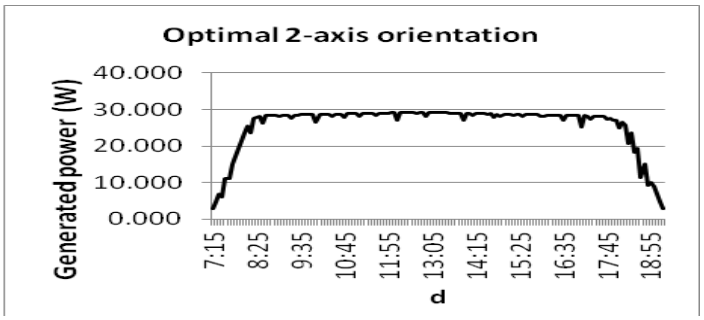

Fig. 2. Generated power for different setups of the photovoltaic system

For the first measurement the photovoltaic panel was positioned at an β inclination of 30 degrees, and it can be seen that the peak daytime appears at about 12:35 and the recorded value of the generated power is around 26W.

Throughout the day, for an inclination of 35 degrees, the conversion efficiency increases by approximately 4% compared to the declination 30 degrees and the maximum instantaneous power approaching 28W.

The gradual increase in the first hour after sunrise or decreasing at the end of the day due to the distance it traverses the light beam from entering the atmosphere to solar cell. Conversion efficiency in this case related to the declination of 45 is higher by 61%.

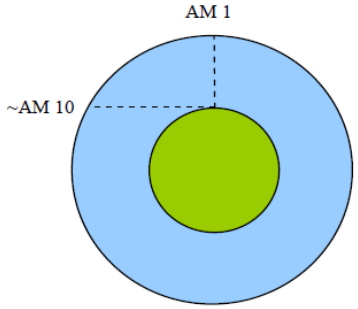

Fig. 3. Schematic illustration of the air mass, representing the relative distance that light travels through the atmosphere

AM = 1 corresponds to the incident radiation and the radiation coming from the horizon can increase the value to more than 10. This factor has the effect of "tempering" of solar radiation in the first and last 1-2 hours of the day thus reducing power generated by photovoltaic panel it is directly proportional to the amount of air mass.

Values of power generated by photovoltaic panel were filtered so as to obtain the arithmetic and they can be used in a comparative chart for a visual assessment to make clear to them.

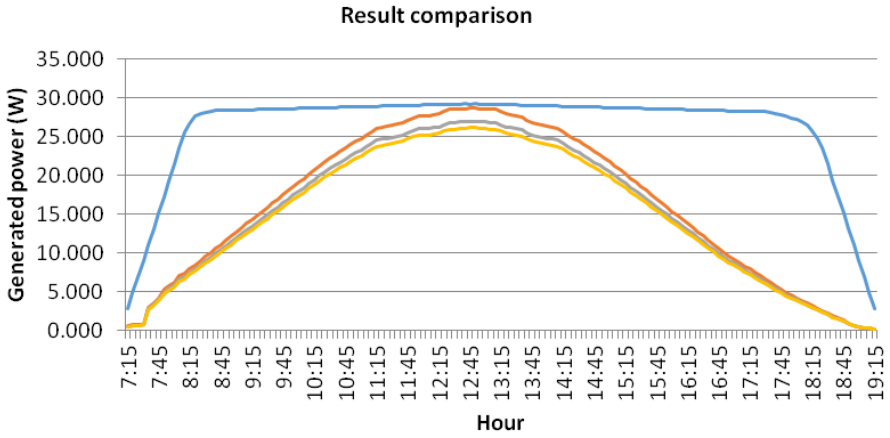

Fig. 4. The values recorded at different inclinations of solar panel during the day

4. CONCLUSIONS

In this paper were studied several positioning systems, that were set at 30, 35, 45 degrees and the biaxial system and from this research resulted that generated electricity with the fixed system at 45 degrees facing south is higher by 9% relative to the amount of energy produced by fixed system at 30 degrees; the amount of electricity produced by the system fixed at 35 degrees southern orientation is higher by 4% relative to the amount of energy produced by the fixed system at 30 degrees and the biaxial orientation system generated 61% more energy than the first setup.

REFERENCES

[1]. **Luis, C., Sivestre, S.,** *Modelling photovoltaic systems using PSpice*, Chichester, John Wiley & Sons Ltd., 2002.

[2]. **Marcu, M., Popescu, F., Pană, L., Slusariuc, I.R.,** *Modeling and simulation of solar radiation*, 3rd International Conference on Nanotechnology, Technology and Advanced Materials ICNTAM, 2014.

[3]. **Naing, L.P.,** *Estimation of solar power generating capacity*, IEEE 11th International Conference on Probabilistic Methods Applied to Power Systems, pp. 95–100, 2010.

[4]. **Rekioua, D., Matagne, E.,** *Optimization of Photovoltaic Power Systems*, Hardcover , XII, pp. 283, 2012.

[5]. **Samoila, B. L., Marcu, M. D., Popescu, F. G.** *Equipment Designed to Control a Heating Hybrid System with Solid Fuel Boiler and Solar Panels*, Proceedings of the 1st International Conference on Environmental Informatics (ENINF '13) Kuala Lumpur, Malaysia April 2-4, 2013, pp. 106-111.

[6]. **Stoicuta O., Pana T.**, *Asymptotic stability study of induction motor sensorless vector control systems with MRAS observer*, In proceedings of the International Conference on Automation, Quality and Testing, Robotics AQTR 2016, Cluj – Napoca; Romania; pp. 1-6, 2016.

Annals of the University of Petrosani, Electrical Engineering, 18 (2016)

THE UTILIZATION OF THE S-FUNCTION BLOCK IN SIMULATION OF THE LUENBERGER ROTOR FLUX OBSERVER FOR INDUCTION MOTORS

OLIMPIU STOICUTA[1]

Abstract: In this paper is presented the procedure of using Matlab-Simulink's S-Function blocks for simulating the Luenberger observer, which has the role of estimating the rotor flux of an induction machine with squirrel-cage rotor. In order to analyze the dynamic performance of the Luenberger estimator, both the effects of electric parameters variations and the effects of noise measurements are highlighted.

Keywords: induction motors, mathematical models, simulation, Luenberger observer.

1. INTRODUCTION

The dynamic performances of the direct vector control schemes with orientation after the rotor flux depend on the quality of rotor flux estimation.

The main rotor flux observers can be classified in three categories [6]:

- *observers derived from the induction machine's equations*, in which *dq* components of the rotor flux are obtained from the differential equation system which defines the mathematical model of the induction machine;
- *linear state observers*, built on the general theory of state observers used in linear systems;
- *optimal observers* (Kalman filters), which rely on the principle of minimizing a certain objective function, in order to estimate optimally the system's state vector.

In the class of linear state observers, both full order observers (in which all components of the induction machine state vector are estimated), and reduced order observers (in which just a part of the state vector components are estimated) are included.

[1] *Associate Professor, Eng., PhD, University of Petrosani, Romania*

The most widely known observers grounded on the general theory of linear state estimators are [6]:

- Luenberger observer (full order observer);
- Gopinath observer (reduced order observer).

The purpose of this article is to present the numerical simulation of the Luenberger estimator using S-function blocks in the Matlab simulation environment. The simulation will show the dynamic performances of the Luenberger observer in various operating modes of the induction machine.

The parallel mathematical model was used for the induction machine during the simulation [6].

The state vector of this model comprises the *dq* components of the: stator currents, rotor flux and air-gap flux.

The parallel model of the induction machine uses an equivalent resistance placed in parallel with the mutual inductance for modeling the iron losses, hysteresis and eddy current losses [2].

2. LUENBERGER OBSERVER

The Luenberger observer, whose simulation is presented in this article, is based on the stator currents-rotor fluxes mathematical model of the induction machine. The block diagram of the system made of static frequency converter (CSF)-induction machine-Luenberger observer is presented in the following figure:

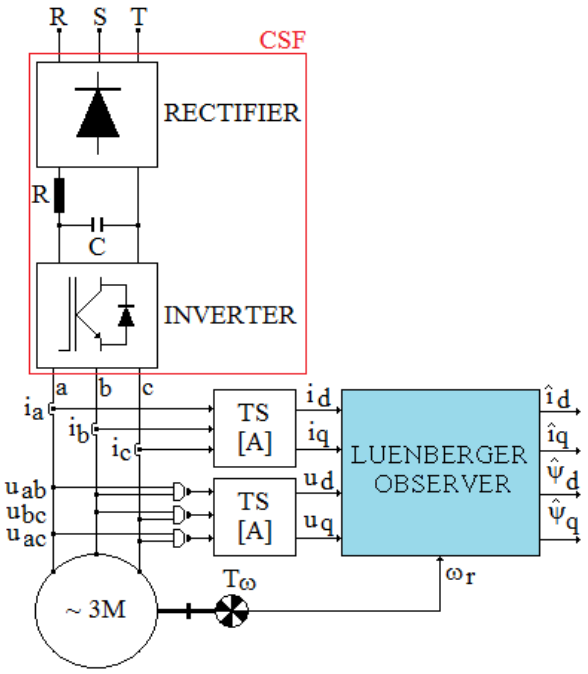

Fig. 1. The block diagram of the assembly CSF-induction machine-Luenberger observer

The equation which defines the Luenberger observer is [3]

$$\frac{d\hat{x}}{dt} = A \cdot \hat{x} + B \cdot u + L \cdot \left(y - C \cdot \hat{x} \right) \tag{1}$$

where $\hat{x} = \begin{bmatrix} \hat{i}_{ds} & \hat{i}_{qs} & \hat{\psi}_{dr} & \hat{\psi}_{qr} \end{bmatrix}^T$; $u = \begin{bmatrix} u_{ds} & u_{qs} \end{bmatrix}^T$; $y = \begin{bmatrix} i_{ds} & i_{qs} \end{bmatrix}^T$;

$$A = \begin{bmatrix} a_{11} & 0 & a_{13} & a_{14} \cdot z_p \cdot \omega_r \\ 0 & a_{11} & -a_{14} \cdot z_p \cdot \omega_r & a_{13} \\ a_{31} & 0 & a_{33} & -z_p \cdot \omega_r \\ 0 & a_{31} & z_p \cdot \omega_r & a_{33} \end{bmatrix}; B = \begin{bmatrix} b_{11} & 0 \\ 0 & b_{11} \\ 0 & 0 \\ 0 & 0 \end{bmatrix}; C = \begin{bmatrix} 1 & 0 & 0 & 0 \\ 0 & 1 & 0 & 0 \end{bmatrix};$$

$$a_{11} = -\left(\frac{1}{T_s \cdot \sigma} + \frac{1-\sigma}{T_r \cdot \sigma} \right);\ a_{13} = \frac{L_m}{L_s \cdot L_r \cdot T_r \cdot \sigma};\ a_{14} = \frac{L_m}{L_s \cdot L_r \cdot \sigma};\ a_{31} = \frac{L_m}{T_r};\ a_{33} = -\frac{1}{T_r};$$

$$b_{11} = \frac{1}{L_s \cdot \sigma}; T_s = \frac{L_s}{R_s}; T_r = \frac{L_r}{R_r}; \sigma = 1 - \frac{L_m^2}{L_s \cdot L_r}.$$

The Luenberger matrix from equation (1), is given by the following expression:

$$L = \begin{bmatrix} la_{11} & -la_{12} \\ la_{12} & la_{11} \\ la_{21} & -la_{22} \\ la_{22} & la_{21} \end{bmatrix} \tag{2}$$

The elements of Luenberger matrix, are obtained through H. Kubota's method, which ensures a certain proportionality between the eigenvalues of the estimator and the eigenvalues of the induction machine.

The elements of Luenberger matrix, given by H. Kubota's method are [3]:

$$\begin{cases} la_{11} = (1-k) \cdot (a_{11} + a_{33}) \\ la_{12} = z_p \cdot \omega_r \cdot (1-k) \\ la_{22} = -\gamma \cdot la_{12} \\ la_{21} = (a_{31} + \gamma \cdot a_{11}) \cdot (1-k^2) - \gamma \cdot la_{11} \end{cases} \tag{3}$$

where $\gamma = 1 / a_{14}$, and k is the proportionality factor between the eigenvalues of the estimator and the eigenvalues of the induction machine.

3. SIMULATION OF THE LUENBERGER OBSERVER

Both the Luenberger observer and the mathematical model of the induction motor are simulated in Matlab-Simulink, using S-function blocks. The Matlab code attached to the S-Function block of the induction machine, is based on the equations which defines the parallel model, stator currents-rotor fluxes-air gap fluxes. The mathematical model of the induction machine, take the iron losses into account.

During the simulation the effects introduced by the static frequency converter are also highlighted. All 6 transistors from the static frequency converter structure are supposed to have an ideal switching. The CSF is designed with a DC intermediary stage. Within the PWM modulator, the carrier is of isosceles triangle type having a frequency f_c [kHz]. The modulation technique is based on a modified suboscillation method [4]. This way, over the stator's reference voltages is injected the 3rd degree harmonic of the phase voltage, having amplitude of 1/6 of the fundamental reference voltage.

The Luenberger observer is tested in open loop, so the estimated values of the stator currents and rotor fluxes are not used to control the induction machine.
In order to get a detailed analysis of the observer dynamic performances, the following tests are realized during the simulation:

- *C1*: testing the dynamic performance of the observer when the electric parameters of the induction motor are the same with the electric parameters used in the implementation of the Luenberger estimator. During this test the measured values of the stator voltages, stator currents and rotor speed are not influenced by noises.
- *C2*: testing the dynamic performance of the observer when the rotor resistance is with 30% higher than the nominal value. The test is done under no noise influence.
- *C3*: testing the dynamic performance of the observer when the stator resistance is with 30% higher than the nominal value. The test is done under no noise influence.
- *C4*: testing the dynamic performance of the observer when the iron losses resistance is with 30% higher than the nominal value. The measurement noise is neglected during this test.
- *C5*: testing the dynamic performance of the observer in the same conditions which exists in the *C1* test, but the noise which affects the measurement process of the stator current and voltages, is taken into account. To generate measurement noise, were used random number generators with normal distribution.

The speed of the induction machine is controlled during this simulation using a scalar control system which employs open loop U/f=ct. control method. The system made of CSF-induction motor-Luenberger observer is simulated for a full load start, when the load has a resistive torque equal with the nominal torque of the induction machine.

Each simulation is done for two frequencies of the stator voltage (f_e^*=20 Hz and f_e^*=50 Hz). The differential equation system on which is based the system CSF - induction motor - Luenberger observer was solved using Dormand – Prince (ode45) numerical method, with a relative and absolute error of $\varepsilon = 10^{-7}$. The Matlab program which simulates the system is presented in Fig.2. The program uses S-Function blocks.

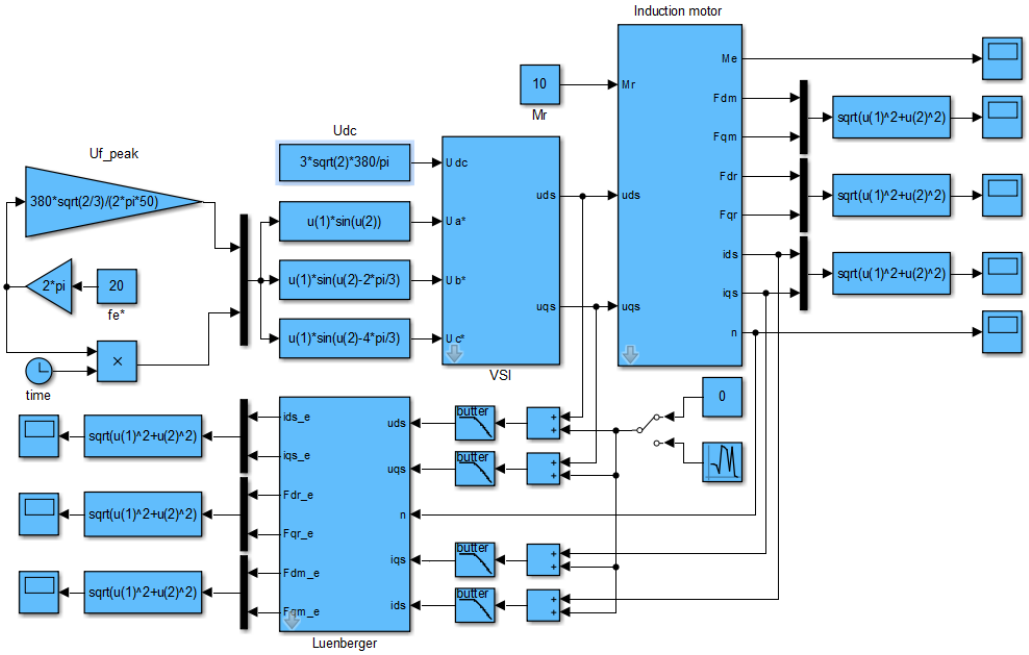

Fig. 2. The simulation program of the CSF-induction motor-Luenberger observer system

The internal structure of the Luenberger block is shown in Fig.3.

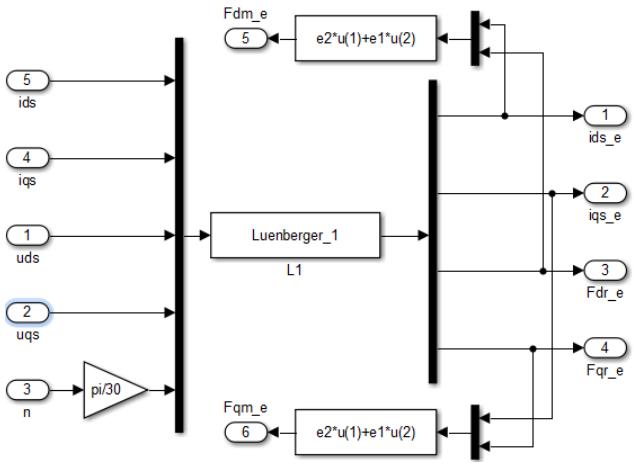

Fig. 3. Luenberger Observer internal structure

The S-Function block which implements the Luenberger estimator is denoted "L1" in Fig.3. The following figure shows the Matlab code associated with this block.

```
function[sys,x0]=Luenberger_1(t,x,u,flag,Rs,Rr,Ls,Lr,Lm,J,F,zp)
k=1.2;
s=1-(Lm^2/(Ls*Lr));
Ts=Ls/Rs;
Tr=Lr/Rr;
a11=-((1/(Ts*s))+((1-s)/(Tr*s)));
a13=Lm/(Ls*Lr*Tr*s);
a14=Lm/(Ls*Lr*s);
a31=Lm/Tr;
a33=-(1/Tr);
b11=1/(s*Ls);
ga=1/a14;
if abs(flag)==1
la11=(1-k)*(a11+a33);
la12=zp*u(5)*(1-k);
la22=-ga*la12;
la21=(a31+ga*a11)*(1-k^2)-ga*la11;
La=[la11 -la12;
    la12  la11;
    la21 -la22;
    la22  la21];
Aa=[a11  0    a13           a14*zp*u(5);
    0    a11  -a14*zp*u(5)  a13;
    a31  0    a33           -zp*u(5);
    0    a31  zp*u(5)       a33];
Ba=[b11  0;
    0    b11;
    0    0;
    0    0];
Xa=[x(1);x(2);x(3);x(4)];
Ua=[u(3);u(4)];
Ma=[u(1)-x(1);
    u(2)-x(2)];
sys=Aa*Xa+Ba*Ua+La*Ma;
elseif flag==3
   sys=x;
elseif flag==0
   sys=[4 0 4 5 0 0];
    x0=[0;0;0;0];
else
   sys=[];
end
```

Fig.4. "L1" block code.

The air gap fluxes *dq* components are estimated using the following equations

$$\begin{cases} \hat{\psi}_{dm} \cong e_2 \cdot \hat{i}_{ds} + e_1 \cdot \hat{\psi}_{dr} \\ \hat{\psi}_{qm} \cong e_2 \cdot \hat{i}_{qs} + e_1 \cdot \hat{\psi}_{qr} \end{cases} \tag{4}$$

where $e_1 = \dfrac{L_m}{L_r}$; $e_2 = \dfrac{L_m \cdot L_{\sigma r}}{L_r}$.

Relations (4) are at the heart of the program shown in Fig.3; they are derived from the flux equations of the induction motor (IM) mathematical model, model which not takes into account the iron losses [6]. In these equations the *dq* components are given by:

$$\begin{cases} i_{dm} \cong i_{ds} + i_{dr} \\ i_{qm} \cong i_{qs} + i_{qr} \end{cases} \tag{5}$$

The internal structure of the simulation block which implements the static frequency converter with intermediary DC voltage circuit is given in Fig.5.

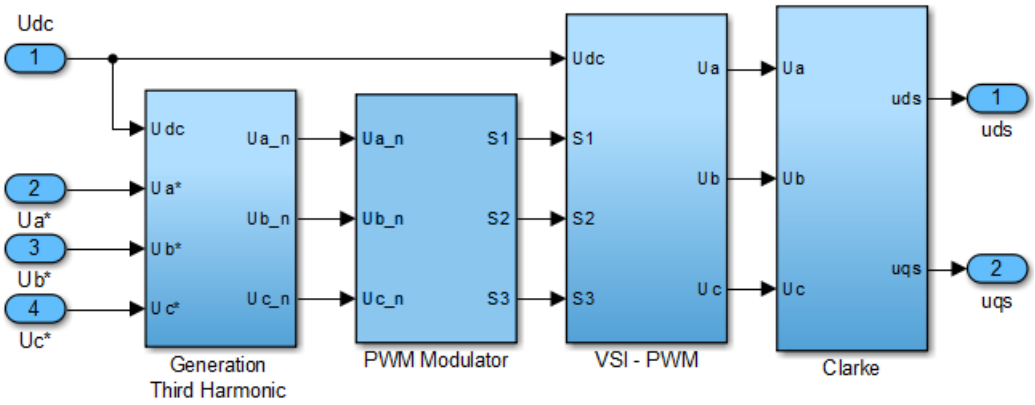

Fig. 5. The Matlab-Simulink of the static frequency converter (CSF)

The equations which define CSF, are:

$$\begin{cases} u_{an} \cong A_a \cdot \left(u_a^* + k_n \cdot \sin\left(3 \cdot \omega_e \cdot t\right) \right) \\ u_{bn} \cong A_a \cdot \left(u_b^* + k_n \cdot \sin\left(3 \cdot \omega_e \cdot t\right) \right) \\ u_{cn} \cong A_a \cdot \left(u_c^* + k_n \cdot \sin\left(3 \cdot \omega_e \cdot t\right) \right) \end{cases} \tag{6}$$

where $A_a = \dfrac{1}{U_{dc}}$; $k_n = \dfrac{|\underline{u}_s|}{6}$; $\sin\left(3 \cdot \omega_e \cdot t\right) = 3 \cdot \sin\left(\omega_e \cdot t\right) - 4 \cdot \left[\sin\left(\omega_e \cdot t\right)\right]^3$;

$\sin\left(\omega_e \cdot t\right) = \dfrac{u_a^*}{|\underline{u}_s|}$; $|\underline{u}_s| = \sqrt{u_{ds}^2 + u_{qs}^2}$; $\omega_e = 2 \cdot \pi \cdot f_e$.

The internal structure of the block which generates the modulating voltages ("Generation Third Harmonic"), is shown in Fig.6.

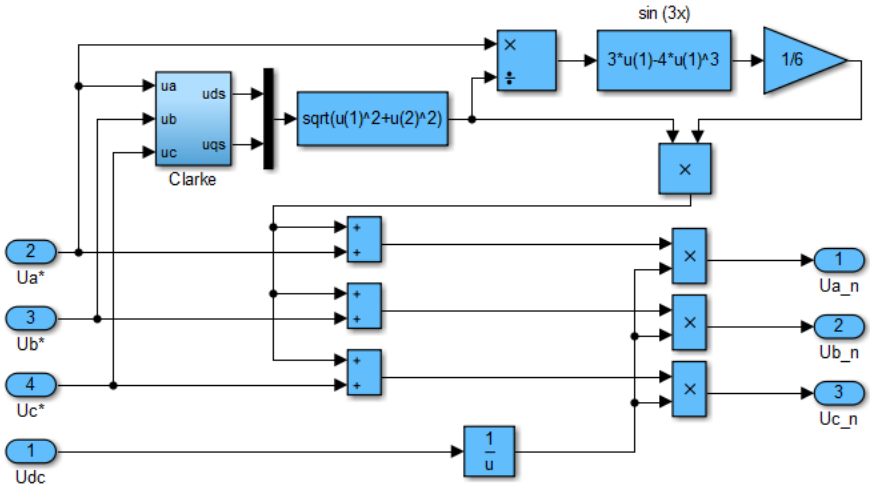

Fig. 6. Internal structure of the block "Generation Third Harmonic".

The signals used to control the transistors in the inverter are generated by comparing the normalized modulating voltages-which contain the third order harmonic- with a triangle signal voltage denoted u_t (see Fig.7). The frequency of the triangle signal is f_c = 5 [kHz].

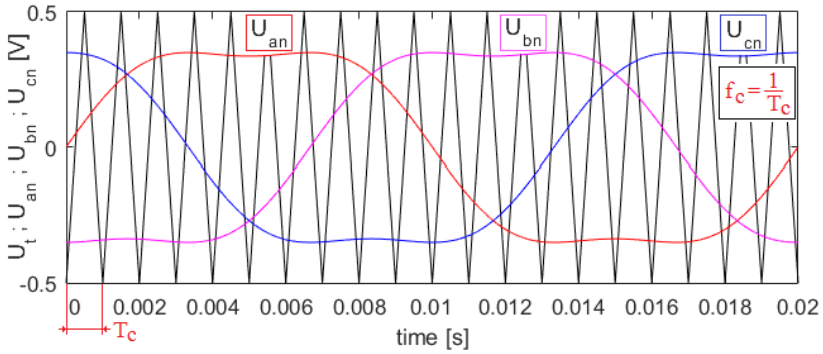

Fig. 7. Time variation of the triangle waveform with a frequency of 1 [kHz]

The control signals are obtained as follows:

- if $u_{an} \geq u_t$ then $S_1 = 1$; the high transistor of phase *a* is open (in conduction);
- if $u_{an} < u_t$ then $S_1 = 0$; the low transistor of phase *a* is open;
- if $u_{bn} \geq u_t$ then $S_2 = 1$; the high transistor of phase b is open;
- if $u_{bn} < u_t$ then $S_2 = 0$; the low transistor of phase *b* is open;
- if $u_{cn} \geq u_t$ then $S_3 = 1$; the high transistor of phase *c* is open;
- if $u_{cn} < u_t$ then $S_3 = 0$; the low transistor of phase *c* is open;

The block "PWM Modulator", used to generate the control pulses according to the logic presented is given in Fig. 8.

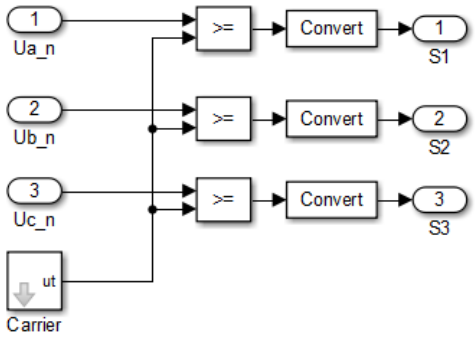

Fig. 8. Internal structure of block "PWM Modulator"

The triangular signal u_t is generated using 3 Simulink blocks (see Fig.9).

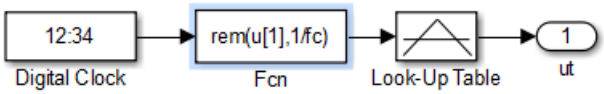

Fig. 9. "Carrier" block internal structure

The sample time property of the block „Digital Clock", is $T_s = 10^{-6}\,[s]$. The components of the input and output vectors contained in the "Look-up table" are:

- input vector:

$$u = \begin{bmatrix} 0 & \dfrac{1}{2 \cdot f_c} & \dfrac{1}{f_c} \end{bmatrix} \tag{7}$$

- output vector:

$$y = \begin{bmatrix} -\dfrac{1}{2} & \dfrac{1}{2} & -\dfrac{1}{2} \end{bmatrix} \tag{8}$$

The phase voltages outputted by the inverter are given by the following equations, assuming that all transistor are ideal.

$$\begin{cases} u_a = \dfrac{U_{dc}}{3} \cdot (2 \cdot S_1 - S_2 - S_3) \\ u_b = \dfrac{U_{dc}}{3} \cdot (2 \cdot S_2 - S_1 - S_3) \\ u_c = \dfrac{U_{dc}}{3} \cdot (2 \cdot S_3 - S_1 - S_2) \end{cases} \tag{9}$$

The equations (9) were used to implement the block „VSI-PWM" which appear in Fig.5. The internal structure of „VSI-PWM" block is shown in Fig.10.

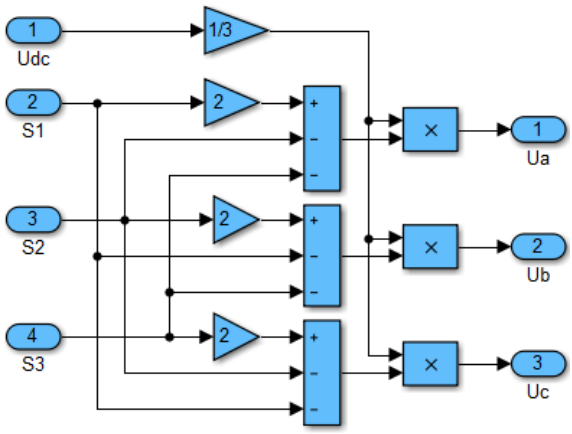

Fig. 10. Internal structure of "VSI-PWM" block

During the simulations, is assumed that the inverter is fed with a voltage (U_{dc}) equal with the average rectified voltage given by a three-phase diode rectifier (6 diodes). The U_{dc} voltage expression is given by

$$U_{dc} = \frac{3 \cdot \sqrt{2}}{\pi} \cdot U_{LL}^{RMS} \tag{10}$$

where U_{LL}^{RMS} is the root mean square value of the rectifier input line-to-line voltage.

The expressions which make the transformation from three-phase system to bi-phase system are:

$$[u_s]_{\perp} = A_c \cdot [u_s] \tag{11}$$

where $[u_s] = [u_a \quad u_b \quad u_c]^T$ and $[u_s]_{\perp} = [u_{ds} \quad u_{qs} \quad u_{s0}]^T$ are the transposed vectors of three-phase stator voltages, respectively biphasic voltages, and A_c matrix is given by:

$$A_c = \frac{2}{3} \cdot \begin{bmatrix} 1 & -\frac{1}{2} & -\frac{1}{2} \\ 0 & \frac{\sqrt{3}}{2} & -\frac{\sqrt{3}}{2} \\ \frac{1}{2} & \frac{1}{2} & \frac{1}{2} \end{bmatrix} \tag{12}$$

Relations (11) and (12) define the Clarke transform applied for stator voltages.
The open loop control law U/f=ct., used in this article is:

$$\left|\underline{u}_s\right| = \left|\underline{\Psi}_s\right| \cdot \omega_e \tag{13}$$

where $\omega_e = 2 \cdot \pi \cdot f_e$ is the angular frequency of the rotating magnetic stator field; $\left|\underline{\Psi}_s\right| = \sqrt{\psi_{ds}^2 + \psi_{qs}^2}$ is the modulus of the stator flux phasor.

The control law given by (13), is derived from the mathematical model stator fluxes-rotor fluxes [6], following the next steps:

- the equations of the induction motor model are written in a reference system which rotates synchronously with the stator current phasor, having an angular frequency of ω_e;
- the module of the stator voltages phasor is expressed as a function of the stator fluxes phasor module;
- in the expression obtained in the previous step the stator resistance and the slip angular frequency are neglected.

In the open loop scalar U/f=ct. control method, the nominal value of the stator flux phasor module is taken into account as follows:

$$\left|\underline{\Psi}_{sN}\right| = \frac{U_N \cdot \sqrt{\frac{2}{3}}}{\omega_N} \tag{14}$$

where $\omega_N = 2 \cdot \pi \cdot f_N$; $f_N = 50\left[Hz\right]$ is the nominal angular frequency of the stator voltages (induction machine supply voltages) , and U_N is the nominal voltage of the induction machine.

The stator voltages imposed by the scalar control law U/f=ct., are:

$$\begin{cases} u_a^* = \left|\underline{u}_s^*\right| \cdot \sin\left(\omega_e^* \cdot t\right) \\ u_b^* = \left|\underline{u}_s^*\right| \cdot \sin\left(\omega_e^* \cdot t - \dfrac{2 \cdot \pi}{3}\right) \\ u_c^* = \left|\underline{u}_s^*\right| \cdot \sin\left(\omega_e^* \cdot t - \dfrac{4 \cdot \pi}{3}\right) \end{cases} \tag{15}$$

where $\left|\underline{u}_s^*\right| = \left|\underline{\Psi}_{sN}\right| \cdot \omega_e^*$; $\omega_e^* = 2 \cdot \pi \cdot f_e^*$.

The electrical and mechanical parameters of the induction machine (IM) used to simulate the system CSF-IM-Luenberger observer, are given in the Table 1.

Table 1. **Induction Motor Parameters** [1]

	Name	**Value**		**Name**	**Value**
R_s	*Stator resistance*	4.85 [Ω]	F	*Friction coefficient*	0.008[N·m·s/rad]
R_r	*Rotor resistance*	3.805 [Ω]	P_N	*Rated power*	1.5 [kW]
R_f	*Iron loss resistance*	500 [Ω]	n_N	*Rated speed*	1420 [rpm]
L_s	*Stator inductance*	0.274 [H]	z_p	*Number of pole pairs*	2
L_r	*Rotor inductance*	0.274 [H]	f_N	*Rated frequency*	50 [Hz]
L_m	*Mutual inductance*	0.258 [H]	U_N	*Rated voltage*	220 Δ/380 Y [V]
J	*Motor inertia*	0.031[kg·m^2]	M_N	*Rated torque*	10 [N·m]

In simulations it is assumed that the rectifier input RMS voltage is equal with the nominal voltage of the induction machine $U_{LL}^{RMS} = U_N = 380[V]$.

Because the first frequency which appears in the stator voltages spectrum is the triangular waveform frequency, both the currents and the stator voltages will be filtered with two pole Butterworth filters, which have de cutoff frequency set 500 [Hz]. The cutoff frequency of the filters is correlated with the frequency of the triangular signal within the inverter, in order to have an optimal aliasing.

In order to demonstrate the dynamic performance of the Luenberger estimator in the presence of the noise which affects the process of measuring the stator voltages and currents, in simulation is used a single random number generator having a normal distribution.

The output of the random number generator is superimposed over the current and voltage inputs within the Luenberger estimator (see Fig. 2).

The sampling time and the dispersion value used to generate the measurement noise is: $T_s = 10^{-6}[s]$, respectively $D = 10$.

The simulated program from Fig.2, was compiled and ran on a numeric system operating Windows 10- 64b. The hardware structure of the system is built around an I7-4720HQ processor (2.6GHz), with 8 GB of available RAM.
The following figure shows the results of the simulation:

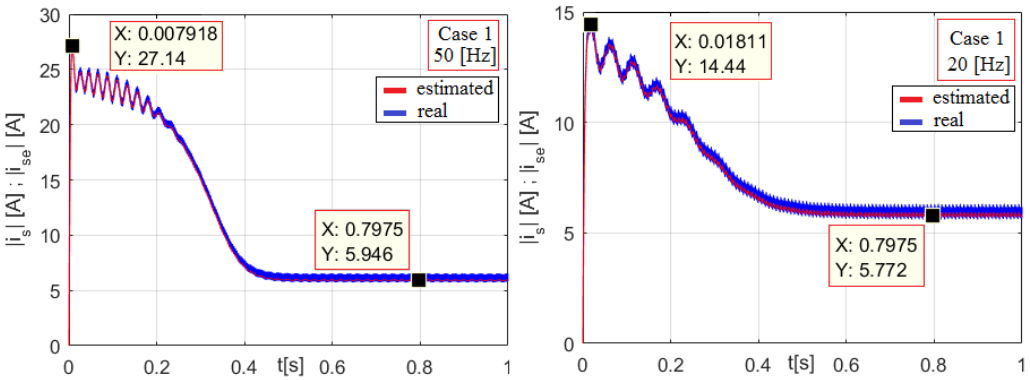

Fig. 11. The module of the estimated and actual stator current phasor – Case 1

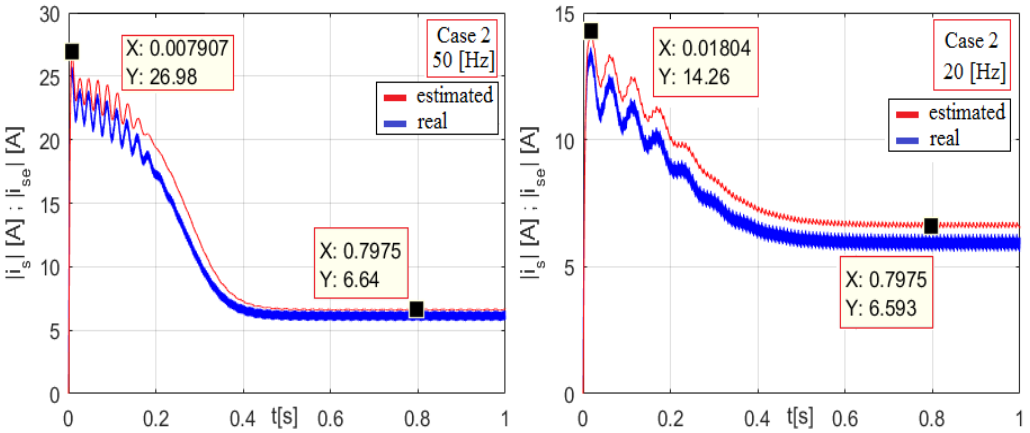

Fig. 12. The module of the estimated and actual stator current phasor – Case 2

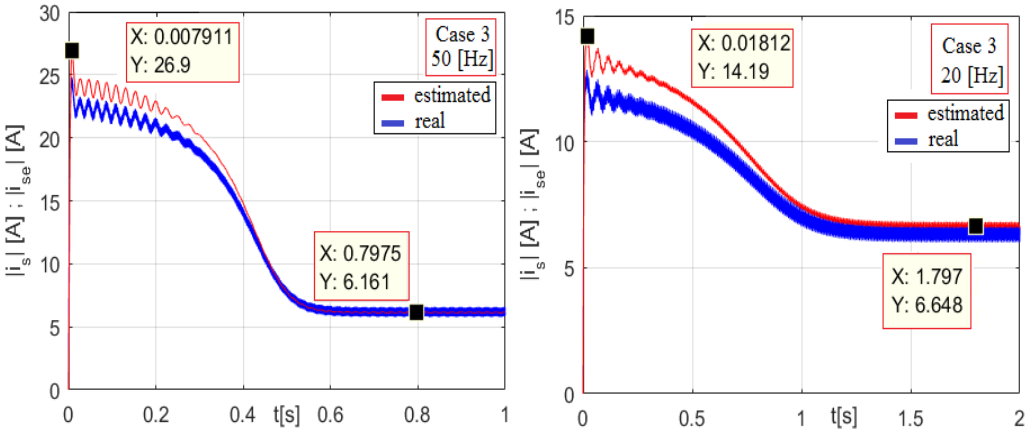

Fig. 13. The module of the estimated and actual stator current phasor – Case 3

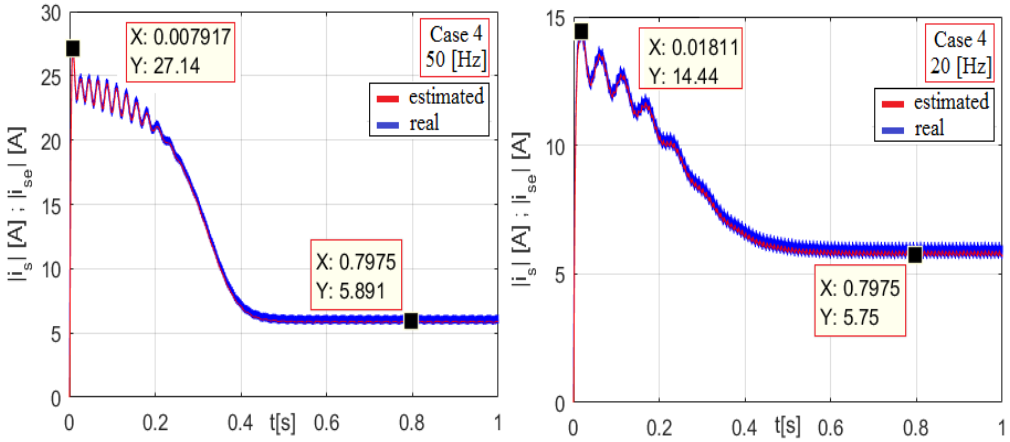

Fig. 14. The module of the estimated and actual stator current phasor – Case 4

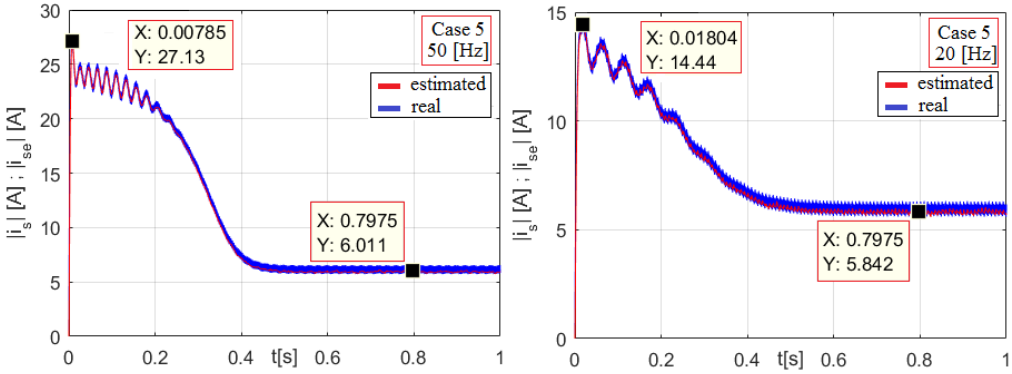

Fig. 15. The module of the estimated and actual stator current phasor – Case 5

From the presented plots, in all 5 cases the module of the stator current phasor is estimated accordingly. The most notable differences appear during the transient response, in cases 2 and 3. It can be observed that when the stator field has a frequency of 20 [Hz], in steady state there is a small error between the actual stator current and the estimated stator current (see Fig. 12).

In the following diagrams it is presented the variation with time of the rotor flux phasor module, in all 5 cases.

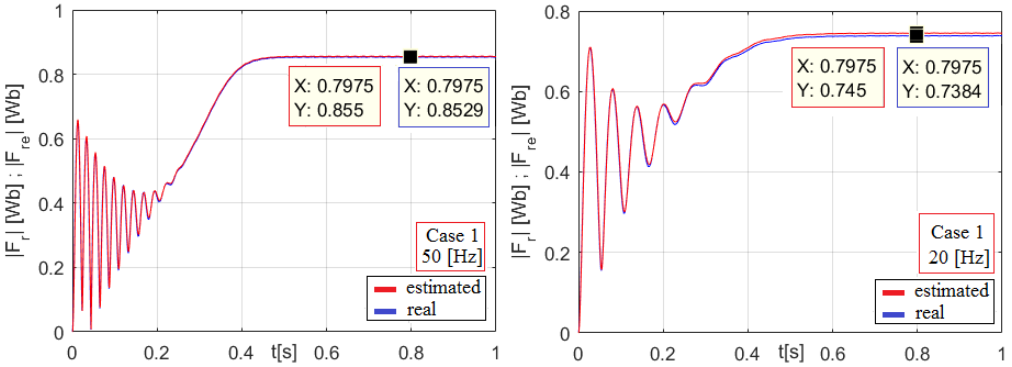

Fig. 16. The module of the estimated and actual rotor flux phasor – Case 1

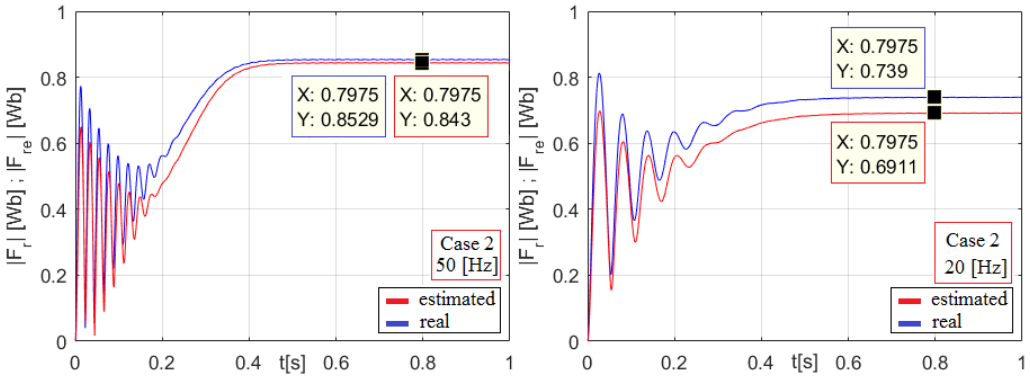

Fig. 17. The module of the estimated and actual rotor flux phasor – Case 2

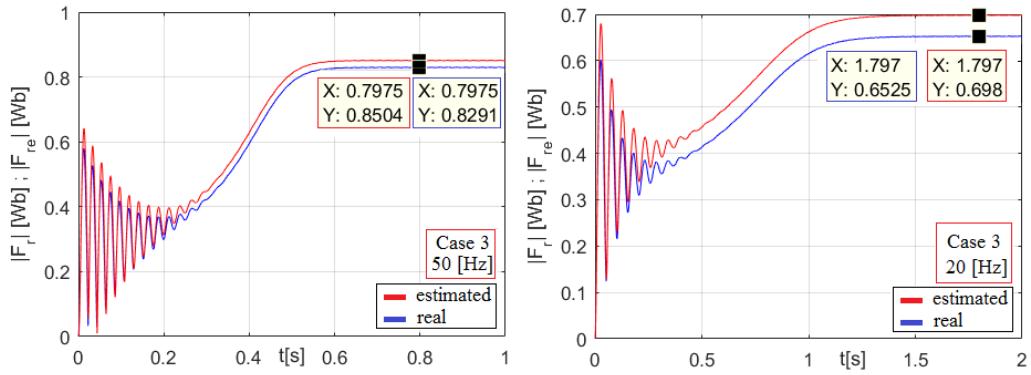

Fig. 18. The module of the estimated and actual rotor flux phasor – Case 3

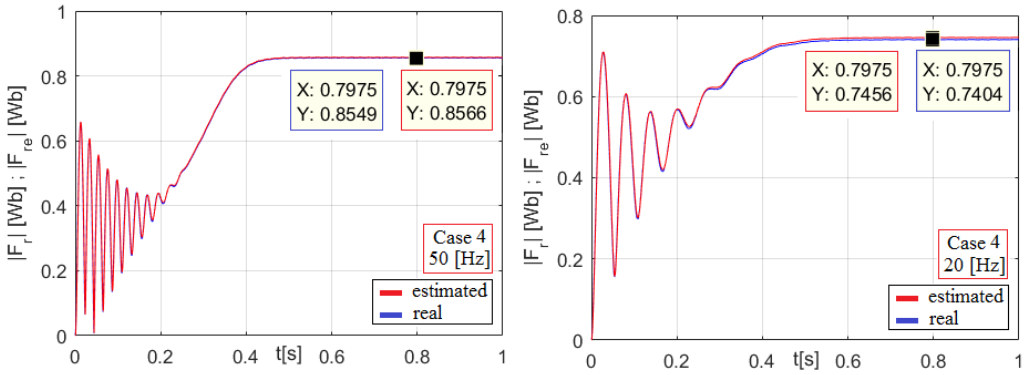

Fig. 19. The module of the estimated and actual rotor flux phasor – Case 4

It can be seen from Fig, 17 and Fig. 18 that there is a certain estimation error of the module of the rotor flux phasor, both in the transient state and in the steady state, error which is noticeably higher when the imposed stator field frequency is 20 [Hz]. In this case, when the frequency of the stator field is 20 [Hz] the highest absolute errors in steady state are $|\varepsilon| = 0.048\,[Wb]$, in case 2, respectively $|\varepsilon| = 0.045\,[Wb]$, in case 3.

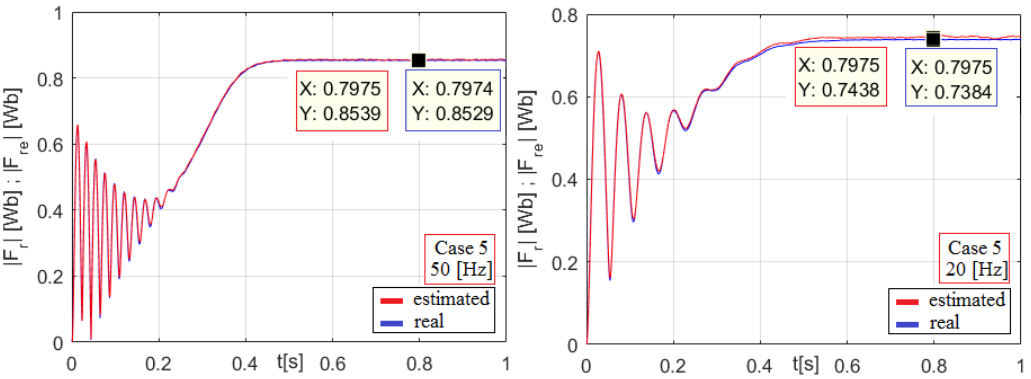

Fig. 20. The module of the estimated and actual rotor flux phasor – Case 5

After the simulation it can be seen that the Luenberger estimator is sensitive to the variations of the stator and rotor resistance. This sensitivity is increasing inversely with the frequency of the rotating stator field. On the other hand, the simulation revealed that Luenberger observer is remarkably robust to the variations of the iron loses resistance and to noises.

4. CONCLUSIONS

The main conclusion which arise from simulation results of the Luenberger observer using S-Function blocks is that the estimator has very good performances, both is transient state and in steady state.

The simulation programs used to test the Luenberger observer are presented in detail offering a useful support for experts within automations and electrical engineering.

REFERENCES

[1]. **Aissa K., Eddine K.D.,** *Vector control using Series Iron Loss Model of Induction Motors and Power Loss Minimization,* World Academy of Science, Engineering and Technology, vol.52, pp. 142-148, 2009.

[2]. **Boldea I., Nasar S.A.,** *Unified Treatment of Core Losses and Saturation in the Orthogonal-Axis Model of Electric Machines,* IEE Proceedings B, Electric Power Applications, vol.134, No. 6, pp.355-363, 1987.

[3]. **Kubota H., Matsuse K.,** *DSP-Based Speed Adaptive Flux Observer of Induction Motor*, IEEE Transactions on Industry Applications, vol. 29, No. 2, pp.344 - 348, 1993.

[4]. **Levi E.,** *Impact of Iron Loss on Behavior of Vector Controlled Induction Machines,* IEEE Transactions on Industry Applications, vol.31, pp.1287-1296, 1995.

[5]. **Pana, L., Popescu**, **F.G., Samoila L., Slusariuc R.**, A*nalysis of thermic stability in short circuit regime of electric distribution networks conductor*. 6th International Multidisciplinary Scientific Symposium, SIMPRO 2014, Conference Proceedings, ISSN 2344 – 4754, Pages: 331-334, 10-11 Octombrie, Petroşani, 2014.

[6]. **Pana T., Stoicuta O.,** *Stability of the Vector Drive Systems with Induction Motors,* Mediamira Publishers, 2016.

[7]. **Uţu, I., Samoilă, L.,** *Senzori şi instrumentaţie pentru sisteme electromecanice,* Editura Universitas, Petroşani, 2011, ISBN 978-973-741-208-9, pp. 222.

[8]. **Uţu, I.,** *Electric drive for winding machines operated by a digital signal processor,* Annals of University of Petrosani, Petrosani, 2014, ISSN 1454-8518, pag. 69 - 72.

Annals of the University of Petrosani, Electrical Engineering, 18 (2016)

VEHICLE COMMUNICATION SYSTEM USING SMARTPHONE

ALEXANDRA ELISABETA LÖRINCZ[1], MARIUS CUCĂILĂ[2], CHARLES ROSTAND MVONGO MVODO[3]

Abstract: With the development of technology, protocols have become more secure, very reliable and give a quick transfer data for vehicle manufacturers. Over the years, have been used several communication protocols, each automobile manufacturer developing or using one of the five communication protocols. OBD2 use the protocols of communication in the automotive industry to create a connection between car and driver. This connection is defined by the transmission of information from the car by the driver, using : Witnesses panel, communication via OBD2.

Keywords: Automotive, K-Line, CAN, ECU, USART, bluetooth.

1. INTRODUCTION

Nowadays, there can be considered that a vehicle has its own "life". It gives information about the problems that it encounters and warns if these minor faults or problems are highly hazardous to the driver of the vehicle and its passengers.

All this communication with the driver is done through the luminous indicators on the car dashboard which are also called WITNESSES PANEL. Some in-car systems can have faults, problems, errors or breaks, and this witnesses panel announces these things. The color of the witnesses panel reflects the seriousness of the problems appeared at the vehicle [1].

[1] *Ph.D. Student, University of Petrosani*
[2] *Ph.D. Student, University of Petrosani*
[3] *Ph.D. Student, University of Petrosani, Institute of Agricultural Research for Development, Yaounde, Cameroon*

All these codes sent by ECU (Electronic Control Unit) through an OBD2 (On Board Diagnostics), announce the detected problem in order to be solved. This OBD2 has 5 communication protocols to decrypt the messages received from the ECU [2].

These 5 protocols are used by various vehicle manufacturers. The most common protocol used today is the CAN (Control Area Network) protocol. The CAN protocol qualities are secure communication, high speed and a big distance.

1.1. Protocol SAE J1850 PWM (Pulse Width Modulation)

It is a protocol used by Ford. It has a transfer speed of up to 41.6 kb / sec through two wires (twisted), the 5V differential signals. The 0 logic signal range is between 0-2.2V and the logical 1 signal range is between 2.8-5V. The data frame has from 0 to 8 bytes as Figure 1.

The message sent consists of a maximum of 12 bytes that includes the CRC (Cyclic Redundancy Check) byte.

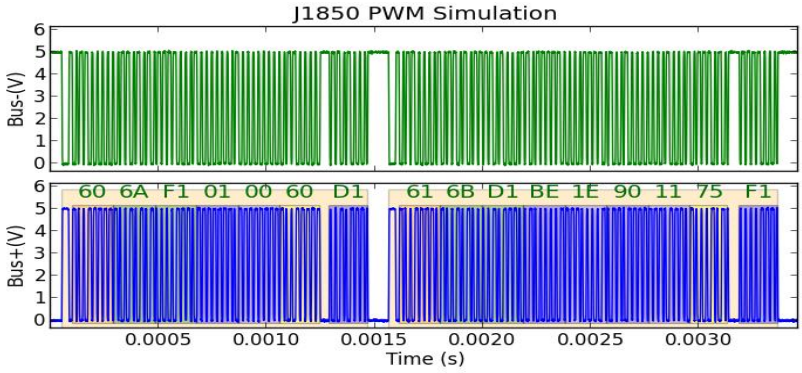

Fig. 1. SAE J1850 PWM protocol [6]

Advantages:

• speed of 41.6 kb/sec, higher than other protocols

Disadvantages:

• message length is 12 bytes, shorter than other protocols

• there are required two wires for communication (pin 2 and pin 10) - differential signals.

1.2. Protocol SAE J1850 VPW (Variable Pulse Width)

This is a protocol used by General Motors, Chrysler, Harley Davidson and Toyota. The transfer speed is up to 10.4 kb / sec. Data transmission is done on a single thread and the maximum voltage is of 20V. The 0 logic signal is in the range 0-3.5V and the logic signal 1 is in the range 20-4.5V. Data frame length is from 0 to 8 bytes as Figure 2.

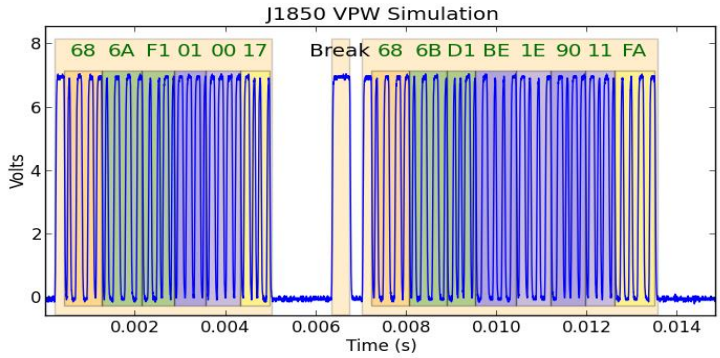

Fig. 2. SAE J1850 VPW protocol [4]

Advantages:

- communication on a single wire (pin 2)
- maximum voltage of 20V, ensuring high flexibility

Disadvantages:

- speed 10.4 kb / sec, lower than other protocols
- message length is 12 bytes that includes the CRC byte, shorter than other protocols

1.3. Protocol ISO 9141-2 (10.4 kB/sec)

This is a protocol used by General Motors, Chrysler, Harley Davidson and Toyota. The transfer speed is up to 10.4 kb / sec. Data transmission is done on a single thread and the maximum voltage is of 20V. The 0 logic signal is in the range 0-3.5V and the logic signal 1 is in the range 20-4.5V. Data frame length is from 0 to 8 bytes [5].

In Figure 3, the message that is sent to the ECU is 0x6A 0x68 0x01 0x00 0xC4 0xF1, that contains the header bytes "0x6A 0x68 0xF1", the byte 0x01 signifying the mode (Mode 01 - show the current date), and the byte 0x00 signifying the PID (Parameter ID) (PIDs supported).

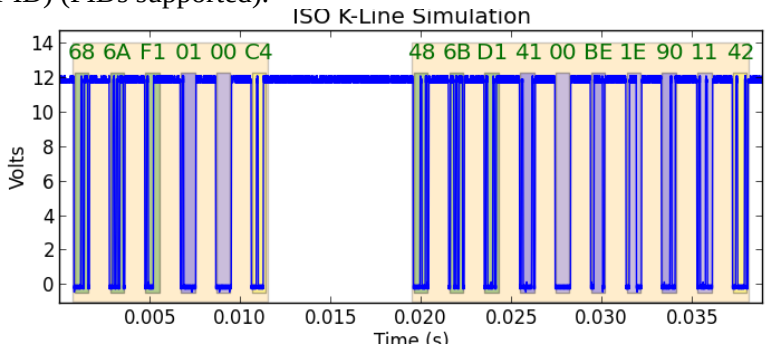

Fig. 3. ISO 9141-2 protocol [4]

The answer received from the ECU is presented in the following table:

Table 1. **The answer received from the ECU**

ex.	B				E				1				E			
in.																
IDs	1	2	3	4	5	6	7	8	9	A	B	C	D	E	F	0
ex.	9				0				1				1			
in.																
IDs	1	2	3	4	5	6	7	8	9	A	B	C	D	E	F	0

PIDs supported: 01,03,04,05,06,07,0C, 0D, 0E, 0F, 11,14,1C 20.

Advantages:

- communication on a single wire (pin 7) and on an optional wire (pin 15)
- message is 260 bytes and data is 255 bytes

Disadvantages:

- speed 10.4 kb / sec, lower than other protocols

initialization 5 bauds, different from the communication speed

1.4. Protocol ISO 14230 KWP 2000 (Keyword Protocol 2000)

It is a protocol similar to ISO 9141-2 and uses pin 7 and optional pin 15 for data transmission. Data transfer speed is in the range 1.2 to 10.4kb / sec and is bidirectional. The received message can contain up to 255 bytes in the data field.

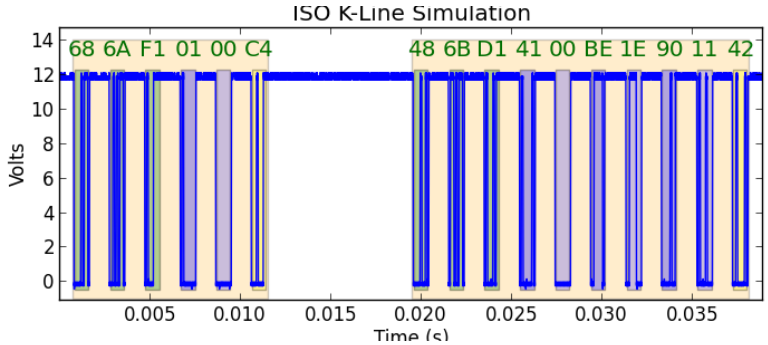

Fig. 4. ISO 14230 KWP2000 protocol [6]

Advantages:

- speed from 1.2 up to 10.4 kb / s, ensuring flexibility in synchronization
- communication on a single wire (pin 7)
- message length of 255 bytes

Disadvantages:

- maxim speed of 10.4 kb / sec, lower than other protocols

1.5. Protocol ISO 15765 CAN (250 kB/sec or 500 kB/sec) (Control Area Network)

This protocol is a product of Bosch and is used in the automotive industry but not only. The data transfer speed is divided into two categories: 250 kb / s and 500 kb / sec. This protocol uses for data transfer the following pins: pin 6 (CAN High) and pin 14 (CAN low). The transmission is done by two twisted wires that transmit the differential signal.

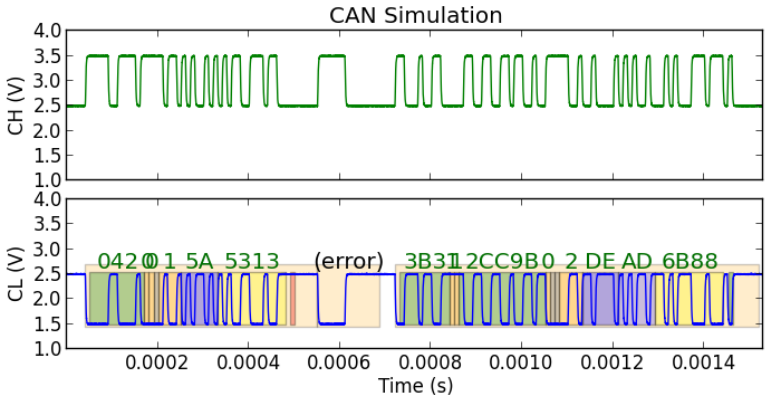

Fig. 5. ISO 15765 CAN protocol [6]

Advantages:

- two speeds of 250 kb / s and 500kb / sec
- most modern communication protocol

Disadvantages:

- high expenses for software development
- undesirable interaction more probable
- danger of incomplete technology for the customer

2. TELEPHONE COMMUNICATION TO ECU WITH STM32

The communication with the ECU can be done using one of the five communication protocols mentioned above. Information such as speed, intake manifold pressure, temperature, etc. can be read and forward to another device.

Using K-line protocol to read this information, it is necessary circuit diagram of connections for this interface protocol and STM32 microcontroller. The Figure 6 illustrates the circuit diagram created in OrCAD Capture program.

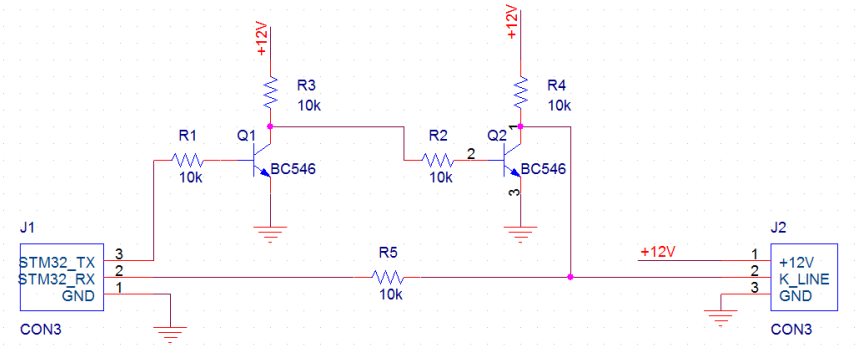

Fig. 6. Electronic Scheme

Parts used to create this device are:
• Resistors (R1, R2, R3, R4, R5) with a value of 10KΩ.
• Connectors (CON3 = J1, J2)
• Amplifier NPN Transistors (Q1, Q2 = BC546)
The power supply is from the vehicle battery (+ 12V DC).
The Figure 7 illustrates the circuit board created in OrCAD Layout.

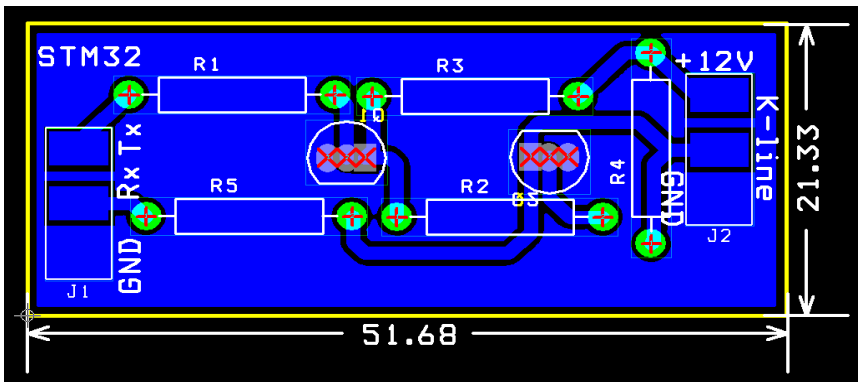

Fig. 7. Electronic Board

Electronic board size is 51.68 x 21.33 mm and is a plus for this system. The small size help placing the device in narrow places in the vehicle.

On the left in Figure 1 are the connectors used in communication with the microcontroller that uses the serial interface functions USART (Universal Synchronous / Asynchronous Receiver / Transmitter). On the right side of the Figure are located the connectors for communication with ECU (using K-line protocol).

Microcontroller creates communication with the ECU using a baud rate of 5 bit / sec for initialization, and 10.4kb / sec for data transfer.

Specific information for each message sent is composed of specific standard addresses.

In the following Figure 8 is an example of function that interrogates the ECU for finding the speed value.

```
void interogate_ecu(void)
{
    if(init_ok_var ==1) // if ok initialization
    {   if(TMR0_proc_IF == 1)
        {
            TMR0_proc_IF =0;
             cnt_inter++;
        }
        if(cnt_inter == 50)
        {
            cnt_inter = 0;
            switch(interogare)
            {
            case(0):
                {
                    send_message(0x68,0x6A,0xF1,0x01,0x0D,0x00);  // speed
                    interogare++;
                    return;
                }break;
```

Fig. 8. Function for interrogate

All the data received are sent to a mobile phone using bluetooth module. Mobile Application is one specific, created in order to interpret the data received and posting on the mobile phone display.

STM32 microcontroller used, converts data received from the ECU and sends a standard series created specifically for the phone application.

Other data that the microcontroller can send from in-vehicle sensors, which are not bound by ECU are transmitted to the phone application (temperature inside the vehicle, the temperature outside the vehicle, etc.).

Block diagram of the system is represented in Figure 9:

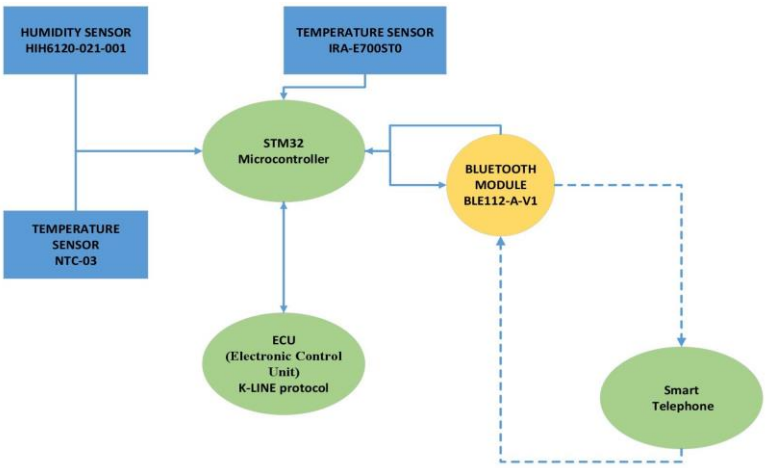

Fig. 9. Block Diagram

3. CONCLUSIONS

The communication protocols used by OBD2 evolved in time and the most modern protocol currently used is CAN. Compared to other protocols, the speed in CAN is very high for data transfer and the cabling has very low costs. It can work in poor conditions (interruptions on wire, grounding or short-circuit to + 12V).

The older protocols have the advantage of time. During the years they were used, they generated a lot of programming experience, they have been refined over time and the software has become simple and highly understandable for programmers.

Communication with your own car is an advantage. All this can be done using the system that transmits real-time data from the ECU to the mobile phone.

Data from ECU and dates from sensors located in the vehicle are displayed on the phone and informs the driver about to the vehicle condition.

REFERENCES

[1]. Dovleac R., Lorincz A.E., Ionica A., Leba M. *A business and technical approach on startups applied on an automotive system*, International Journal of Economics and Management Systems, Vol.1/2016, pp. 153-157, ISSN: 2367-8925, 2016.

[2]. Dzhelekarski P. *Initializing communication to vehicle OBDII system*, [Online], Available at: http://fett.tu-sofia.bg/et/2005/pdf/Paper097-P_Dzhelekarski1.pdf , 2005.

[3]. Marcu, M. D., Samoila, L. B., Popescu, F.G., *Simulation Software for Power Electronics*, Computer science and Software Techniques in 2011, Ed. Silhavy Sro, Czech Republic, pg. 121-127, ISBN 978-80-904741-0-9, 28 Ianuarie, 2011.

[4]. Samoila, B. L., Popescu, F. G., Slusariuc, R., *Virtual instruments used in direct current circuits learning process.* Annals of University of Petrosani, Electrical Engineering, Vol. 15, pag.47-52, Petroşani, 2013, ISSN 1454-8518, Ed. Universitas.

[5]. International Standard ISO 9141-2, first edition 1994-02-01

[6]. http://kevinpt.github.io/ripyl/rst/protocols.html#kline

Annals of the University of Petrosani, Electrical Engineering, 18 (2016)

STUDY ON THE USE OF ARDUINO BOARDS TO MONITOR POWER CONSUMPTION

NICOLAE PĂTRĂŞCOIU[1], COSMIN RUS[2]

Abstract: This paper details how to build a simple energy monitor that can be used to measure how much electrical energy you use in home place. It measures current, but uses an assumed fixed value for voltage and calculates apparent power and show the dates in one web page. Although not as accurate as a monitor that measures voltage as well as current, it is a method commonly used in commercially available whole house energy monitors for reasons of simplicity and cost. This paper then highlights selected approaches to monitoring and evaluation and the conditions under which each might be useful, and how and by whom lessons are to be learned. Attention is paid to key elements of monitoring and evaluation such as the development of indicators and the measurement of impacts. In the light of the many failed energy projects, this paper closes with some suggestions of how monitoring and evaluation processes and capacity may be improved.

Keywords: arduino, webserver, energy, monitoring.

1. INTRODUCTION

Everyone wishes to save energy and money. Minimizing your monthly electricity bill is a good place to start. What makes it difficult, is that your bill only tells the total amount of electric energy that was consumed during a long time window, typically one month. Hence, testing the effect of a change in behavior as an energy consumer is not practical. A working solution would be to frequently log the values from your energy meter to a notebook, and then draw a graph to reveal the before-after effect. But things like this need to be automated to become practical. So we will use a home PC, and build a measurement device that can be simply attached on top of the electricity meter [4].

[1] *PhD. Associate Professor Eng. University of Petrosani*
[2] *Ph.D. Student, University of Petrosani*

With increasing fuel costs and electricity to large consumers it became necessary to optimize consumption. In most production activities, energy consumption has a significant impact on cost, so it is imperative to know the real situation of consumption and efficiency.

Achieving this requirement requires the collection of information on water consumption, heat, natural gas, industrial water, process steam, compressed air, wastewater or any other specific size and profile beneficiary involving energy consumption of different types.

Using these systems ensures automatic data reading from specialized measuring equipment and metering, data storage in databases, data processing and their transformation into information and displaying the information obtained in the form of reports [8].

Energy consumption monitoring systems provide a complete solution for energy management. For this purpose require the use of the most modern measurement technology, communications and information processing. For example, the electric field they must be used in exchange points of the producing companies, transmission, electricity distribution and commercial and industrial consumers.

2. SPECIFICATIONS AND IMPLEMENTATION OF METERING SYSTEMS

Metering systems provide information used to streamline the operations of the companies and improve energy management, implementing the latest technologies in monitoring and energy management in a system with an open architecture. These provide the capability to monitor and analyze the production, distribution and consumption of energy and to identify potential methods to reduce costs.

Such a system must meet the following requirements:

• to be able to monitor hundreds or thousands of analog electrical quantities (current, voltage, power factor) and non (temperatures, pressures, velocities, flow rates); analog values originating either from sensors or transducers, either from the local control loops.

• to be able to track tens or hundreds of digital sizes (electric switches state);

• frequency readout input channels to be large enough. It is considered that the minimum performance that we have to provide a system for monitoring energy parameters are read at intervals of one second and the maximum state parameters of the process reading within 5 seconds. Frequency readings must, of course, coupled with dynamic parameters monitored process and shape characteristics of energy used.

• to store the input values over a fairly large[2].

• to issue warning signals operator in an emergency or overcoming preset limits in the process, or if a fault in the monitoring system.

• to be able to work, put in a usable form for operator and display the monitored values in a manner most advantageous, easy to interpret (tables of values, drawings, graphics and three-dimensional plane, histograms etc.).

In addition to these general requirements may include others such as:

• allowing identification of the facility monitored loss, damage or parasites consumers;

• allow consumption analysis separately for each part of the installation monitored (sections, important individual consumers, etc.);

• ensure electronic data reading;

• in certain circumstances it is necessary to provide simultaneous reading of all measuring points;

• the possibility of centralized dispatching display of measured values;

• ensure all consumptions reading in one system

• comply with the requirements of an open system, so as to enable further development and expansion of the system.

Continuous monitoring and evaluation of energy efficiency (Monitoring and Targeting, M&T) is a structured system of management of energy consumption within a socioeconomic system. It aims to achieve control and management of energy consumption [1].

Monitoring energy consumption is achieved using a system of meters and other measuring equipment. They are installed within an area called "center energy management."

The use of energy performance parameters are determined by the correlation between energy consumption and other quantities which influence (the amount of products produced within the specified period). The result of this analysis is to determine the laws of limit values (or target) for consumption - an action called "targeting".

Performance evaluation of energy consumption is achieved through regular reports highlighting deviations from target values, generally in the form of financial gains or losses.

After this analysis should be established and responsibilities for energy consumed regularly, conducting analyzes in order to find methods to improve the energy performance of the process and ways of practical application of these methods.

It is necessary to create a feedback mechanism within the socio-economic system by implementing a system to motivate staff so as to engage in action to find new ways to increase energy efficiency [6].

Steps to be taken to implement such a system are:

1. Conducting an audit to estimate its efficiency

The purpose of this audit is to establish the maximum amounts that can be spent to achieve the system so that these expenses are justified.

2. The data collection

The main data to be collected by the monitoring system are:

- Consumption of energy carriers;
- Production values;
- The values of environmental factors (temperature, etc.)
- Other auxiliary data.

Data collection frequency is variable being preferred automatic collection. Generally not recommended to collect data that can not be processed. One must also consider that the frequency readings can influence the quality of analysis.

3. Data Analysis

The first stage of determining objective values in terms of energy consumption to establish for each center energy management quantities shaping the energy values, and so that will be monitored. These quantities are called variables[7].

The purpose of the analysis stage is to establish a new feature that gives dependence on energy consumption of variable values. These functions can be simple phrases (ie linear) or complex, depending on the specific monitored system.

Data analysis can be performed manually (very difficult when the number of variables is large), using spreadsheets or using a specialized software for operating monitoring systems. The latter solution is the simplest but requires the existence of specialized personnel. The operational phase of collection continuously monitored quantities and values of objective comparison of consumption.

4. Application of measures to reduce energy consumption

An M&T seeks not only evaluating energy performance in one unit, but also the establishment of a system for the use of this information in order to establish concrete measures to reduce energy consumption. A monitoring system is always a special case, which must conform to actual installation of surveillance. To implement the beneficiary of the app, is based on a monitoring system "standard", which contains many core modules, hardware and software, and is performed onsite concrete equipment specific for each major energy consumer [7].

Often the implementation of such a system is achieved in stages, milestone dates are:

a. Initially, there are a relatively small number of monitored parameters (e.g., analog inputs 2-300) from the main machine, or which has the greatest consumption.

b. Based on preliminary results, the software modules are redesigned to meet the requirements of effective monitoring process. Also, the graphical user interface is adapted.

c. It identifies problems to be solved.

d. It gradually expanding network of sensors and transducers to other machines or production sections, the structure with suitable hardware and application programs.

e. In the next phases, the system is developed according to the specific needs of the beneficiary, both quantitatively (increasing the number of entries, to inspect all machinery) and in terms of functionality.

3. PRACTICAL IMPLEMENTATION

Project to undertake monitoring electrical energy consumption of a home via the Internet, that supervision power consumption of the house in which we live. It will measure the current and voltage consumed instantaneously and on a timeframe that will be displayed in a web page as a graph.

Materials required:

- Arduino Nano or Arduino Mini
- a current sensor (preferably 30 A).
- a voltage sensor that we will achieve power transformer and installation, to separate all the installation of network galvanic 220v the house to prevent damage caused by a short circuit. It is 12V and 1A.
- a stabilized source of 5V and 1A.
- an alternating current circuit to recover read current sensor (coil version). The circuit is actually a precision rectifier with a gain of about 40. It converts the output of the negative peak of the current sensor voltage of about 0 ... 5V in a range of about 0 - 50 A, the linearity and accuracy of approximately 0.1A.
- memory database that can store data recorded on 4 weeks.

and a network card, Arduino W5100.

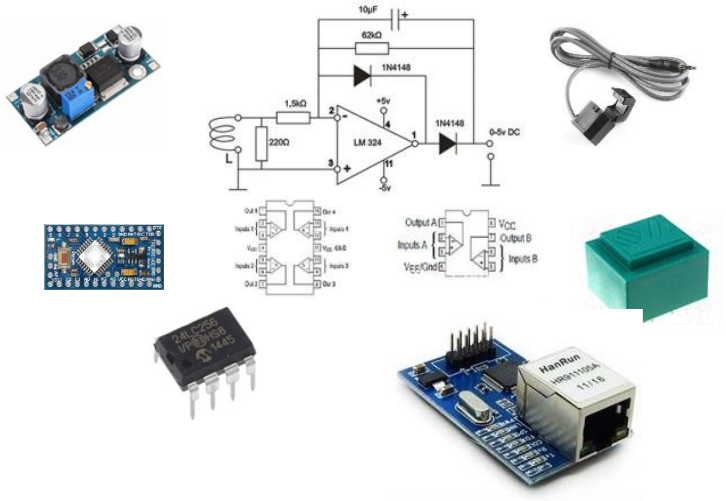

Fig.1. The hardware project

Programming is made in Arduino programming environment. Codebase contains several files:

serverWeb_Energy.ino
database.h
debug_out.h
general_string_data.h
page_printer.h
page_string_data.h

Actual loading of the source code and then compiled to run is via a module FTDI interface - USB (type FT232R) with reset.

After making installation and loading of source code (sketch), the current sensor is mounted on the housing phase wire or thread phase of a prize for illustration. Network card LEDs begin to pulsate, a sign that it is trying to connect. You have to look in the settings from Internet router IP whom received the device achieved.

Open a browser and the IP that the webpage.

Now you can read the instantaneous current and voltage power network of the dwelling and active electrical energy displayed depending on the time displayed on the buttons at the bottom. Reset button deletes the entire database.

Of course, if the code is modified, it can make various patterns web page or Internet can send various other measurements from other sensors.

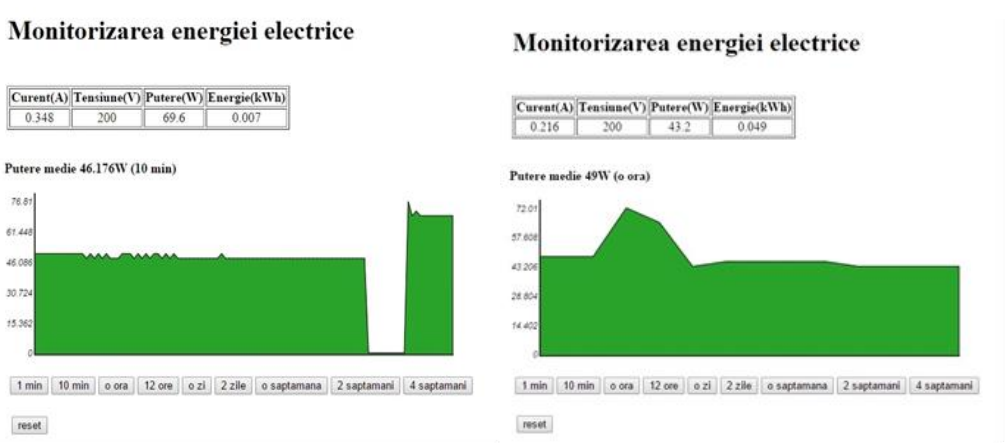

Fig. 2. Data representation through a diagram on a web page

4. CONCLUSIONS

Monitoring electricity consumption of a home is a good start to achieve technical and functional infrastructure to ensure the reduction of electricity consumption in order to reduce overall costs. In other news regarding infrastructure major energy Romania has adopted the standard EN 16001: 2009, which specifies the requirements for establishing, implementing, maintaining and improving a system of energy management for continuous improvement in the sense of energy use sustainable and more efficient. Development and adoption of EN 16001: 2009 helps stimulate

continuous improvement process leads to more efficient use of energy. This encourages organizations to implement a plan to monitor and analyze energy. According to the specifications of EN 16001: 2009 management system Efficient energy use is due in practice: the possibility of taking decisions to improve energy efficiency, continuous improvement Annual and improving performance in energy consumption, a deeper analysis areas with potential for energy saving. Developing predictive management by managing data and statistics on the development for long term secured with online monitoring systems and data transmission to dispatcher station for centralizing and storing them in a database.

The data can be used for studies and projects of modernization and efficiency, energy audits, for comparison with data subsequently recorded modernization processes. An argument pro - level management of public lighting and domestic lighting is the degree of comfort and safety in use they offer a well-controlled and monitored. It is essential that a study to implement a monitoring system for public lighting in a city or in a housing estate to be done within an organization competent and neutral, to remove temptations traders to sell the equipment in any form. Information obtained through monitoring are essential for optimal measures to improve power quality and energy efficiency. From measurements made in network studied (electronic laboratory) values were obtained in addition to those specified quality standards on consumption. From their analysis gave directions to reduce costs while preserving or even improving the quality of energy. As regards public lighting to increase power factor, for example, it needs to replace some electronic electromagnetic ballasts equipped with controls to reduce lumen. An important component in monitoring the efficiency of public lighting, household or business is the data. This allows optimization of the systems within the limits set. The proposed solution enables monitoring and wireless data transfer via a router. For offline monitoring, data are recorded on the internal memory. High energy savings achieved by implementing energy efficiency grade grow the plant optimized with positive influences on cost reduction.

REFERENCES

[1]. Arad, S., Samoila, L. *Electricity generation in coal-fired plants in Romania*, Revista Minelor, nr. 4/2014, pag. 8-15, ISSN-L 1220-2053, ISSN 2247-8590.

[2]. Leba M., Pop E., *New Distributions Properties and Applications in Digital Control*, Proceedings of the 7th WSEAS International Conference on SIGNAL PROCESSING, ROBOTICS and AUTOMATION (ISPRA '08), ISSN: 1790-5117 48, ISBN: 978-960-6766-44-2, University of Cambridge, UK, February 20-22, 2008.

[3]. Leba M., *Programare in limbaj de asamblare. Aplicatii in ingineria sistemelor*, Editura Didactica si Pedagogica, Bucuresti, 2007.

[4]. Leba M., *Contributii privind conducerea numerica ierarhizata a sistemelor de actionare cu motor asincron*, Ph.D.Thesis, Petrosani, 2002.

[5]. Leba M., Pop E., Badea A., *Adaptive Software Oriented Automation for Industrial Elevator*, Proceedings of the 11th WSEAS International Conference on Automatic

Control, Modeling and Simulation ACMOS'09, ISBN 978-960-474-082-6, ISSN 1790-5117, pp.128-133, Istanbul, Turkey, 2009.

[6]. Marcu, M.D., Popescu, F.G., Niculescu, T., Pana, L., Handra, A.D., *Simulation of power active filter using instantaneous reactive power theory*. Harmonics and Quality of Power (ICHQP), 2014 IEEE 16th International Conference, Page(s):581 – 585, Bucharest, Romania, 25-28 May 2014.

[7]. Pătrăşcoiu N., *Tehnici de instrumentaţie virtuală*, Editura Universitas, Petroşani, 2015.

[8]. Pătrăşcoiu N., *Sisteme de achiziţie şi prelucrare a datelor*, Editura didactică şi Pedagogică, 2004.

[9]. Pop E., Leba M., *Applications of Distribution Theory in Digital Control Systems*, Annals of University of Petrosani, Vol. 5, 2003, pp.23-34.

[10]. Pop E., Leba M., *Simulation and Design of Nonlinear Controllers based on Distributions Theory*, Proceedings of the 6th WSEAS International Conference on SYSTEM SCIENCE and SIMULATION in ENGINEERING, ISBN 978-960-6766-14- 5, ISSN 1790-5117, 2007, pp.103-108.

[11]. Pop E., Leba M., *Microcontrollere şi automate programabile*, Editura Didactica si Pedagogica, Bucuresti, 2003.

[12]. Pop E., Bubatu R., *Teoria sistemelor educaţie prin e-learning*, Editura Universitas, Petroşani, 2012.

[13]. Sochirca, B., Poanta, A., *Proiectarea şi dezvoltarea aplicaţiilor cu microcontroler*, Editura Universitas, Petroşani, 2012.

[14]. Uţu, I., Păsculescu, D., *Power Quality Study in Order to Comply with European Norms*, Revista Calitatea, Supplement of "Quality - Access to Success" Journal, Vol.18, S1, January 2017, ISSN 1582-2559, pag. 366-371.

[15]. http://www.engineerathome.com/elektronica/log+arduino+data+to+a+web+server/34

[16]. http://www.open-electronics.org/how-to-create-an-intelligent-web-enabled-power-meter-with-arduino/

[17]. http://www.instructables.com/id/Green-power-live-data/

[18]. http://www.arduino.cc/

[19]. http://documents.tips/documents/capitolul-6-despre-arduino.html

[20]. http://www.robofun.ro

[21]. http://www.unitbv.ro/faculties/biblio/interfete_specializate/curs.pdf

[22]. http://www.chip.ro

Annals of the University of Petrosani, Electrical Engineering, 18 (2016)

VIRTUAL INSTRUMENT FOR SIMULATING A DC GENERATOR BEHAVIOUR

BRANA LILIANA SAMOILA[1], SUSANA LETITIA ARAD [2]
STOCHITOIU MARIA DANIELA [3]

Abstract: The paper deals with a LabView simulation we made for studying the operation of a d.c. generator with separate excitation. This virtual instrument is meant to allow studying the behavior of such generators when the working conditions change. The virtual instrument we achieved shows the external characteristic for different values of resistances, excitation voltage and driving speed.

Keywords: virtual instrument, d.c. generator, electrical engineering education.

1. INTRODUCTION

Traditional hardware instrumentation is made up of digital or analogical specific measurement devices. These systems are limited in their use comparing to virtual instrumentation systems.

Virtual Instrumentation is the use of customizable software and modular measurement hardware to create user-defined measurement systems, called Virtual Instruments [9].

Comparing hardware instrumentation and virtual instrumentation we can see that software is used to replace a large amount of hardware.

Modeling and simulation are meant to evaluate the results of certain actions in a virtual environment comparing to similar actions performed in a real environment.

New graphical programming languages are more and more used in modeling and simulation [2], such as:

SPICE, Electronics WorkBench are destined to electrical and electronic circuits;

[1] *PhD., Associate Professor, Eng., University of Petrosani*
[2] *PhD, Professor, Eng., University of Petrosani*
[3] *PhD., Associate Professor, Eng., University of Petrosani*

- *Working Model* is a simulator for mechanical systems;
- LabVIEW (Laboratory Virtual Instrument Engineering Workbench);
- *MATLAB* (MATrix LABoratory) is package of programmes dedicated to calculations and graphical representations. *Simulink* is a component of this software;
- *Modelica* is an object oriented language used in modeling physical systems;
- *Dymola (*Dynamic Modeling Laboratory) is an environment used in modeling and simulating complex systems;
- *20-SIM (Twente Sim)* is used for modeling and dynamic simulation of complex systems.

LabView is a programming environment conceived for virtual instrumentation. A Virtual instrument –*VI* - has 2 components:

- *front panel* –the user graphical interface, that is what the user sees on the display;
- *block diagram* –the code of the program which defines the functionality of the *VI* – it uses operators, functions, etc;

LabView uses the concept of "modular programming", likewise the C, C++, and PASCAL programming environments [1], [8].

LabVIEW is very effective in interactive simulations in education [5]. Using virtual instruments, students have the possibility of getting answers of "what – if" type to certain changes of input values.

Users may interactively change the signal and virtual instrument characteristics and witness the appropriate response.

2. CONSIDERATIONS ABOUT THE DC GENERATOR WITH SEPARATE EXCITATION

Figure 1 shows the electrical diagram of a d. c. generator with separate excitation [3] [6]. The excitation winding is powered by a separate continuous voltage source.

The equivalent diagram of the circuit formed by the rotor winding of the generator and the load, R_S, is presented in Figure 2, where: R_r is the electrical resistance of the rotor winding, r_p - brush - collector contact resistance, E – induced electromotive force in the rotor winding [6].

Applying the law of Ohm to the circuit in Figure 2, we obtain the operating equation for this type of generator:

$$U_S + I_r\left(R_r + r_p\right) = E \Rightarrow U_S = E - I_r \tag{1}$$

where:

$$U_S = R \cdot I_S \tag{2}$$

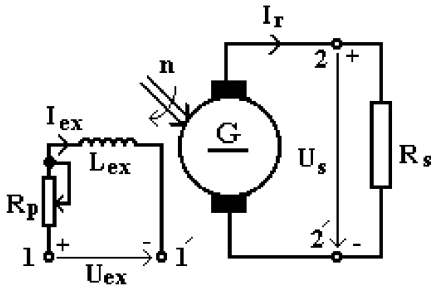

Fig. 1. Electrical diagram of a d. c. generator with separate excitation.

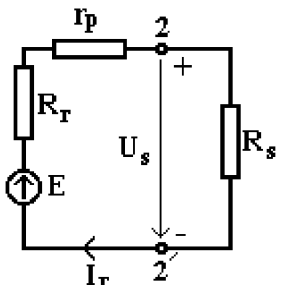

Fig. 2. Equivalent diagram of the d. c. generator rotor winding and load

The current through the rotor winding, which is the same as through the load, is:

$$I_r = \frac{E}{R_r + r_p + R_S} \tag{3}$$

It results that the value of the current through the rotor winding depends on the load.

The polarity of the voltage between 2 and 2 'depends on the sense of the rotor rotation and the sense of the excitation current [4].

The external characteristic (Figure 3) represents the variation of the output voltage depending on the load current U = f (I) when the generator speed and magnetizing current are kept constant [6].

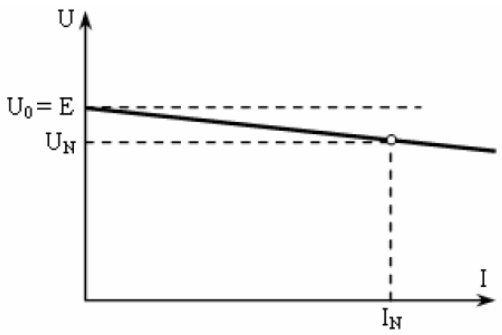

Fig. 3. External characteristic of a d.c. generator with separate excitation

3. VIRTUAL INSTRUMENT FOR SIMULATING A DC GENERATOR WITH SEPARATE EXCITATION

We have created a virtual instrument (VI) that can simulate the work of a d. c. generator with independent excitation.

The front panel of the application is shown in Figure. 4. The similarity of the symbols represented for the different input or output values with the displays of

industrial equipment (sources, numeric fields, tachometers, digital displays, buttons and graphics) can be noticed.

The controls we used are:

• Horizontal Pointer Slide - for rotor resistance;
• Horizontal Pointer Slide - for starting rheostat;
• Horizontal Pointer Slide - for excitation rheostat;
• Horizontal Pointer Slide - for load rheostat;
• Knob - for excitation voltage;
• Dial - for speed;
• Numerical Indicators for displaying numerical values of input and output quantities;
• Waveform Graph - Graphic Indicator;
• String type indicator.

Using the relations between the characteristic values in the circuit of a d.c. generator with separate excitation, presented in chapter 1, simulating the measurement of real values [7], we developed the algorithm and the program.

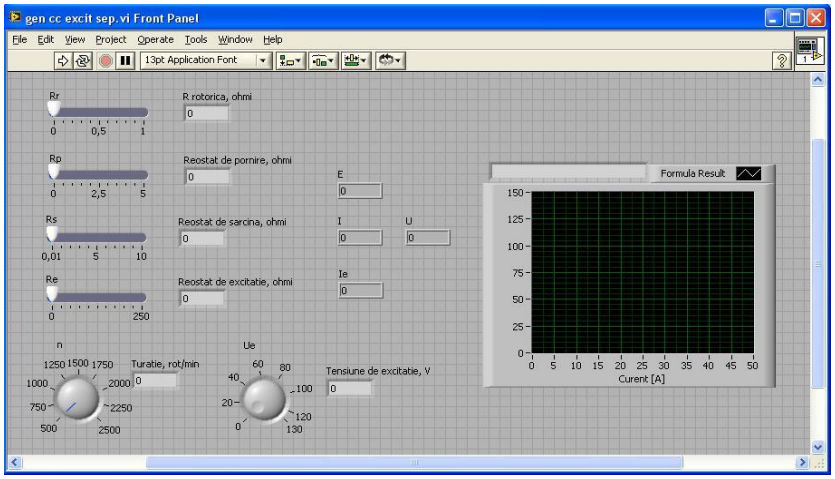

Fig. 4. The front panel of the vitrual instrument for simulating a d.c. generator with independent excitation

In the block diagram, we used:

• a FOR cycle;
• two Formula Nodes;
• Bundle elements for obtaining dynamic sizes;
• Formula block to enter the graphical function.

The block diagram of the VI is shown in Figure 5.

The virtual instrument that we achieved allows simulating the external characteristic of the separate excitation d. c. generator.

The result of the simulation is shown in Figure 6.

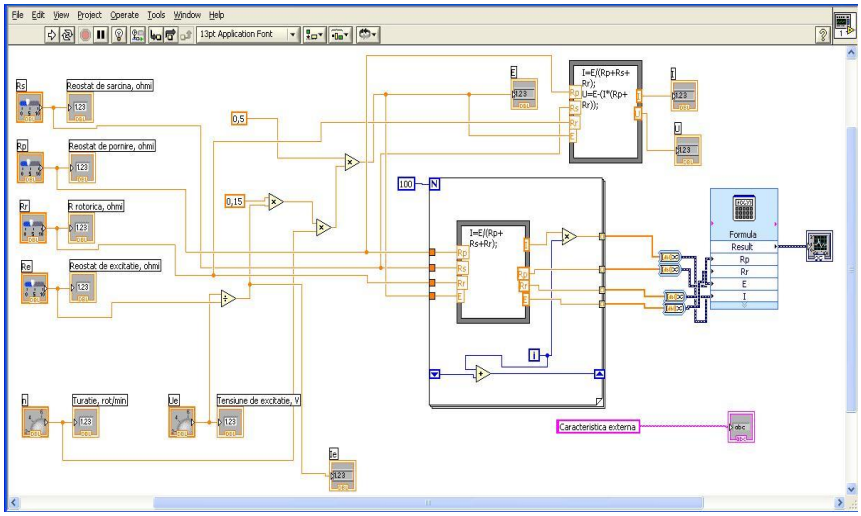

Fig. 5. Block diagram of the VI for simulating the external characteristic of a d. c. generator with separate excitation

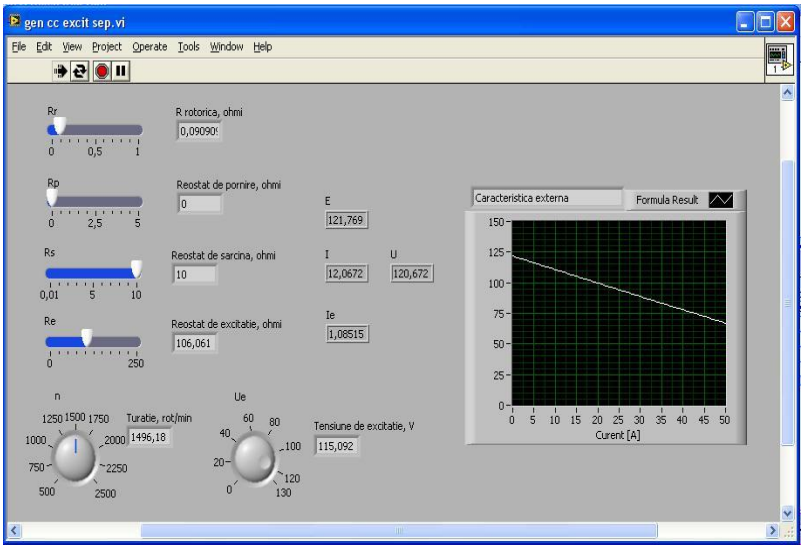

Fig. 6. The simulated external characteristic of a d.c. genarator with independent excitation

The virtual instrument allows visualizing the changes in the external characteristic, due to the variation of the input values:

- rotor resistance;
- starting resistance;
- load resistance;
- resistance in the excitation circuit;
- speed;
- excitation voltage.

4. CONCLUSIONS

Learning is a challenging intellectual process and new technologies have tremendous potential to make an immense difference with their interactive (computational) and multimedia features.

For a learner, "the virtual-reality", if it is well designed, may have many advantages over the reality itself Confucius said: *"I hear…and I forget, I see…and I remember, BUT, I do…and I understand!"* That is why kids love video games, like TV, but hate old-fashioned lectures.

The LabVIEW has an advantage to further enhance the simulation applications due to its powerful features and an appealing, real-like "front panel" interface.

This virtual instrument we made is used in learning and teaching activities where it turned out to be very helpful for students aiming a better understanding of the d. c. generator behavior under different conditions given by rheostats values.

We made it simple, easy to use and intuitive, being a more flexible, alternative method to the practice using hardware devices in laboratories.

REFERENCES

[1] Pătrăşcoiu N., *Achiziţie de date. Instrumentaţie virtuală,* Didactic and Pedagogical Publishing House, Bucharest, Romania, 2004.

[2] Dolga V., Golga L., *Modelling, Simulation and Virtual Instrumentation in Mechatronics*, Annals of the Oradea University. Fascicle of Management and Technological Engineering, Volume VI (XVI), PP. 1108-1117, 2007.

[3] Marcu M.D., Popescu F.G., *Convertoare statice - lucrări de laborator*, Editura Universitas, Petroşani, 2010.

[4] Niculescu T., Marcu M., Popescu F. G., *Study of switching electric circuits with DC hybrid breaker, one stage*, EUROINVENT, International Conference on Innovative Research, Iasi, 19th–20th of May 2016, Romania.

[5] Kostic M., *Interactive Simulation with a LabVIEW Virtual Instrument*, NIWeek2000 Annual International Conference, National Instruments, Austin, TX, 2000.

[6] Tăbăcaru T., Uţu I., *Maşini electrice şi acţionări: culegere de probleme*, Universitas, 2012.

[7] Uţu I., Samoilă L., *Măsurarea mărimilor electrice*, Editura Universitas, 2010.

[8] www.ni.com/labview/

[9] https://en.wikipedia.org/wiki/Virtual_instrumentation

Annals of the University of Petrosani, Electrical Engineering, 18 (2016)

TECHNICAL AND LEGAL ASPECTS ON THE USE OF DRONES

COSMIN RUS[1], NICOLAE PĂTRĂŞCOIU[2]

Abstract: This paper discusses initial application of drone technology in the surveilance and collect data. In this study, a small-scale aerial drone was used as a tool for exploring potential benefits to collect data. A drone is an aerial quadcopter that can be piloted remotely using a smart phone, tablet device or a computer. Since the drone is equipped with video cameras, it can provide safety managers with fast access to images as well as real time videos from a range of interes locations. Autonomous navigation, vocal interaction, high-resolution cameras, and collaborative user-interface environment are some examples of features that can be used. This application of the aerial drone has the potential to improve general safety but need to be traced a clear border between Big Data and Big Brother.

Keywords: drones, big data, big brother.

1. INTRODUCTION

This paper explains some general principles of drone regulation by national governments and asks how both air safety and privacy will be shaped by new technologies. It puts forth the claim that taking property rights in the air seriously is a way to allow innovation while protecting safety and privacy. As far back as 1944, when the Chicago Convention on International Civil Aviation established the International Civil Aviation Organization (ICAO), the international umbrella body for aviation regulators, authorities were considering the implications of "pilotless aircraft." Article 8 of the convention prohibited "aircraft capable of being flown without a pilot" from trespassing over the territory of contracting states without permission and further obligated the fifty-two signatories (nearly all sovereign states now adhere to the convention) to "insure that the flight of such aircraft without a pilot in regions open to civil aircraft shall be so controlled as to obviate danger to civil aircraft". [35]

[1] *Ph.D. Student, University of Petrosani*
[2] *PhD. Associate Professor Eng. University of Petrosani*

Just what it means to obviate that danger is a question that national aviation regulators around the world are wrestling with.

2. DRONES - THE POSSIBLE HAZARDS

The chief danger that unmanned aircraft pose to manned aircraft is accidental collision. This is for two reasons. The first is the sheer number of small unmanned aircraft. There are already more small drones than exist general aviation aircraft, and that number will only grow. The air will become more crowded than ever before. The second is the limited situational awareness that drones have. Though drones can be flown with so-called "First Person View" (FPV) cameras that provide some such awareness, regulators believe (based on a track record of military drones with somewhat similar systems) that FPV systems do not provide awareness comparable to a pilot within an aircraft. At some point in the future, drones may commonly have onboard systems that algorithmically avoid collisions. The vast majority of drones do not have such systems at present. In a century of manned aviation, a number of techniques for airspace management have been developed to prevent collisions. These might sound similar to a layperson but in fact entail distinct technical solutions. The first is to segregate airspace. If manned aircraft and unmanned aircraft fly at entirely different altitudes, then there is no risk they can collide. At worst, unmanned aircraft could collide with one another, which would not involve loss of life [12]. This approach means excluding drones from the vicinity of airports used by manned aircraft and confining them to low altitudes where manned aircraft are already prohibited from flying. However, because of exceptions like medevac helicopters, which must fly at low altitudes and must have freedom to go almost anywhere at short notice to complete their missions total segregation is not possible. It is, however, the principle behind restrictions, in many jurisdictions, that confine small drones to low altitudes. However, low-altitude flight implicates privacy; low-flying drones can more easily take pictures that infringe on privacy and can create noise that is an "intrusion upon seclusion"[13].

Thus, some have proposed segregated bands for drone flight between, say, 500 and 700 feet (150-200 m) above the ground that would be reserved for unmanned aircraft. Similar bands for larger unmanned aircraft at higher altitudes could segregate them from manned aircraft. If airspace control systems were being designed from scratch, such bands would be a logical solution. However, they are not likely to be implemented in any jurisdiction because they run counter to the legacy of how airspace has been regulated. The next mechanism for preventing crashes is to maintain "separation" between aircraft. This works in controlled airspace, where air-traffic controllers keep track of where both manned and unmanned aircraft are. It allows, for example, Predator drones flown by the U.S. government to patrol the U.S.-Mexico border. It also is what has allowed the airport in Kandahar, Afghanistan, to function. The airport was for some time the world's busiest single runway airport, with more than 800 takeoffs and landings per day civilian and military, manned and unmanned, all mixed together. Air-traffic controllers managed this airspace by keeping a

minimum of 1,000 feet (300 m) of separation between drones and manned aircraft and 500 feet (150 m) between one drone and another. There does not exist, for the moment, a system for maintaining separation between small drones. For such a system to work, controllers must be able to both see all relevant aircraft and direct them. Small drones fly at lower altitudes, where radar coverage is difficult; there are many more of them, and because small drones have very limited payload capacity, systems that allow them to interact with air-traffic control and other aircraft must be carefully designed. NASA is developing a system that would act as a global surveillance system for small drones at low altitudes. As a backup in case separation measures fail, passenger aircraft are required (throughout the world) to have a Traffic Collision Avoidance System (TCAS), which is an automated system in which transponders on aircraft communicate with one another and alert pilots to the risk of collision. In smaller aircraft, a pilot's eyes can suffice the pilot is required to be able to "see and avoid" other aircraft. Developing systems for drones to "sense and avoid" other aircraft is an active area of research, as is determining how to regulate such new technologies. Some consumer drones already have limited autonomous sense-and-avoid technologies, such as DJI's "Guidance" system. The capabilities of such autonomous systems are changing rapidly. It is difficult to venture predictions about how they will improve. Systems that work at low speeds won't do much good at high speeds; systems that work well in controlled testing may not be resilient in the real world. However, much may change quickly [14].

Larger drones can carry sophisticated sensors, cameras and gimbals that give the pilot good situational awareness (though not as good as that of a pilot in a manned aircraft).

The FPV systems that smaller drones have provide a similar, though more limited capability. Such FPV systems can be used to race around obstacles at high speed. This does not mean, however, that they provide the sort of peripheral awareness that a pilot in an airplane cockpit has. Latency with such systems is also an issue. Many countries, particularly in the developing world, still do not have explicit regulations governing drones. However, in the United States, Canada, Europe, Australia, and elsewhere, a broad consensus on how to regulate drones has emerged in the past decade. The similarities among the various regulatory regimes outnumber the differences. That consensus is to allow more flexibility for smaller drones. These generally can be flown at low altitudes, far from airports, far from crowds, and within the line of sight. Some countries, France, for instance, permit flight beyond the line of sight for very lightweight drones. This is sensible and likely to become more common. The United States has lagged behind the United Kingdom, France, Germany, Australia, Canada, and elsewhere in the implementation of commercial drone flight regulations, however, the proposed rules which the Federal Aviation Administration (FAA) [13].

In 1942 a chicken farmer outside of Greensboro, North Carolina, sued the U.S. government. He said the frequent, low overflight of military aircraft on the adjacent runway was scaring his birds and damaging his livelihood, and he wanted compensation. The case made it all the way to the Supreme Court in 1946. And one

result of United States v. Causby was that the Court set the limits of private airspace: If you own a house, your property rights extend 83 feet (25 m) up into the air [22].

That's a quaint, and thankfully irrelevant, limit when it comes to manned aircraft. The Federal Aviation Administration keeps planes much higher than that, save on approach and take-off, and even then most airports require a decent buffer around them. But the 70-year-old ruling has new importance in the age of drones. It remains the only clear federal statement of law on how far above the ground your property ends. And that has raised concerns among some privacy advocates, who question whether anyone from a pesky neighbor to a police department to Amazon's planned delivery service should be allowed to fly above private property, potentially shooting video from the level of the treetops [24].

Now a federal lawsuit, which was argued today in the D.C. Circuit Court of Appeals, is trying to force the Federal Aviation Administration to set rules protecting citizens from such privacy intrusions. The action was brought by the Electronic Privacy Information Center (EPIC); among other points, EPIC wants the FAA to make it easy for citizens to find out whether drones flying overhead have surveillance capabilities. The group also wants to protect the privacy rights of drone pilots, who have been required to register with the FAA since December.

This isn't the first time that EPIC has tried to compel the FAA to focus on drones and privacy, but the agency argues that its authority is limited to making sure that drones are safe. For now, the question remains: If the FAA isn't protecting your right to privacy from drone spying, who is?[24]

3. WORKING WITH DRONES - TECHNICAL ISSUES

While discussing multirotor construction and piloting, it will certainly be useful to have a way of communicating different movements of the multirotor. Fortunately, mathematicians way back in the 1700s came up with a way of describing the orientation of rigid bodies in space. The system they developed uses a set of three angles to describe, in this case, the orientation of the multirotor around the three spacial dimensions. You have probably heard of these angles before, they are called roll, pitch, and yaw.[19]

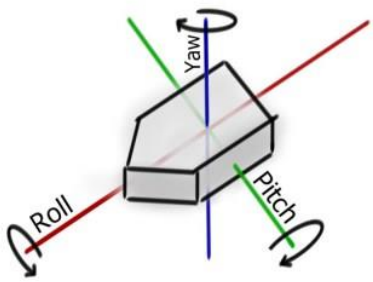

Fig.1. Angles of rotation

The roll angle of the multirotor describes how the craft is tilted side to side. Rotation about the roll axis is like tilting your head towards one of your shoulders. Rolling the multirotor causes it to move sideways.

The pitch angle of the multirotor describes how the craft is tilted forwards or backwards. Rotation about the pitch axis is like tilting your head in order to look up or down. Pitching the multirotor causes it to move forwards or backwards.

The yaw angle of the multirotor describes its bearing, or, in other words, rotation of the craft as it stays level to the ground. Rotation about the yaw axis is like when you shake your head to say "no."

There is one final bit of terminology we will use to discuss flying the multirotor, and that is throttle. Throttle simply controls the altitude of the multirotor.[19]

Steering

While flying your multirotor, it is very important to understand how the multirotor moves and how we control it. At the root of all the multirotor's movements is the rotational speed of the motors. By adjusting the relative speeds of the motors in just the right ways, keeping in mind that the rotational speed of the motors determines how much lift each prop produces, the flight controller is able to cause the multirotor to rotate around any of the directional axes (roll, pitch, and yaw), or make the multirotor gain or lose altitude.[19]

Roll and Pitch

To make the multirotor rotate about the roll or pitch axes, the flight controller makes the motors on one side of the multirotor spin faster than the motors on the other side. This means that one side of the multirotor will have more lift than the other side, causing the multirotor to tilt.

So, for example, to make a quadcopter roll right (or rotate about the roll axis clockwise), the flight controller will make the two motors on the left side of the multirotor spin faster than the two motors on the right side. The left side of the craft will then have more lift than the right side, which causes the multirotor to tilt.

Similarly, to make a quadcopter pitch down (rotate about the pitch axis clockwise) the flight controller will make the two motors on the back of the craft spin faster than the two motors on the front. This makes the craft tilt in the same way that your head tilts when you look down. [19]

Yaw

Controlling the multirotor's rotation about the yaw axis is a bit more complex than controlling its rotation about the roll or pitch axes. First, let's discuss how we prevent rotation about the yaw axis. When assembling and programming multirotors, we set up the motors so that each motor spins in the opposite direction than its neighbors. In other words, using a quadcopter as an example again, starting from the front-left motor and moving around the multirotor clockwise, the motors' rotational

directions alternate, CW, CCW, CW, CCW. We use this rotational configuration to neutralize, or cancel out, each motor's tendency to make the multirotor rotate.

When a prop spins, for example, clockwise, conservation of angular momentum means that the body of the multirotor will have a tendency to spin counter-clockwise. This is due to Newton's third law of motion, "for every action, there is an equal and opposite reaction." The body of the multirotor will tend to spin in the direction opposite the rotational direction of the propellers.

For example, helicopters have two rotors. One big main rotor responsible for lifting the aircraft, and one small rotor on the tail that adjusts how the helicopter spins. Imaging what would happen if in mid-flight, a helicopter's tail rotor fell off the aircraft while the big main rotor kept spinning (this by the way is something we hope never happens to any helicopter pilots). You can probably imagine that the helicopter would start spinning. Well this rotation would be caused by the rotation of the propeller in the opposite direction, according to the law of conservation of angular momentum.[19]

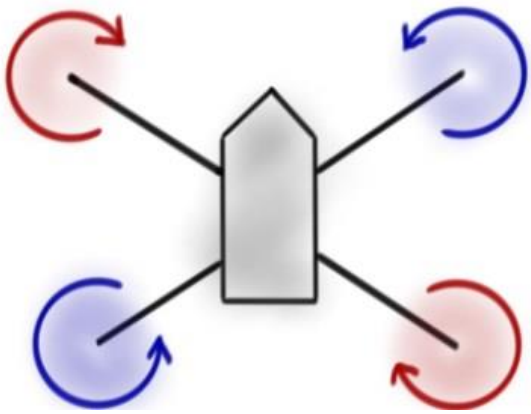

Fig.2. Motors rotation directions

Bringing it all together now, each of the quadcopter's four rotors tends to make the multirotor rotate in the opposite direction than their spin. So by using pairs of rotors spinning in opposite directions, we are able to cancel out this effect and the multirotor does not spin about the yaw axis.

So therefore, when we actually want the multirotor to rotate about the yaw axis, the flight controller will slow down opposite pairs of motors relative to the other pair. This means the angular momentum of the two pairs of props will no longer be in balance and the craft rotates. We can make the multirotor rotate in either direction by slowing down different pairs of motors.[19]

Hovering/Altitude Control

Now that we understand how steering the multirotor works, let's quickly discuss a much simpler maneuver, hovering. To make the multirotor hover, which means the multirotor stays at a constant altitude without rotating in any direction, a

balance of forces is needed. The flight controller will need to counteract the force of gravity with the lift produced by the rotors.

Throwing a bit of math into the picture now, the force of gravity acting on the multirotor is equal to the mass of the multirotor times gravitational acceleration (which, as far as we are concerned, is a constant as long as we are staying on Earth). The lift produced by the multirotor is equal to the sum of the lift produced by each of the rotors. Therefore, if the force of gravity equals the force of the lift produced by the motors, the multirotor will maintain a constant altitude.

To ascend or descend, therefore, the flight controller disrupts this balance. If the lift produced by the multirotor is greater than the force of gravity, the craft will gain altitude. If the opposite is true, that is, if the lift produced by the multirotor is less than the force of gravity acting on the multirotor, then the multirotor will fall.

Movement

Adjusting the relative speeds of the motors, the flight controller can make the multirotor tilt. Well, the reason we want to be able to tilt the multirotor is that tilting the multirotor causes it to move. By tilting the multirotor in different directions, it can be made to move forward, backward, left, or right (neither altitude control nor yaw control involve tilting). For example, when the multirotor pitches down (clockwise around the pitch axis) it moves forward.

The reason the multirotor moves when it tilts is because while the multirotor is tilting, some of the lift produced by the rotor is directed horizontally while normally all of the lift is directed downward. This sideways component of the lift pushes the multirotor.

Now, you might have realized the problem that happens when we sacrifice some of the multirotor's downward thrust to move the craft horizontally. Since less thrust is directed downward while the multirotor is tilting, multirotors tend to lose altitude while moving around. Now some flight controllers have a feature called "altitude hold" which means that the flight controller automatically adjusts the motor speeds in order to make the craft maintain a constant altitude while moving. Unfortunately, the KK2.1 flight controller used in the tutorials on this site lacks this feature. This helps keep costs down, but also means that the pilot must manually adjust the throttle to maintain altitude while maneuvering.

4. PRIVACY LAWS

Big data is a term for data sets that are so large or complex that traditional data processing applications are inadequate. Challenges include analysis, capture, data curation, search, sharing, storage, transfer, visualization, querying, updating and information privacy. The term often refers simply to the use of predictive analytics, user behavior analytics, or certain other advanced data analytics methods that extract value from data, and seldom to a particular size of data set. Accuracy in big data may lead to more confident decision making, and better decisions can result in greater

operational efficiency, cost reduction and reduced risk. Big brother means a person or organization exercising total control over people's lives.

Privacy concerns can lead to hot tempers. Last year, a Kentucky man use a shotgun to blast a drone out of the air above his home. A New Jersey man did the same thing in 2014, and a woman in Seattle called the police when she feared a drone was peeping into her apartment. (The drone belonged to a company conducting an architectural survey). And in November, repeated night-time overflights by a drone prompted calls to Albuquerque police complaining of trespassing, the police concluded that the flyer wasn't breaking any laws.

State laws already on the books offer some privacy protections, especially if a drone is shooting photos or video. Erin E. Rhinehart, an attorney in Dayton, Ohio, who studies the issue, says that existing nuisance and invasion-of-privacy statutes would apply to drone owners. If you could prove you were being harassed by a drone flying over your house, or even that one was spying on you from afar, you might have a case against the drone operator. But proof is difficult to obtain, she says, and not everyone agrees on how to define harassment.

Some states are trying to strengthen their protections. In California, nervous celebrities may benefit from a law signed by Governor Jerry Brown this past fall. The meat of the legislation reads, "A person is liable for physical invasion of privacy when the person knowingly enters onto the land or into the airspace above the land of another person without permission…in order to capture any type of visual image, sound recording, or other physical impression of the plaintiff." And a similar privacy law in Wisconsin makes it illegal to photograph a "nude or partially nude person" using a drone. (Dozens of states have passed or are considering drone-related laws).

Most of these statutes are carefully worded to focus on capturing images, because the states can't control where drones are allowed to fly—that's up to the FAA. Robert Kirk, an attorney who advocates on the part of companies that want to use drones for surveying, thinks that privacy laws that single out drones could be challenged in court. "The FAA has taken the position that any regs that deal with air safety reside solely with the FAA," he says. "The trouble is going to be whenever someone comes after a drone operator and we're moving into privacy and trespass, areas that are more traditionally in the realm of state and local authority." The upshot: Authority is split between the federal government and the states. And no one currently has the authority to broadly protect privacy by preventing drones from flying over people's homes.

5. CONCLUSIONS

Someday soon, Amazon promises, drones will zip around neighborhoods, quickly and efficiently delivering small packages. If they do, they are very likely to have the legal right to fly over your house—and the same goes for commercial land surveyors using cameras to prepare maps.

When it comes to the use of drones by law enforcement, the situation is less clear-cut. The Supreme Court has ruled that aerial surveillance by police forces is legal, whether the subject is on private or public property. This came up in two cases in the 1980s, when the Court decided that the police hadn't needed a warrant to take aerial photos of marijuana plants growing in residential backyards. However, the advent of drone technology has made it much easier and cheaper for police departments to conduct such surveillance. And states have been grappling with the implications. Both Nevada and Virginia have passed legislation requiring the police to obtain a warrant before using a drone for surveillance. However, Texas has gone in the opposite direction, saying that law enforcement agencies need only probable cause. This is an issue that could end up being decided in federal court.

The EPIC lawsuit is not the only effort to expand the FAA's role into the privacy realm. A law proposed by Massachusetts Senator Ed Markey, the Drone Aircraft Privacy and Transparency Act, would require the agency to ensure baseline privacy and transparency safeguards, which would apply to both private drone operators and law enforcement.

The ACLU, which supports the Markey bill, argued as far back as 2011 that a lack of oversight could lead to excessive surveillance by law enforcement using drones. Yet some legal analysts warn that the opposite situation also poses dangers: If regulations were poorly written, they could end up protecting government and commercial operators of drones, while restricting everyone else. For instance, some states are considering laws that would prevent journalists from using drones to photograph conditions on big industrial farms, according to Margot Kaminski, a law professor at Ohio State. Kaminski urges patience on the federal level. "Clarity comes at the cost of experimentation, and early law is likely to be over-reaching," she says.

Some restrictive laws could end up being struck down in the courts. But by letting states, counties, and towns try to get this right, Kaminski argues, we may end up with a reasonable understanding of when and how drones fit into our daily lives.

And that includes how drones can be used for good, not just as intrusions. These aircraft are already being used for everything from stunning film-making to search-and-rescue operations to water conservation work on farms. Drones can also enhance safety by taking over both such mundane applications as inspections of leaky roofs, and high-profile tasks such as monitoring natural disaster sites. The challenge is to find the right balance between the right to the skies and the right to privacy. Big Data or Big Brother?

REFERENCES

[1]. Barbu C. Pătrăşcoiu N., Roşulescu C., *Using virtual instrumentation in distributed control systems*, Proceedings of International Multidisciplinary Symposium "Universitaria SIMPRO 2014", Petroşani, 2014.

[2]. Pătrăşcoiu N., Poanta A., Tomuş A., Sochirca B., *A software solution for mechanical change measurement through virtual instrumentation*, WSEAS Transactions on Circuits and Systems, v.9 n.12, p.746-755, December 2010.

[3]. Pop E., Leba M., *Applications of Distribution Theory in Digital Control Systems*, Annals of University of Petrosani, Vol. 5, 2003, pp.23-34.

[4]. Pop E., Leba M., *Simulation and Design of Nonlinear Controllers based on Distributions Theory,* Proceedings of the 6th WSEAS International Conference on SYSTEM SCIENCE and SIMULATION in ENGINEERING, ISBN 978-960-6766-14- 5, ISSN 1790-5117, 2007, pp.103-108.

[5]. Pop E., Leba M., *Microcontrollere si automate programabile*, Editura Didactica si Pedagogica, Bucuresti, 2003.

[6]. Pop E., Bubatu R., *Teoria sistemelor educaţie prin e-learning*, Editura Universitas, Petroşani, 2012.

[7]. Leba M., Pop E., *New Distributions Properties and Applications in Digital Control,* Proceedings of the 7th WSEAS International Conference on SIGNAL PROCESSING, ROBOTICS and AUTOMATION (ISPRA '08), ISSN: 1790-5117 48, ISBN: 978-960-6766-44-2, University of Cambridge, UK, February 20-22, 2008.

[8]. Leba M., *Programare in limbaj de asamblare. Aplicatii in ingineria sistemelor*, Editura Didactica si Pedagogica, Bucuresti, 2007.

[9]. Leba M., *Contributii privind conducerea numerica ierarhizata a sistemelor de actionare cu motor asincron*, Ph.D.Thesis, Petrosani, 2002.

[10]. Leba M., Pop E., Badea A., *Adaptive Software Oriented Automation for Industrial Elevator*, Proceedings of the 11th WSEAS International Conference on Automatic Control, Modeling and Simulation ACMOS'09, ISBN 978-960-474-082-6, ISSN 1790-5117, pp.128-133, Istanbul, Turkey, 2009.

[11]. Sochirca, B., Poanta, A., *Proiectarea şi dezvoltarea aplicaţiilor cu microcontroler*, Editura Universitas, Petroşani, 2012.

[12]. **Uţu, I., Samoilă, L.,** *Senzori şi instrumentaţie pentru sisteme electromecanice*, Editura Universitas, Petroşani, 2011, ISBN 978-973-741-208-9, pp. 222.

[13]. http://www.consumerreports.org/electronics/drone-privacy-is-anyone-in-charge/

[14]. http://consumerreports2032-yahoopartner.tumblr.com/post/139074748311/drone-privacy-is-anyone-in-charge

[15]. http://palliation4.rssing.com/chan-3776278/all_p375.html

[16]. http://consumer1105.rssing.com/chan-5393842/all_p371.html

[17]. http://trifacial3.rssing.com/chan-3467305/all_p183.html

[18]. https://cielotech.wordpress.com/category/privacy-concerns/

[19]. https://cielotech.wordpress.com/2016/06/05/quadcopters/

[20]. http://id5wv4auh.xiagao.us/author/admin/page/4

[21]. http://ivebeenmugged.typepad.com/my_weblog/2016/02/drone-privacy.html

[22]. https://samnoakes.wordpress.com/tag/digc310/

[23]. https://samnoakes.wordpress.com/tag/regulation/

[24]. https://samnoakes.wordpress.com/2016/04/19/cmon-uow-lets-drone-race/

[25]. https://www.researchgate.net/publication/306237285_Feasibility_of_use_UAVs_drones_in_construction

[26]. https://www.researchgate.net/publication/285484026_Usability_Assessment_of_Drone_Technology_as_Safety_Inspection_Tools

[27]. http://docplayer.net/7556639-Feasibility-study-to-determine-the-economic-and-operational-benefits-of-utilizing-unmanned-aerial-vehicles-uavs-by.html

FUZZY FEED_BACK CONTROL FOR INVERTED PENDULUM

STELIAN VALENTIN CASAVELA[1], ANTONIO CASAVELA[2], CRISTOFOR CASAVELA[3]

Abstract: A fuzzy feed back system solves partially the inverted pendulum control, but this is designed as a component in a Model Reference Adaptive Fuzzy Control (MRAFC). Also, we performed modelation and simulation of a MRAFC, via the use of this fuzzy feed back system, inside the fuzzy direct and inverse controllers. A fuzzy feed back system scheme is simulated for performing an asymptotic tracking of a reference signal for the inverted pendulum, signal with quickly or slowly time-varying parameters.

Keywords: fuzzy, feed back, model reference, adaptive fuzzy control, controller.

1. THE MATHEMATICAL MODELATION OF PENDULUM

1.1. The equilibrium of forces

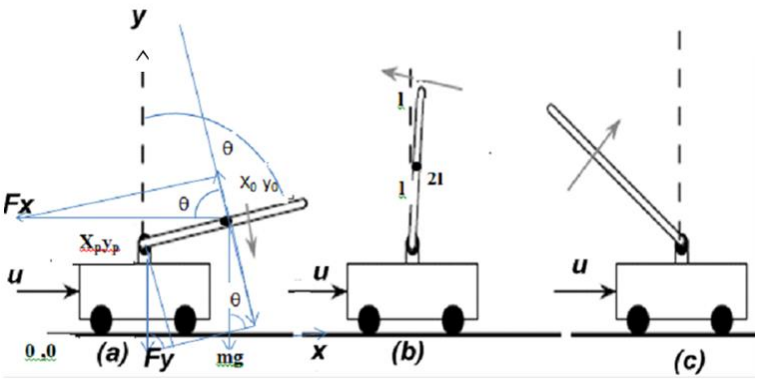

Fig 1. Inverted pendulum in 3 base positions

[1] *PhD., Associate Professor, Eng., University of Petrosani*
[2] *Ph.D. Student., Victor Babes University of Medicine and Pharmacy, Timisoara*
[3] *Ph.D. Student., Victor Babes University of Medicine and Pharmacy, Timisoara*

x_0 and y_0 are the coordinates of the center of gravity of the pendulum. Its length is 2*l. Displacements, speeds and accelerations:

$$x_0 = x_p + 1\sin\theta\,;\; x_0^{'} = x_p^{'} + 1\theta^{'}\cos\theta\,;\; x_0^{''} = x_p^{''} + 1\theta^{''}\cos\theta - 1(\theta^{'})^2\sin\theta \quad (1)$$

$$y_0 = y_p + 1\cos\theta\,;\; y_0^{'} = y_p^{'} - 1\theta^{'}\sin\theta\,;\; y_0^{''} = y_p^{''} - 1\theta^{''}\sin\theta - 1(\theta^{'})^2\cos\theta \quad (2)$$

Let note with *M*, the mass of the trolley and with *m*, the mass of the pendulum.

Forces on Ox axis are the active force: *f*, the inertial force of the pendulum *Fx*, the inertial force of the trolley: $M\,x_p''$ and the force due the coefficient of friction between pendulum and trolley: *b*.

$$f = F_x + Mx_p^{''} + bx_p^{'} \quad (3)$$

$$F_x = mx_0^{''} = m[x_p^{''} + 1\theta''\cos\theta - 1(\theta^{'})^2\sin\theta] \quad (4)$$

$$f - mx_p^{''} - m1\theta^{''}\cos\theta + m1\left(\theta^{1}\right)^2\sin\theta = Mx_p^{''} + bx_p^{'} \quad (5)$$

Let neglect the coefficient of friction b, and also b* x_p', and we suppose that the angle θ is limited at a little one and, so, sin θ=0 and cosθ=1;we obtain[2]:

$$f = (M+m)x_p^{''} + m1\theta^{''} \quad (6)$$

$$x_p^{''} = \left(f - m1\theta^{''}\right)/(M+m) \quad (7)$$

$$\theta^{''} = \left[f - (M+m)x_p^{''}\right]/(m1) \quad (8)$$

1.2. The equilibrium of the couples

Let us see now the equilibrium of the couples, for motionless pendulum.

$$\sum M_0 = 0 = J\theta^{''} + c\theta^{'} + F_x 1\cos\theta - F_y 1\sin\theta \quad (9)$$

"J" is the moment of inertia for pendulum and "c" is the coefficient of friction for trolley. Let we calculate Fy, using the equilibrium of forces on 0y axis, for motionless pendulum. The gravity is supported by the acceleration in up of the pendulum [3].

$G + my_0^{''} = 0\,;\; mg + my_0^{''} = 0\,;$ from (2), we obtain:

$$mg + m[y_p^{''} - 1\theta^{''}\sin\theta - 1\left(\theta^{'}\right)^2\cos\theta] = 0 \quad (10)$$

Fy appears as a reaction against the forces in the center of gravity of the pendulum, but in the support, upon trolley, that is, Fy is the force at the base of the pendulum. The inertia has a component which push in up, the pendulum. From (10):

$$F_y = my''_p = mg - m1\theta''\sin\theta - m1(\theta')^2\cos\theta \tag{11}$$

From (4), (8) and (9), we obtain:

$$\begin{gathered} mx''_p l\cos\theta + ml^2(\cos\theta)^2 - ml^2(\theta')^2\sin\theta\cos\theta - mgl\sin\theta + ml^2\theta''(\sin\theta)^2 + \\ ml\left(\theta'\right)^2\sin\theta\cos\theta = -J\theta'' - c\theta' \\ mgl\sin\theta - ml^2\theta' - mx''_p l\cos\theta = J\theta'' + c\theta' \end{gathered} \tag{12}$$

If θ is little, sin θ≈0, cosθ≈1. For the length equal with 2l, the moment of inertia for pendulum: $J=ml^2/3$ and we neglect "c" the coefficient of friction for trolley: c=0 and obtain[8]:

$$gl\theta - ml^2\theta'' - mlx''_p = \frac{ml^2}{3}\theta'' \tag{13}$$

or

$$g\theta - l\theta'' - x''_p = \frac{l}{3}\theta'' \tag{14}$$

1.3. The transfer functions

We calculate first the Laplace transfer function, H(s)= θ(s)/f(s), but the position (x_p,y_p) being without interest, for moment.

From (7) and (8) we obtain:

$$mgl\theta - ml^2\theta'' - \frac{ml\left(f - ml\theta''\right)}{M+m} - \frac{ml^2}{3}\theta'' = 0 \tag{15}$$

$$\left(4\frac{l}{3} - \frac{ml}{M+m}\right)\theta - g\theta + \frac{f}{M+m} = 0 \tag{16}$$

But $\mathcal{L}(\theta'')=s^2\,\theta(s)$ and $\mathcal{L}(f)=\mathcal{L}(f(t))=f(s)$. Then:

$$H_1(s) = \theta(s)/\,f(s) = -\frac{\dfrac{l}{M+m}}{\left(4\dfrac{l}{3} - \dfrac{ml}{M+m}\right)s^2 - g} \tag{17}$$

or

$$\theta(s) = -\frac{\dfrac{f(s)}{M+m}}{\left(4\dfrac{l}{3} - \dfrac{ml}{M+m}\right)s^2 - g} \tag{18}$$

We may calculate also the Laplace transfer function, $H(s)= x_p(s)/f(s)$, y_p being constant, but the angle θ being dependent of x_p. From (8) and (14) it may be obtained:

$$g\theta - \frac{l[f-(M+m)x_p^{"}]}{ml} - x_p^{"} = \frac{l}{3}\frac{f-(M+m)x_p^{"}}{ml} \tag{19}$$

$$x_p^{"} = \frac{g\theta - \dfrac{4f}{3m}}{1 - \dfrac{4(M+m)}{3m}} = 3m\frac{g\theta - \dfrac{4f}{3m}}{4M+m} \tag{20}$$

But $\mathcal{L}(x_p^{"})=s^2\, x_p(s)$ and (18) determine:

$$x_p(s) = -3m\frac{-g\dfrac{\dfrac{f(s)}{M+m}}{\left(4\dfrac{l}{3} - \dfrac{ml}{M+m}\right)s^2 - g} - \dfrac{4f(s)}{3m}}{s^2(4M+m)} \tag{21}$$

Finally:

$$H_2(s) = \frac{x_p(s)}{f(s)} = \frac{3mg\dfrac{\dfrac{1}{M+m}}{\dfrac{l}{3}\left(\dfrac{4M+m}{M+m}\right)s^2 - g} + 4}{s^2(4M+m)} = \frac{3mg\dfrac{3}{(4M+m)ls^2 - 3g(M+m)} + 4}{s^2(4M+m)} \tag{22}$$

$$H_2(s) = \frac{x_p(s)}{f(s)} = \frac{4ls^2 - 3g}{l(4M+m)s^4 - 3g(M+m)s^2} \tag{23}$$

Usually, the situations described by formulas (17) and (18), but not (19), are often encountered, and these will be developed in this paper.

As physical constants let us take: m=0.5Kg, M=1kg and l=0.5m. Then:

$$H_1(s) = \frac{0(s)}{f(s)} = \frac{\frac{1}{1+0.5}}{\left(\frac{4 \cdot 0,5}{3} - \frac{0,5 \cdot 0,5}{0,5+1}\right)s^2 - 9,8} \tag{24}$$

$$H_1(s) = \frac{0,66}{0,5s^2 - 9,8} \tag{25}$$

2. SIMULATION OF THE CONTROL FOR INVERTED PENDULUM

2.1. Inputs and Outputs for Fuzzy Controller

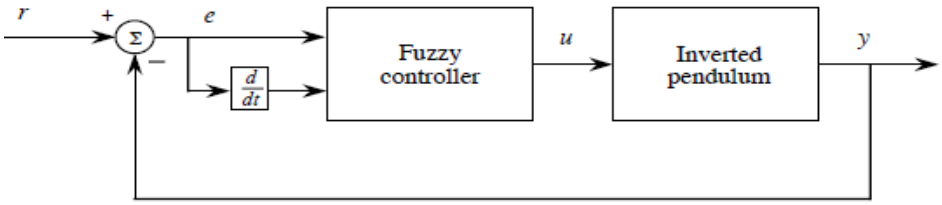

Fig 2. Fuzzy direct controller with feed back

The linguistic variables are inputs and outputs. The inputs mean the error $e(t)$ and the change-in-error de/dt, while the output is described by the force $u(t)$- newton (previously denoted with $f(t)$), $e(t) = r(t) - y(t)$, where $r(t)$ (angle -radians) is the reference input, $y(t)$ means the output angle, made by pendulum with the vertical (previously denoted with θ). "l" is the half of length of the pendulum (meters). See next figure 3.

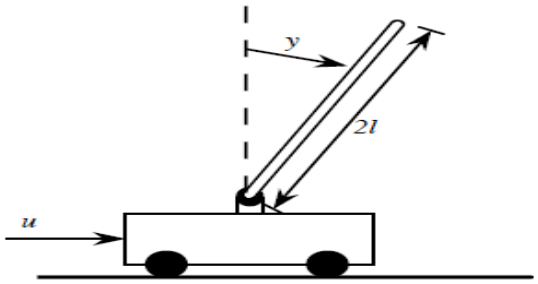

Fig 3. Force and angle

Error and change-in-error are framed in domains: "−2" means "neglarge" , "−1" means "negsmall" (for right side), "0" means "zero","1" means "possmall" and "2" means "poslarge" (for left side). The force has reverse sign, because if $r = 0$, then $e = r - y = -y$ and $de/dt = -dy/dt$.

Table 1. **Rule Table, heuristic created**

1. If (e is NB) and (de is NB) then (u is PB) (1)
2. If (e is Z) and (de is NB) then (u is PB) (1)
3. If (e is NS) and (de is NB) then (u is PB) (1)
4. If (e is PS) and (de is NB) then (u is PS) (1)
5. If (e is PB) and (de is NB) then (u is Z) (1)
6. If (e is NB) and (de is NS) then (u is PB) (1)
7. If (e is PS) and (de is NS) then (u is Z) (1)
8. If (e is PB) and (de is NS) then (u is NB) (1)
9. If (e is NB) and (de is Z) then (u is PB) (1)
10. If (e is PS) and (de is Z) then (u is NS) (1)
11. If (e is PB) and (de is Z) then (u is NB) (1)
12. If (e is NB) and (de is PS) then (u is PS) (1)
13. If (e is PS) and (de is PS) then (u is NB) (1)
14. If (e is PB) and (de is PS) then (u is NB) (1)
15. If (e is NB) and (de is PB) then (u is Z) (1)
16. If (e is PS) and (de is PB) then (u is NB) (1)
17. If (e is PB) and (de is PB) then (u is NB) (1)
18. If (e is Z) and (de is NS) then (u is PS) (1)
19. If (e is NS) and (de is NS) then (u is PB) (1)
20. If (e is Z) and (de is Z) then (u is Z) (1)
21. If (e is NS) and (de is Z) then (u is PS) (1)
22. If (e is NS) and (de is PB) then (u is NB) (1)
23. If (e is NS) and (de is PS) then (u is Z) (1)
24. If (e is Z) and (de is PB) then (u is NB) (1)
25. If (e is Z) and (de is PS) then (u is NB) (1)

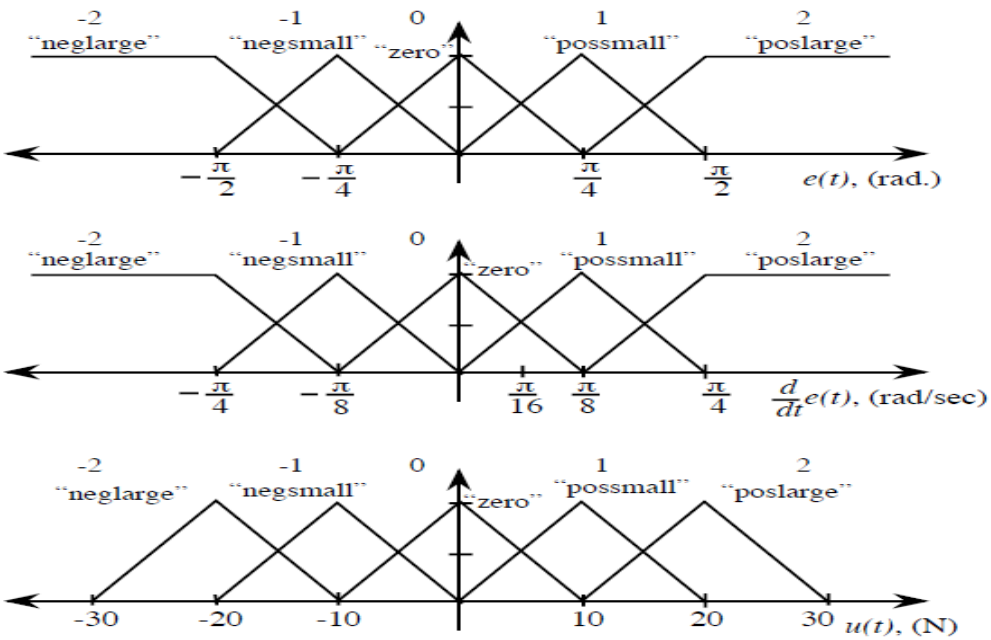

Fig 4. Membership functions

2.2. The Matlab programs for System with Fuzzy Controller

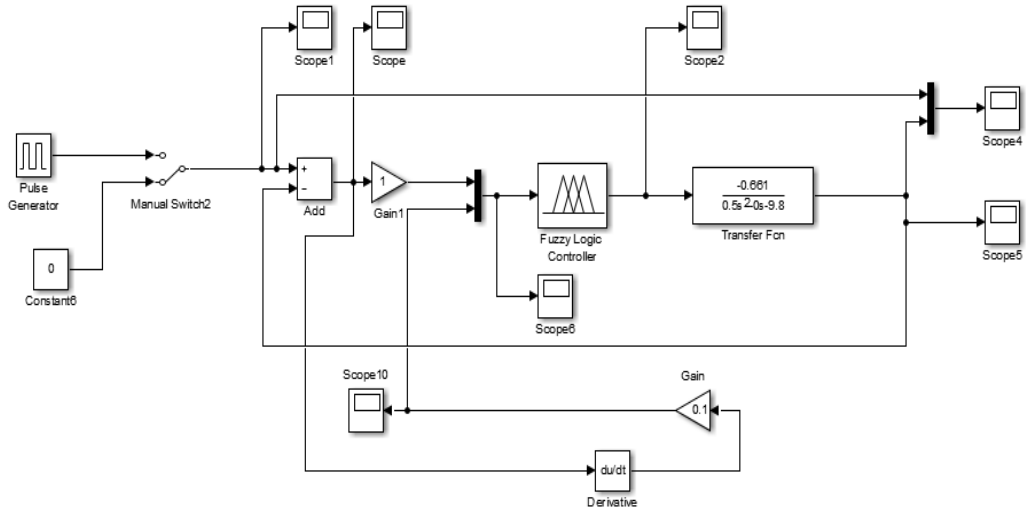

Fig 5. Simuling in Matlab for Fuzzy feed back controller for inverted pendulum

We may see that the input is $\theta_{set}=0$ (Scope1). The outputs will be seen on Scope2 (force), Scope 5 (θ) and Scope 10 (de/dt).

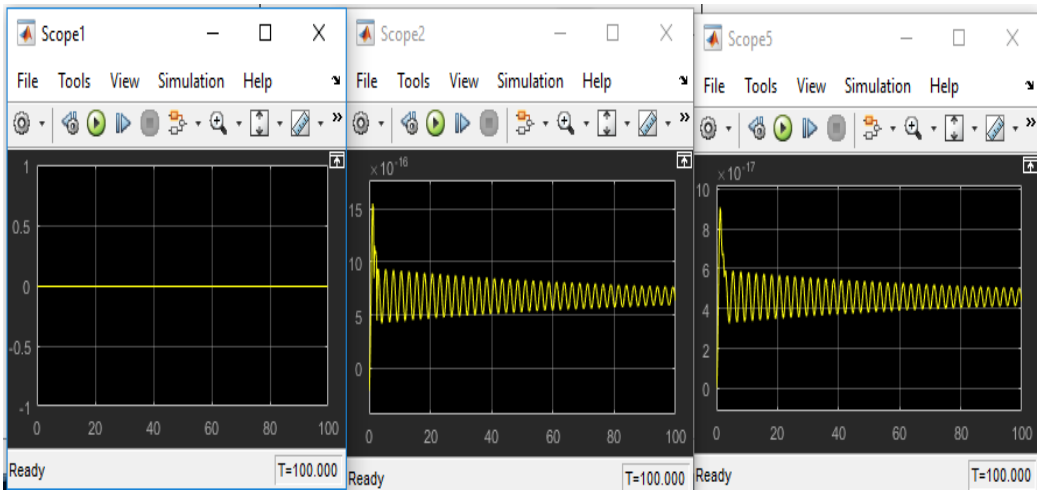

Fig 6. $\theta_{set}=0$, force and θ

If we modify the input, in pulses with maximum $\theta_{set}=1.150$ (Scope 1), the outputs would be seen next. Scope 2 (force), Scope 5 (θ).

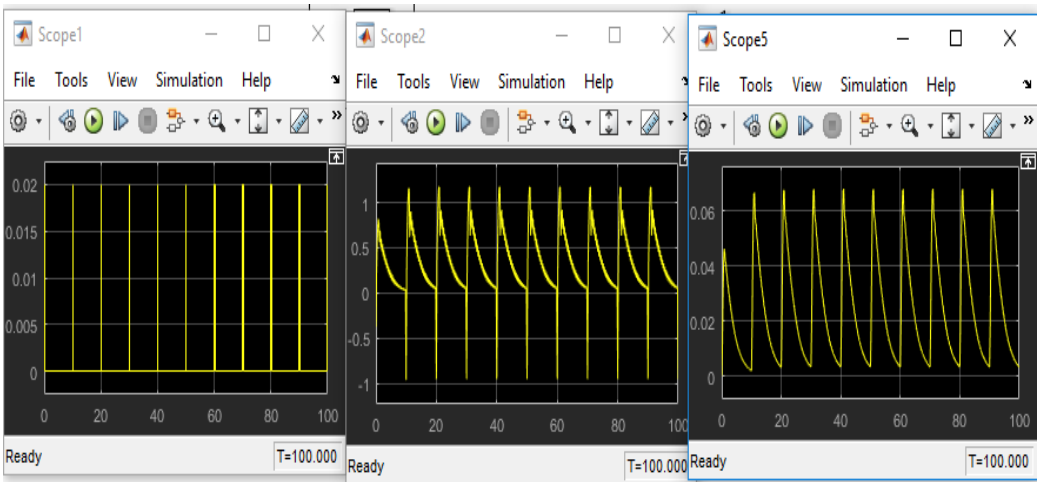

Fig. 7. $\theta_{set}=1.15^0$, force and θ

3. CONCLUSIONS

The results seem to be quite modest, but this program is used in a Model Reference Adaptive Fuzzy Control (MRAFC), as a direct controller and the performance is increased significantly.

REFERENCES

[1]. Barbu C. Pătrăşcoiu N., Roşulescu C., *Using virtual instrumentation in distributed control systems*, Proceedings of International Multidisciplinary Symposium "Universitaria SIMPRO 2014", Petroşani, 2014.

[2]. Navale R. L., *Development of an adaptive fuzzy logic controller for HVAC system*, Retrospective Theses and Dissertations, 2006.

[3]. Oltean S. E., Dulau M., Duka A. V., *Model Reference Adaptive vs. Learning Control for the Inverted Pendulum. A Comparative Case Study*, Journal of Control Engineering and Applied Informatics, 2007.

[4]. Passino K. M., Yurkovich S., *Fuzzy Control*, Addison Wesley Longman, Inc., 1998.

[5]. Pătrăşcoiu N., Poanta A., Tomuş A., Sochirca B., *A software solution for mechanical change measurement through virtual instrumentation*, WSEAS Transactions on Circuits and Systems, v.9 n.12, p.746-755, December 2010.

[6]. Pătrăşcoiu N., *Tehnici de instrumentaţie virtuală*, Editura Universitas, Petroşani, 2015.

[7]. Pătrăşcoiu N., *Sisteme de achiziţie şi prelucrare a datelor*, Editura didactică şi Pedagogică, 2004.

[8]. Samoila, B. L., Popescu, F. G., Slusariuc, R., *Virtual instruments used in direct current circuits learning process.* Annals of University of Petrosani, Electrical Engineering, Vol. 15, pag.47-52, Petroşani, 2013, *I*SSN 1454-8518.

[9]. Zadeh L. A., Berkeley, C. A., *Fuzzy Logic Toolbox, For Use with MATLAB, User's Guide Version 2*, January 10, 1995.

INDEX OF AUTHORS

REVIEWERS:

Professor Susana Arad, PhD.
Associate Professor Marius Marcu, PhD.
Associate Professor Nicolae Pătrăşcoiu, PhD.
Associate Professor Liliana Samoila, PhD.
Associate Professor Olimpiu Stoicuta, PhD.
Associate Professor Ilie Uţu, PhD.
Lecturer Dragoş Păsculescu, PhD.
Lecturer Florin Gabriel Popescu, PhD.